Improving Network Performance Through Multipath Utilization for Wireless Mesh Networks

Manolis Ploumidis

Computer Science Department,

University of Crete

March 13, 2015

UNIVERSITY OF CRETE
COMPUTER SCIENCE DEPARTMENT

Improving Network Performance Through Multipath Utilization for Wireless Mesh Networks

Dissertation submitted by

Manolis Ploumidis

in partial fulfillment of the requirements for the
Doctor of Philosophy Degree in Computer Science

Author:

Manolis Ploumidis

Examination Committee:

Apostolos Traganitis, Professor Emeritus, University of Crete

Panagiotis Tsakalides, Professor, University of Crete

Vasilios Siris, Associate Professor, Athens University of Economics and Business

George D. Stamoulis, Professor, Athens University of Economics and Business

Maria Papadopouli, Associate Professor, University of Crete

Stavros Toumpis, Assistant Professor, Athens University of Economics and Business

Vangelis Angelakis, Assistant Professor, Linköping University

Departmental approval:

Panagiotis Tsakalides, Professor Head of the Department

Heraklion, March 2015

Η παρούσα έρευνα έχει συγχρηματοδοτηθεί από την Ευρωπαϊκή Ένωση (Ευρωπαϊκό Κοινωνικό Ταμείο - ΕΚΤ) και από εθνικούς πόρους μέσω του Επιχειρησιακού Προγράμματος «Εκπαίδευση και Δια Βίου Μάθηση» του Εθνικού Στρατηγικού Πλαισίου Αναφοράς (ΕΣΠΑ) – Ερευνητικό Χρηματοδοτούμενο Έργο: Ηράκλειτος ΙΙ. Επένδυση στην κοινωνία της γνώσης μέσω του Ευρωπαϊκού Κοινωνικού Ταμείου.

Ευρωπαϊκή Ένωση
Ευρωπαϊκό Κοινωνικό Ταμείο

ΕΠΙΧΕΙΡΗΣΙΑΚΟ ΠΡΟΓΡΑΜΜΑ
ΕΚΠΑΙΔΕΥΣΗ ΚΑΙ ΔΙΑ ΒΙΟΥ ΜΑΘΗΣΗ
επένδυση στην κοινωνία της γνώσης
ΥΠΟΥΡΓΕΙΟ ΠΑΙΔΕΙΑΣ ΚΑΙ ΘΡΗΣΚΕΥΜΑΤΩΝ
ΕΙΔΙΚΗ ΥΠΗΡΕΣΙΑ ΔΙΑΧΕΙΡΙΣΗΣ

ΕΣΠΑ
2007-2013
πρόγραμμα για την ανάπτυξη
ΕΥΡΩΠΑΪΚΟ ΚΟΙΝΩΝΙΚΟ ΤΑΜΕΙΟ

Με τη συγχρηματοδότηση της Ελλάδας και της Ευρωπαϊκής Ένωσης

This research has been co-financed by the European Union (European Social Fund – ESF) and Greek national funds through the Operational Program "Education and Lifelong Learning" of the National Strategic Reference Framework (NSRF) - Research Funding Program: Heracleitus II. Investing in knowledge society through the European Social Fund.

European Union
European Social Fund

OPERATIONAL PROGRAMME
EDUCATION AND LIFELONG LEARNING
investing in knowledge society
MINISTRY OF EDUCATION & RELIGIOUS AFFAIRS
MANAGING AUTHORITY

NSRF
2007-2013
programme for development
EUROPEAN SOCIAL FUND

Co-financed by Greece and the European Union

Ευχαριστίες

Κατάρχήν, θα ήθελα να ευχαριστήσω θερμά τον επόπτη μου, κ. Απόστολο Τραγανίτη για την υποστήριξη, υπομονή, και βοήθεια κατά τη διάρκεια της διατριβής. Θερμές ευχαριστίες επίσης και στον Νικόλαο Παππά για την πολύ ουσιαστική συνεργασία και βοήθεια του σε όλη την προσπάθεια. Χωρίς την κρίσιμη βοήθεια και των δύο, η διατριβή αυτή δεν θα είχε ολοκληρωθεί. Ευχαριστώ επίσης τον κ. Βασίλειο Σύρη για την συνεργασία και την ευκαιρία που μου έδωσε να μετέχω σε project του εργαστηρίου.

Θα ήθελα επίσης να ευχαριστήσω και τα υπόλοιπα μέλη της επιτροπής, Παναγιώτη Τσακαλίδη, Μαρία Παπαδοπούλη, Σταύρο Τουμπή, Γεώργιο Σταμούλη, και Βαγγέλη Αγγελάκη για τα χρήσιμα σχόλια και τις συμβουλές όσον αφορά την παρούσα διατριβή.

Αξίζει να αναφερθούν επίσης οι συνεργάτες και άτομα που βοήθησαν από το εργαστήριο τηλεπικοινωνιών και δικτύων, το "κλουβί", αλλά και άλλα εργαστήρια: Στέφανος Παπαδάκης, Μανώλης Σπανάκης, Μανώλης Σουρλίγκας, Φώτης Νικολαΐδης, Μανώλης Χουρδάκης, Νίκος Παππάς, Γιώργος Σταματάκης.

Έξω από το χώρο του πανεπιστημίου και του ΙΤΕ, σημαντική ήταν η υποστήριξη από: Βαγγέλη, Κίμωνα, Βάσω.

Και τέλος, να ευχαριστήσω τους αφανείς και κλασσικούς "ήρωες" κάθε τέτοιας προσπάθειας, τους γονείς μου, Μαρία Βεντούρη και Λάμπρο Πλουμίδη.

Η διατριβή αυτή πραγματοποιήθηκε στο πλαίσιο υλοποίησης του έργου «ΗΡΑΚΛΕΙΤΟΣ ΙΙ Πανεπιστημίου Κρήτης» του Επιχειρησιακού Προγράμματος «Εκπαίδευση και Δια βίου Μάθηση 2007 – 2013» (Ε.Π.Ε.Δ.Β.Μ.) του Ε.Σ.Π.Α. (2007 – 2013), το οποίο συγ-

χρηματοδοτείται από την Ευρωπαϊκή Ένωση (Ευρωπαϊκό Κοινωνικό Ταμείο) και από εθνικούς πόρους

Abstract

In order to meet the increased demand for quality of service over wireless mesh networks, a large number of studies have suggested employing multiple paths in parallel, in order to aggregate the scarce resources. Multipath utilization comes in many different flavours including schemes that perform routing, resource allocation, flow and congestion control, and opportunistic forwarding. Multipath utilization has been shown to be advantageous in terms of delay, throughput, reliability, and load balancing. Two common performance goals are increased throughput and fault tolerance. For achieving reliability, multipath utilization is combined with redundancy. However, multipath utilization in wireless networks, is more complicated compared to their wired counterparts since transmissions across a link interfere with neighbouring links and may result in reduced network performance.

In this thesis, static, random access, wireless mesh networks are considered, where receivers have multi-packet reception capabilities. Multiple unicast flows are forwarded to their destinations through node-disjoint paths.

In the first part of the thesis, different forwarding schemes, employing multiple paths and different degrees of redundancy are compared in terms of delay and throughput. An analytical framework for expressing the throughput and delay of these schemes is evaluated, through Ns2 simulations of various scenarios and is also extended for the case where link success probability is captured through the SINR model.

In the second part of the thesis, multipath utilization for maximizing average aggregate flow throughput is addressed, for the aforementioned type of networks. A distributed flow rate allocation scheme that maximizes average aggregate flow throughput, while also providing

bounded delay is proposed, that does not employ any kind of redundancy. For the purposes of the suggested scheme, flow rate allocation is formulated as an optimization problem. A simple model for the average aggregate flow throughput is employed that captures both intra- and inter-path interference through the SINR model. As far as interference is concerned, two different variants of the suggested scheme are explored. In the first one, interference is approximated by considering only that link's dominant interferers. In the second variant, a simple topology is employed where receivers apply successive interference cancellation, instead of treating interference as noise. For the evaluation process, Ns2 simulations of some illustrative topologies, along with several random wireless ones are employed. The proposed scheme is compared with three other simple flow allocation schemes both in terms of average aggregate flow throughput and flow delay.

Περίληψη

Προκειμένου να ικανοποιηθούν οι αυξανόμενες απαιτήσεις για ποιότητα υπηρεσίας πάνω από ασύρματα δίκτυα πλέγματος, ένας μεγάλος αριθμός μελετών προτείνει την αξιοποίηση πολλαπλών μονοπατιών ταυτόχρονα με σκοπό να αθροιστούν οι πόροι τους. Υπάρχουν αρκετές διαφορετικές προσεγγίσεις αξιοποίησης πολλαπλών μονοπατιών οι οποίες περιλαμβάνουν σχήματα που πραγματοποιούν δρομολόγηση, δέσμευση πόρων, έλεγχο ροής και ευκαιριακή προώθηση κίνησης. Η ταυτόχρονη αξιοποίηση πολλαπλών μονοπατιών έχει αποδειχτεί επωφελής ως προς την καθυστέρηση, το ρυθμό διαμεταγωγής δεδομένων, την αξιοπιστία και την ισοκατανομή φόρτου κίνησης. Δύο διαδεδομένοι στόχοι είναι ο αυξημένος ρυθμός διαμεταγωγής δεδομένων και η αξιοπιστία. Προς επίτευξη της αξιοπιστίας συγκεκριμένα, η αξιοποίηση πολλαπλών μονοπατιών συνδυάζεται με πλεονασμό. Παρ΄ όλα αυτά, η αξιοποίηση πολλαπλών μονοπατιών στα ασύρματα δίκτυα είναι πιο περίπλοκη, από ότι στα ασύρματα καθώς μεταδόσεις σε μία ζεύξη παρεμβάλλουν γειτονικές ζεύξεις και μπορεί να οδηγήσουν σε μειωμένη δικτυακή απόδοση.

Στην παρούσα διδακτορική διατριβή, θεωρούνται στατικά, ασύρματα δίκτυα πλέγματος, τυχαίας προσπέλασης, όπου τα μονοπάτια αποτελούνται από πολλαπλές ζεύξεις. Επιπλέον, οι παραλήπτες έχουν δυνατότητα για λήψη πολλαπλών πακέτων. Πολλαπλές ροές κίνησης, τύπου μονοεκπομπής, προωθούνται προς τους προορισμούς, μέσω μονοπατιών που δεν έχουν κοινούς κόμβους.

Στο πρώτο τμήμα της διατριβής, διαφορετικά σχήματα προώθησης κίνησης που αξιοποιούν πολλαπλά μονοπάτια και διαφορετικούς βαθμούς πλεονασμού συγκρίνονται ως προς την καθυστέρηση και το ρυθμό διαμεταγωγής δεδομένων. Αξιολογείται, μέσω προσομοι-

ώσεων διαφόρων σεναρίων, στον προσομοιωτή δικτύων Ns2, ένα αναλυτικό πλαίσιο το οποίο εκφράζει την καθυστέρηση και το ρυθμό διαμεταγωγής δεδομένων για τα προαναφερθέντα σχήματα προώθησης κίνησης. Το συγκεκριμένο αναλυτικό πλαίσιο επεκτείνεται και αξιολογείται επίσης για την περίπτωση όπου η πιθανότητα λάθους μίας ζεύξης εκφράζεται μέσω του μοντέλου σηματοθορυβικής σχέσης.

Στο δεύτερο μέρος της διατριβής, εξερευνάται το θέμα της αξιοποίησης πολλαπλών μονοπατιών με σκοπό την αύξηση του μέσου αθροιστικού ρυθμού διαμεταγωγής δεδομένων, για τον προαναφερθέντα τύπο δικτύων. Προτείνεται ένα κατανεμημένο σχήμα κατανομής ροής, το οποίο μεγιστοποιεί τον μέσο αθροιστικό ρυθμό διαμεταγωγής δεδομένων για όλες τις ροές, ενώ ταυτόχρονα, παρέχει πεπερασμένη καθυστέρηση. Δεν χρησιμοποιείται κανενός είδους πλεονασμός. Για τους σκοπούς του συγκεκριμένου σχήματος, η κατανομή ροής σε πολλαπλά μονοπάτια διατυπώνεται σαν ένα πρόβλημα βελτιστοποίησης. Το προτεινόμενο σχήμα βασίζεται σε ένα απλό μοντέλο για το μέσο αθροιστικό ρυθμό διαμεταγωγής δεδομένων, το οποίο εκφράζει τις παρεμβολές από γειτονικά μονοπάτια, αλλά και τις παρεμβολές από κόμβους του ίδιου μονοπατιού, μέσω του μοντέλου σηματοθορυβικής σχέσης. Αναφορικά με τις παρεμβολές, εξετάζονται δύο εκδοχές του προτεινόμενου σχήματος κατανομής ροής. Στην πρώτη εκδοχή, η παρεμβολή σε μία ζεύξη προσεγγίζεται λαμβάνοντας υπόψη μόνο τους σημαντικότερους παρεμβολείς. Στη δεύτερη εκδοχή, οι παραλήπτες εφαρμόζουν την τεχνική της διαδοχικής απαλοιφής παρεμβολών. Για την διαδικασία αξιολόγησης, αξιοποιούνται προσομοιώσεις, τόσο ενδεικτικών όσο και τυχαίων ασύρματων σεναρίων, χρησιμοποιώντας τον προσομοιωτή δικτύων Ns2. Το προτεινόμενο σχήμα κατανομής ροής συγκρίνεται με άλλα απλά σχήματα κατανομής ροής, τόσο ως προς την καθυστέρηση όσο και ως προς το ρυθμό διαμεταγωγής δεδομένων.

Contents

List of Figures

List of Tables

Chapter 1

Introduction

Meeting the increasing user demand for Quality of Service (QoS), in wireless multi-hop networks, is a challenging issue. Wireless networks are more error-prone and unreliable, compared to their wired counterparts, while wireless spectrum is limited. Moreover, transmissions on a specific link interfere with transmissions on neighbouring links, lowering network performance [1]. Many studies, have suggested utilizing different network paths in parallel, in order to overcome wireless networks limitations by aggregating their scarce resources. However, multipath utilization for wireless networks, is a challenging issue due to interference. In wireless mesh networks for example, where multiple multi-hop paths may be employed in parallel, receivers experience both inter- and intra-path interference. Adjusting the utilization of a specific link, also affects the performance of neighbouring links. This inherent coupling among links in a wireless environment, makes modeling and controlling several aspects a complicated problem. Deriving accurate models for the performance of such networks and designing efficient multipath utilization schemes, is a challenging issue.

1.1 Combining multipath utilization with redundancy to improve network reliability

The idea of using redundancy is central in channel coding theory. Several studies have employed diversity coding for link-, or path-error recovery. The work in [2], suggests an error recovery approach, called diversity coding, where M parity symbols are transmitted along with the original N symbols, allowing for recovery from simultaneous failures of M communication lines. The work of [3], suggests a scheme utilizing multiple paths, aimed at maximizing the probability of successful packet reception. Redundant bits are added to each packet and each resulting packet is fragmented and dispersed among the available paths. The work of [4], extends [3] in the case where the failure probabilities are different for different paths, and when the paths are not necessarily independent.

Numerous studies suggest achieving redundancy by combining network coding with multipath utilization. Network coding is a generalization of the traditional store-and-forward technique. The core notion of network coding, introduced in [5], is to allow and encourage mixing of data at intermediate network nodes. Error correcting network coding is introduced in [6], as a generalization of classical error correcting codes. Several network coding related studies explore code design issues. The work in [5], is aimed at characterizing the admissible code rate region. The work in [7], suggests a coding scheme for both unicast and multicast traffic and also studies the coding delay in packet networks that support network coding. In [8], efficient algorithms for the construction of robust network codes for multicast connections are proposed. The work in [9], presents an approach for designing network codes by considering path failures in the network, instead of edge failures. The work in [10], explores a multipath transmission scheme employing network coding for providing better rate-delay trade-offs, being also adjustable according to QoS constraints.

There is a significant body of work concerning opportunistic routing in wireless mesh networks, with or without network coding [11]. COPE [12], MORE [13] and MC^2 [14], explore network coding with opportunistic routing, in wireless networks with broadcast transmissions, focusing exclusively on the throughput improvements. ExOR [15] and ROMER [16], explore opportunistic routing in broadcast wireless networks without network coding. These studies focus on throughput improvements, except [16], which also considers the packet delivery ratio. In [17], the authors discuss several issues that affect the computational complexity of practical network coding implementations. These issues are related to network coding parameters, such as, generation and field size and also platform dependent, and protocol related issues. CoMP suggested in [18], is an online multipath network coding scheme that is aimed at improving the performance of TCP sessions in multi-hop wireless mesh networks. The rate at which linear independent combinations are injected in the network, depends on estimates of link loss rate. In [19], an adaptive multipath routing protocol is suggested, that switches between single path, multipath with network coding, and multipath routing that replicates packets on all paths, based on the observed channel loss conditions. The work in [20], explores the advantage of network coding over standard routing, for the multiple unicast network communication problem and shows that under certain connection requirements, it is bounded by three.

Most of the theoretical results in network coding consider multicast traffic, the vast majority of Internet traffic though, is unicast. Applying network coding in wireless environments, has to address multiple unicast flows, if it has any chance of being used. Especially for the case of multicast traffic, where all receivers are interested for all packets, intermediate nodes can encode any packets together, without worrying about decoding, which will be performed eventually at the destinations.

In the first part of this thesis, static wireless multihop networks (also referred to as, wireless mesh networks) are considered, with random access to the shared medium. Multiple paths are employed, between a source and a destination node, for forwarding flows carrying unicast traffic. Source and destination nodes are equipped with multiple interfaces and hop-by-hop retransmissions are assumed for achieving reliability. The aim of this part of the thesis, is to compare in terms of delay and throughput, different forwarding schemes employing multiple paths and different degrees of redundancy.The forwarding schemes explored are: *single path*, that employs zero redundancy and one path, *multipath*, that employs multiple paths and zero redundancy, *multicopy*, that replicates each packet on every path, and *network coding-based* forwarding. For expressing the throughput and delay of these schemes, the analytical framework presented in [21] is utilized. Ns2 simulations, of several wireless scenarios, are employed, for validating the accuracy of this framework on capturing the throughput and delay trends of the aforementioned schemes. The analytical framework presented in [21] however, considers fixed link error probabilities. In the first part of the thesis, an extension of this framework is also presented and evaluated through Ns2 simulations, where link error probability is captured through the SINR model.

Part of the work, presented in the first part of the thesis, has alse been published in [22,23].

1.2 Throughput optimal flow allocation on multiple paths

In the second part of the thesis, static, random access, wireless mesh networks are also considered. Flows carrying unicast traffic, are forwarded to their corresponding destinations over multiple node disjoint paths. Different from the first part of the thesis, no form of redundancy is assumed. Apart from that, instead of expressing the throughput and delay of different schemes, the goal is to identify the rate at which the available paths should be utilized, in order to maximize the average aggregate flow throughput, given the intra- and inter-path interference relations among different flows.

A wide range of different schemes, have been proposed in literature, focusing on multipath utilization for improving network performance, including routing schemes, resource allocation, flow control, and opportunistic-based forwarding ones. A significant amount of studies focuses on identifying the set of paths that will guarantee improved performance in terms of some metric [24–27]. However, such studies mostly address the issue of, *which*, paths should be utilized and rely on heuristic-based approaches concerning the issue of, *how*, should these paths be utilized (e.g. allocation of traffic on these paths) [24–26, 28]. In [26] for example, traffic is allocated on a round-robin fashion among the available paths.

Several studies focus on coordinating the access of multiple flows, employing different paths, to shared network resources, suggesting scheduling, routing, power control, or channel assignment schemes. Authors in [29] for example, suggest a scheme that performs joint channel assignment, scheduling and routing for maximizing system throughput. A resource allocation scheme, for multiple flows in wireless networks, that performs joint scheduling, routing and power control is suggested in [30], while the authors in [31], address the problem of joint routing, scheduling and power control, for multiple information flows in interference limited ad hoc networks. The problem is modelled as a mixed-integer one and a polynomial time framework for solving it is suggested. Authors in [32], study an MPLS-based forwarding paradigm and aim at identifying a feasible routing solution for multiple flows employing multiple paths. Links whose transmissions have a significant effect on each others success probability are considered to belong to the same collision domain and cannot be active at the same time. [33] suggests a technique for combining multipath forwarding with packet aggregation over IEEE 802.11 wireless mesh networks. Multipath utilization is accomplished by employing Layer-2.5, a multipath routing and forwarding strategy, that aims at utilizing links in proportion to their available bandwidth.

As far as flow allocation on multiple paths and rate control is concerned, a well studied approach associates a utility function to each flow's rate and aims at maximizing the sum of these utilities, subject to cross-layer constraints. Several studies, suggest joint rate control and scheduling approaches [34–36]. Authors in [37], instead of employing a utility function of a flow's rate, they employ a utility function of flow's effective rate, in order to take into account the effect of lossy links.

The aforementioned method, based on utility functions related to flow rates, has also been applied for wireless random access networks to derive joint rate and MAC-layer control schemes [38–40]. As far as the interference model adopted by these approaches is concerned, two concurrent transmissions on links, that interference with each other, result in a packet failure. In the interference model employed in both parts of this thesis however, link error probability is captured through the SINR model.

Based on back-pressure scheduling and utility maximization, Horizon [41] constitutes a practical implementation of a multipath forwarding scheme that interacts with TCP. There is also a significant amount of studies that suggest opportunistic forwarding/routing schemes that exploit the broadcast nature of the wireless medium. A multipath routing protocol called Multipath Code Casting, that employs opportunistic forwarding combined with network coding, is suggested in [42]. It also employs a rate control mechanism that achieves fairness among different flows by maximizing an aggregate utility of these flows. The work in [43], suggests an optimization framework that performs optimal flow control, routing, scheduling and rate adaptation, employing multiple paths and opportunistic transmissions.

The issue addressed in this part of the thesis is: allocation of flow on multiple paths that exhibit both intra- and inter-path interference, in order to maximize Average Aggregate flow Throughput (AAT), while also providing bounded delay, for random access, wireless mesh networks, with multi-packet reception capabilities. A distributed flow rate allocation scheme, that formulates flow rate allocation as an optimization problem, is suggested. The proposed scheme also employs a simple model for the AAT, capturing intra- and inter-path interference through the SINR model. As far as interference is concerned, two variants of the proposed scheme are explored. In the first one, interference is approximated, by considering the dominant interfering nodes only, for each link. Additionally, a variant of the proposed scheme is also explored, where certain receivers employ successive interference cancellation (SIC), instead of treating interference as noise.

A simple topology is employed to demonstrate flow allocation, derive the conditions for the corresponding optimization problem's non-convexity, and also illustrate the application of successive interference cancellation. The suggested scheme is evaluated, both in terms of flow delay and AAT, through Ns2 simulations of, both some illustrative wireless scenarios and several random ones. As part of the evaluation process, the proposed scheme is also compared with three other simple flow allocation schemes in terms of flow delay and AAT.

Part of the work presented in this part of the thesis has been published in [44, 45].

Chapter 2

Throughput and delay of schemes employing multiple paths and different degrees of redundancy

2.1 Introduction

In this chapter, the throughput and delay is explored, for forwarding schemes employing different degrees of redundancy. Random access, wireless mesh networks are assumed. Moreover, flows carry unicast traffic and hop-by-hop retransmissions are assumed, for achieving link-layer reliability. In the first part of this chapter, the analytical framework presented in [21], for expressing the throughput and delay of forwarding schemes, employing different degrees of redundancy, is extended, for the case where success probability for a link is captured through the SINR model. In the second part of this chapter, Ns2 simulations are used, to validate the accuracy with which the aforementioned framework and its extension, capture the throughput-delay trade-off for the various schemes explored.

Section 2.2, presents the system model along with the extension of the analytical framework considered, for the case where link success probabilities are derived based on the SINR-criterion. Section 2.3, compares the forwarding schemes discussed, both in terms of delay and throughput, using simulation results and numerical ones derived from the aforementioned analytical framework.

The work in this chapter, extends the work of [21, 22] and part of the results presented have also been published in [22, 23]. This extension is along two directions. First, simulation results are derived for several wireless scenarios, for validating and extending the throughput and delay trends presented in [21, 22]. Secondly, the analytical framework presented in [21], is extended, for the case where link success probability is captured through the SINR model.

2.2 Analytical framework extension

2.2.1 System model

A wireless acyclic network is assumed, where a single source sends unicast traffic to a single destination node, through multiple paths that consist of lossy links. The paths available, between the source and the destination, can be, either node-disjoint, or share common nodes and are assumed to be given by some multipath routing protocol [46]. Moreover, source routing is assumed, ensuring that packets of the same flow will be forwarded to the destination through the same path. As far as MAC layer is concerned, hop-by-hop retransmissions are assumed, for achieving reliability, while time is slotted and packet transmission requires one time slot. When an error occurs at the transmission of a packet between two nodes, for example node i and $i + 1$, node i retransmits the packet to $i + 1$. Moreover, each node transmits with a probability equal to 1.0 on each time slot. Acknowledgements for successfully received packets are assumed to be instantaneous and error free. Nodes, are also assumed to have multi-packet reception capabilities, being thus able to decode more than one packets at the same time. Two different approaches for interference are employed, for deriving numerical results. In the first one, also presented in the analytical framework of [21], fixed link error probabilities are assumed for each link. In the extension of this framework, presented in the rest of the current section, link error probabilities are derived through the SINR model.

2.2.1.1 Forwarding Schemes

In this work, the delay and throughput achieved is modelled, for the following schemes:

- *Single path (SP)*, also depicted in Fig. 2.1(a), utilizes only a single path, to forward a packet to the destination. Among the available paths, it selects the one with the highest end-to-end success probability.

- *Multipath (MP)*, utilizes multiple paths in parallel, employing zero redundancy, by forwarding different packets over different paths. For the case of Fig. 2.1(c), where three paths are available between the source and the destination, MP assigns packet N on the first path, packet $N + 1$ on the second one, e.t.c.

- *Multicopy (MC)*, utilizes multiple paths in parallel along with maximum redundancy, by replicating a specific packet on all the available paths. As also shown in Fig. 2.1(b), packet N is replicated on all three paths.

- *Multipath with network coding (NC)*, or also referred to as, *network coding based forwarding*, for the rest of the paper, combines multipath utilization with network coding. Data packets are grouped in sets of size k, constituting different *packet generations*. Packets of each packet generation, are coded together, through linear network coding, resulting in $m = 2^k - 1$ linearly independent combinations, excluding the one that contains only zero values. Each such linear independent combination constitutes a coded packet that is assigned on a specific path. A packet generation can be decoded and the original data can be extracted, if k, or more coded packets, are received at the destination. All coded packets are forwarded in parallel. Fig. 2.1(d) explores the case of a packet generation of size two. Two packets, namely, N and $N+1$ are coded together, resulting in three coded packets, assigned on one of the three available paths each.

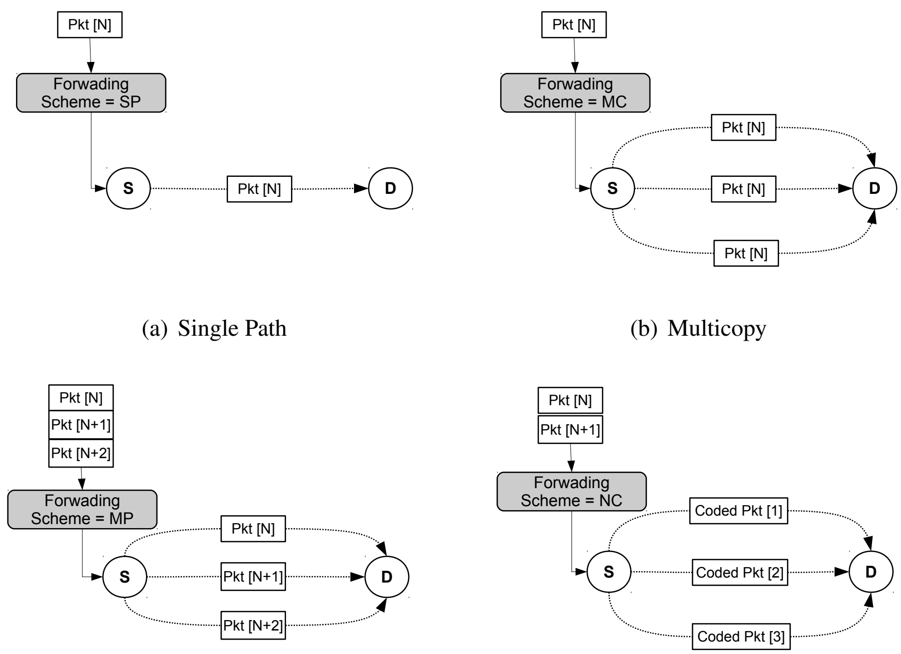

(a) Single Path

(b) Multicopy

(c) Multipath

(d) Multipath with network coding

Figure 2.1: Forwarding schemes considered.

Following the assumptions presented in [21], for the case of multicopy, when a packet is successfully received by the destination, all other nodes are assumed to remove it from their queues. Similarly, for the case of network coding-based forwarding, when a packet generation is successfully decoded at the receiver, all traffic sources, or relays, remove from their queues coded packets that belong to the same generation.

2.2.1.2 Channel model

The channel model used in this part of the thesis, is a generalized form of the packet erasure model [47]. In the wireless environment, a packet can be decoded correctly by the receiver, if the received SINR exceeds a certain threshold. More precisely, suppose that a given set of nodes, denoted by $\mathcal{T}$, are also active, during the same slot, with node i. Let $\mathcal{P}_{rx}(i,j)$ be the signal power received from node i at node j. Treating interference from neighbouring links as noise, $\mathrm{SINR}(i,j)$, is then expressed through:

$$\mathrm{SINR}(i,j) = \frac{\mathcal{P}_{rx}(i,j)}{\eta_j + \sum_{k \in \mathcal{T} \setminus \{i\}} \mathcal{P}_{rx}(k,j)}. \tag{2.1}$$

In the above equation, η_j denotes the receiver noise power at j. We assume that, a packet transmitted by i, is successfully received by j, if and only if, $\mathrm{SINR}(i,j) \geq \gamma_j$, where γ_j is a threshold characteristic of node j. The wireless channel is subject to fading; let $\mathcal{P}_{tx}(i)$ be the transmitting power of node i and $r(i,j)$ be the distance between i and j. The power received by j, when i transmits, is $\mathcal{P}_{rx}(i,j) = \mathcal{A}(i,j)g(i,j)$, where $\mathcal{A}(i,j)$ is a random variable representing channel fading. Under Rayleigh fading, $A(i,j)$ is exponentially distributed [48]. The received power factor, $g(i,j)$, is given by $g(i,j) = \mathcal{P}_{tx}(i)(r(i,j))^{-\alpha}$, where α is the path loss exponent, with typical values between 2 and 4. The success probability of link (i,j), when the transmitting nodes in $\mathcal{T}$ are also active, is given by:

$$p^j_{i/T} = \exp\left(-\frac{\gamma_j \eta_j}{v(i,j)g(i,j)}\right) \prod_{k \in \mathcal{T} \setminus \{i,j\}} \left(1 + \gamma_j \frac{v(k,j)g(k,j)}{v(i,j)g(i,j)}\right)^{-1}, \tag{2.2}$$

where $v(i,j)$ is the parameter of the Rayleigh random variable for fading. The analytical derivation for this success probability, which captures the effect of interference on link (i,j), from transmissions of nodes in set $\mathcal{T}$, can be found in [49]. It should also be noted that, nodes i and j in the above equations, can either represent nodes with a single interface or a specific interface of a node equipped with more than one interfaces. In a similar manner, the link error probability for link l, between i and j, given that nodes in $\mathcal{T}$ are transmitting simultaneously with node i, denoted by $e^j_{i/\mathcal{T}}$, is expressed by

$$e^j_{i/\mathcal{T}} = 1 - p^j_{i/\mathcal{T}}. \tag{2.3}$$

Accordingly, using link indexes instead of node indexes, $e^j_{i/\mathcal{T}}$ can also be written as $e_{l/\mathcal{L}}$, where $\mathcal{L}$ denotes the links that are simultaneously active with l.

2.2.2 Throughput and delay expressions assuming SINR-based link success probabilities

The throughput and delay expressions presented in this section, for the aforementioned forwarding schemes, constitute the extension of the analytical framework presented in [21]. In this framework, throughput and delay expressions were derived for single-path, multipath, multicopy, and multipath with network coding, assuming fixed link error probabilities. In this section, this framework is extended, for the case of a network consisting of three single hops paths, where link error probability is captured through the SINR model.

Before proceeding with the analysis, for the delay and throughput of various schemes, the following definitions concerning throughput and delay for the various forwarding schemes considered, are needed: For single path forwarding (SP), SP delay, denoted as D_{sp}, is defined as the average time, measured in slots, required to receive a packet. Since each packet trans-

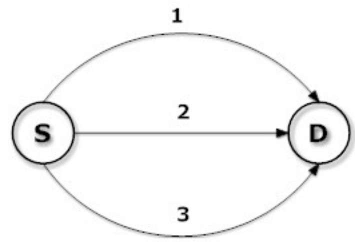

Figure 2.2: A wireless network with three single hop paths.

mission requires one time slot, it can be expressed as the average number of transmissions required for a successful packet reception. Since one packet is received on D_{sp} slots, on average, the throughput for SP, is $1/D_{sp}$. For multipath (MP), and the case where m paths are employed in parallel, delay is defined through the average time, in slots, required to receive m packets (D^m_{mp}). For example, consider the case of the topology depicted in Figure 2.2. The average time to receive three packets can be expressed through the average number of transmissions required to receive three packets. Consequently, delay of multipath (denoted as D_{mp}) is defined as, the average delay per packet, defined through: $D_{mp} = D^m_{mp}/m$. Thus, throughput for MP is $1/D_{mp}$. For multicopy (MC) and the case of m paths, the same copy is replicated on each path available. Delay for MC, denoted as D_{mc}, is defined as the average time required to receive at least one copy of the packet. This can be expressed through the average number of transmissions required to receive at least one copy of the packet. Since one packet is received on D_{mc} slots on average, MC throughput is expressed through: $1/D_{mc}$. Finally, let us consider the case of multipath with network coding (NC) and a packet generation of size N. NC delay, denoted as D_{nc}, is defined as the average time required to receive at least N coded packets. Consider as an example, the case of a packet generation of size two. Applying linear network coding on two data packets, results in three coded packets (and a fourth one consisting of only zero values). In order to successfully decode a packet generation, we need to receive at least two coded packets, so we have to take into account all the cases of different packet combinations. Since N packets are successfully decoded in D_{nc}, the achieved throughput for NC is N/D_{nc}.

In this section, throughput and delay are expressed, for all aforementioned forwarding schemes, for a network consisting of three single hop paths (shown in Fig. 2.2), where link error probability is determined based on the SINR model presented in Section 2.2.1. Source node S forwards three unicast flows to destination D through single-hop paths 1, 2, and 3 according to Fig. 2.2. Both S and D, are assumed to be equipped with three interfaces each.

- Single or Best Path: the link j (path) with the lowest link error probability is selected to forward traffic to the destination and is provided by:

$$j = \arg\min_i e_{i/i},\ i = 1, 2, 3. \tag{2.4}$$

SP delay is given by:

$$\mathcal{D}_{\text{sp}} = \frac{1}{1 - e_{j/j}}, \tag{2.5}$$

where $e_{i/i}$ denotes the probability of a packet error on link i given that only the transmitter of link i is active, and is given by (2.3). The throughput is given by:

$$Thr_{\text{sp}} = 1/\mathcal{D}_{sp}. \tag{2.6}$$

- Multipath: The packets are transmitted in parallel through all available paths.

$$\mathcal{D}_{\text{m}p} = \frac{\sum_{k=1}^{3} \frac{1}{1-e_{k/1,2,3}}}{3}. \tag{2.7}$$

The achieved throughput:

$$Thr_{\text{mp}} = \sum_{k=1}^{3} 1 - e_{k/1,2,3}. \tag{2.8}$$

- Multicopy (MC): The delay is

$$\mathcal{D}_{\text{mc}} = \frac{1}{1 - \prod_{k=1}^{3} e_{k/1,2,3}}. \tag{2.9}$$

The throughput is given by $Thr_{\text{mc}} = 1/\mathcal{D}_{\text{mc}}$.

- Multipath with Network Coding: Assuming a packet generation of size two, applying linear network coding on two data packets, results in three coded packets and a fourth one containing only zero values. In order to successfully decode a packet generation thus, we need to receive two or three coded packets. If only one coded packet is received through path *i*, the receiver will wait for the other paths to accomplish a successful coded packet delivery. Recall that NC delay, for a packet generation of size N, is defined as the average time required to receive at least N coded packets. Thus, in order to express NC delay ($\mathcal{D}_{nc}$), all different events that result in a successful packet generation decoding, need to be enumerated. In order to estimate the contribution to the average time for decoding a packet generation, for each such event, its probability along with the time required to receive the corresponding coded packets, are needed. Consider for example the case where all three coded packets transmitted over the three different paths in Fig. 2.2, are successfully received. Since each packet transmission requires one time slot and the probability of receiving successfully all three coded packets is $(1 - e_{1/1,2,3})(1 - e_{2/1,2,3})(1 - e_{3/1,2,3})$, then the contribution of this event to the average time required to decoded a packet generation is $(1-e_{1/1,2,3})(1-e_{2/1,2,3})(1-e_{3/1,2,3})$ slots. In case where all three transmissions fail, one time slot is spent and the whole packet generation needs to be retransmitted which will required an additional $\mathcal{D}_{nc}$ until it is successfully decoded. The probability of this event is $e_{1/1,2,3}e_{2/1,2,3}e_{3/1,2,3}$. Based on the previous discussion, NC delay is expressed through:

$$
\begin{aligned}
\mathcal{D}_{\mathrm{nc}} = {} & (1-e_{1/1,2,3})(1-e_{2/1,2,3})(1-e_{3/1,2,3}) + (1-e_{1/1,2,3})(1-e_{2/1,2,3})e_{3/1,2,3} \\
& + (1-e_{1/1,2,3})(1-e_{3/1,2,3})e_{2/1,2,3} + (1-e_{2/1,2,3})(1-e_{3/1,2,3})e_{1/1,2,3} \\
& + (1-e_{1/1,2,3})e_{2/1,2,3}e_{3/1,2,3}(1+\mathcal{D}^1_{\mathrm{nc}}) + (1-e_{2/1,2,3})e_{1/1,2,3}e_{3/1,2,3}(1+\mathcal{D}^2_{\mathrm{nc}}) \\
& + (1-e_{3/1,2,3})e_{1/1,2,3}e_{2/1,2,3}(1+\mathcal{D}^3_{\mathrm{nc}}) + e_{1/1,2,3}e_{2/1,2,3}e_{3/1,2,3}(1+\mathcal{D}_{nc}).
\end{aligned} \tag{2.10}
$$

In the previous equation, $\mathcal{D}^1_{\mathrm{nc}}$ denotes the delay required, to receive at least one more coded packet, given that the destination has already received one from the first path and is given by the following expression:

$$
\begin{aligned}
\mathcal{D}^1_{\mathrm{nc}} = {} & (1-e_{2/2,3})(1-e_{3/2,3}) + (1-e_{2/2,3})e_{3/2,3} \\
& + e_{2/2,3}(1-e_{3/2,3}) + e_{2/2,3}e_{3/2,3}(1+\mathcal{D}^1_{\mathrm{nc}}).
\end{aligned} \tag{2.11}
$$

$$
\begin{aligned}
\mathcal{D}^2_{\mathrm{nc}} = {} & (1-e_{1/1,3})(1-e_{3/1,3}) + (1-e_{1/1,3})e_{3/1,3} \\
& + e_{1/1,3}(1-e_{3/1,3}) + e_{1/1,3}e_{3/1,3}(1+\mathcal{D}^2_{\mathrm{nc}}).
\end{aligned} \tag{2.12}
$$

$$
\begin{aligned}
\mathcal{D}^3_{\mathrm{nc}} = {} & (1-e_{1/1,2})(1-e_{2/1,2}) + (1-e_{1/1,2})e_{2/1,2} \\
& + e_{1/1,2}(1-e_{2/1,2}) + e_{1/1,2}e_{2/1,2}(1+\mathcal{D}^3_{\mathrm{nc}}).
\end{aligned} \tag{2.13}
$$

$\mathcal{D}^2_{\mathrm{nc}}$ and $\mathcal{D}^3_{\mathrm{nc}}$ are calculated through (2.12) and (2.13) respectively. The throughput for network coding is:

$$
Thr_{\mathrm{nc}} = 2/\mathcal{D}_{\mathrm{nc}}. \tag{2.14}
$$

As the analysis above shows, capturing in an exact manner the interference experienced by a specific link, requires exhaustive enumeration of all possible subsets of interfering transmitters. For larger networks, such an approach would be computationally intractable.

2.3 Throughput-delay trade-off for different wireless setups

In this section, the throughput and delay is explored for the aforementioned forwarding schemes and different wireless setups. For expressing delay and throughput for these schemes, the analytical framework of [21] is employed, along with its extension presented in the previous section, where link error probability is derived through the SINR model. More precisely, the accuracy of the corresponding analytical framework, for capturing the throughput and delay trends, for various forwarding schemes is evaluated. The main reason for the deviation, between numerical and simulation results, both in terms of throughput and delay trends, is the analytical framework's inaccuracy for capturing the actual interference in the simulation scenarios.

Each wireless setup, is characterized by the following parameters: a)type of topology (number of paths, number of hops per path), b)type of coding (end-to-end or hop-by-hop), c)path disjointness, d)link error probability. As far as link error probability is concerned, it is either assumed fixed, on an SNR-based manner, or defined through the SINR model. For

Parameter	Value
Transmit Power	0.1 W
Noise Power	7×10^{-11} W
Max Retransmit Threshold	Inf
Path Loss Exponent	4.0
Contention Window (CW)	7 (fixed used for relays only)
Transmission probability for traffic sources	0.2

Table 2.1: Parameters used in the simulations.

the cases of fixed link error probabilities, they can either be the same for all links, or different for each link. For the rest of the chapter, the term *symmetric* will be used to denote links that share the same success probability. The main goal of this section, is to validate through Ns2 simulations, if the analytical framework discussed, along with the suggested extension for link success probability, accurately captures the throughput and delay for the various forwarding schemes considered. It should be noted that, directly comparing throughput and delay values between numerical and simulation results, is meaningless, due to the different assumptions in the analysis and simulation setup. The main difference is that, in the analytical framework considered, fixed link error probabilities are assumed, while in the simulated scenarios, link error probability is determined through the SINR model (more details concerning Ns2 simulator setup in Appendix A). Moreover, in the aforementioned analytical framework, transmission probability for each node is assumed 1.0, while different transmission probabilities are considered in the simulated scenarios, due to the half-duplex operation of nodes. In Section 2.3.3.2 however, where the extension of the analytical framework presented in the previous section is considered, numerical and simulation results are directly compared. Instead, the *rank* achieved by each scheme is compared, in terms of delay and throughput, in the simulation and numerical results for each wireless setup explored. As far as rank is concerned, the lower the rank of a scheme, the lower its delay and the higher its throughput.

Implementation details for the Ns2 network simulator setup (Ns2) are presented in Appendix A. The values for certain simulation parameters used, for deriving simulation results, are summarized in Table 2.1.

As also discussed in Appendix A, time is slotted. Transmission probabilities are fixed for sources of traffic, while relay nodes wait for a random number of slots, uniformly drawn from [0, CW], prior to transmitting. Traffic sources employ static predefined routes to the destination and generate constant bit rate UDP flows. Additionally, all nodes share the same channel, transmission rate, and power (parameter values summarized in Table 2.1). In each simulated scenario, the source node generates a flow f, of $R = 9$ Mbps, constant bit rate UDP traffic consisting of same sized packets, routed to the destination over n multiple paths in parallel. Mulipath splits f into n subflows of rate $R_i = R/n, i = 1...n$. Each subflow, is forwarded to the destination through a specific interface of the source node and a predefined path. Multicopy, replicates f on all paths assigning a subflow of rate $R_i = R$ on each one. For the case of network coding, assuming a packet generation of size k (number of data packets coded together), a subflow or rate $R_i = R/k$ is assigned on each path. Single path on the other hand, routes f to the destination through the shortest path available to it.

Following the assumptions of the analytical framework presented in [21], the following two characteristics concerning network-coding based forwarding are simulated. In the lemma presented in the appendix of [50], the minimum and maximum number of linear combinations, needed to decode a packet generation was derived. For the case of a network where seven paths are utilized in parallel, the minimum and maximum number of coded packets required to decode a specific packet generation, are three and four, respectively. Based on this, two different NC variants are simulated for the scenarios where seven paths are available. In the first variant, denoted by *NC-L*, a packet generation can be successfully decoded when three coded packets are received at the destination. For the second variant, denoted by *NC-U*, four packets are required, in order to decode a specific packet generation. The second characteristic concerning network coding-based forwarding, is whether packets of a subsequent packet generation are allowed to be injected into the network, without requiring for the previous packet generation to have been successfully decoded. Based on this, a NC variant is explored, that allows only one packet generation to be on the network each time. Subsequent packet generations, are injected into the network only when the previous one is fully decoded at the destination. For the rest of the study, the notation used for this variant will be *NC*, or *NC-L* and *NC-U*, for the case of seven paths (also explained in [21]). The second network coding variant explored, is a greedy one that continually injects packet generations into the network, without waiting for the previous ones to be decoded. For the rest of the chapter, this variant will be referred to as *G-NC*, or *G-NC-L* and *G-NC-U*, for scenarios consisting of seven paths.

Before presenting and discussing simulation results, a brief discussion about how delay and throughput are measured for each scheme, is provided. For the case of single path (SP) and multipath (MP), delay is estimated as the average per-packet delay, with per-packet delay denoting the time interval between the first transmission of that packet at source node S and successful reception of that packet at destination D. As far as multicopy (MC) is concerned, delay is also estimated as average per-packet delay. However, in this case, per-packet delay denotes the interval between the first transmission of a packet with sequence number k at the source node and the time when the first packet with sequence number k is received at destination. In case of network coding based schemes and assuming a packet generation of size n, delay is estimated as average per-generation delay, where per-generation delay, is the interval between transmitting the first coded packet of a specific packet generation i at source node S and the time when destination D receives the n^{th} coded packet for that generation. Recall that, the destination is able to decode a generation when it receives at least n coded packets of that generation. For the case of network coding-based schemes, *inter-arrival time* reports the average inter-arrival time, over all coded packets, of all generations received at the destination, with inter-arrival time denoting the interval between the successful reception of two successive coded packets at the receiver. For the rest of the chapter, the term *failed packets* will be used to refer to packets that are not successfully received due to noise, signal attenuation, interference, and fading. Accordingly, the row labelled *Failed pkts*, presents the total number of failed data (or coded for the case of network coding) packets.

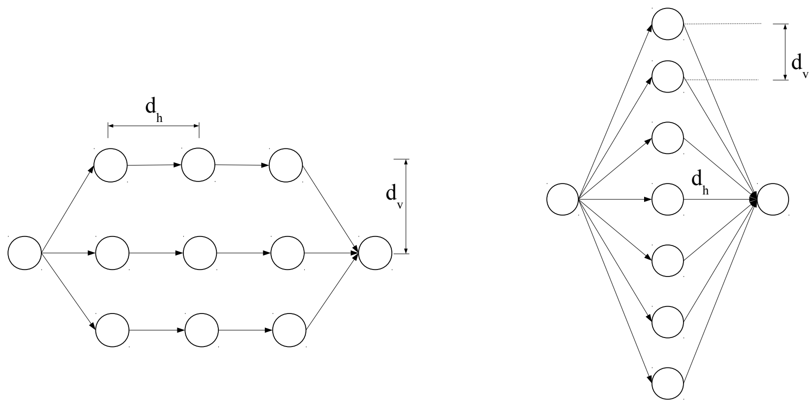

(a) Three paths with four hops each (b) Seven paths with two hops each

Figure 2.3: Indicative topologies consisting of node disjoint paths.

	MP	MC	NC	G-NC	SP
Delay (Slots)	324.1	123.6	43.5	537.3	80.2
Throughput (Pkts/Slot)	0.092	0.052	0.087	0.076	0.109
Inter-arrival times (Slots)			12.7	207.6	
Failed pkts	28342	36981	12328	30293	3386

Table 2.2: Simulation results for the topology depicted in Fig. 2.3(a). Three paths with four hops each, where $d_h = 40$ m and $d_v = 80$ m.

2.3.1 Node disjoint paths, end-to-end coding, symmetric links

In this section, the setup explored, consists of node disjoint paths, where end-to-end coding is assumed, for the case of network coding-based forwarding. Moreover, similar success probabilities and thus, error probabilities are assumed for all links. Analytical results are compared with simulation ones, for the two topologies presented in Fig. 2.3(a) and Fig. 2.3(b). In Fig. 2.3(a), the source forwards data to the destination, through three paths with four hops each, while in Fig. 2.3(b), source employs seven paths with two hops each.

Simulation results for these two different topologies are presented in Tables 2.2-2.4.

Table 2.5 compares the throughput and delay trends for the numerical results presented in Table I of [21] and the simulation results of Tables 2.2, 2.3, for the case of a network consisting of three node-disjoint paths with four hops each. Moreover, end-to-end coding is assumed for network coding.

The numerical results included in this table show that, lowest end-to-end delay is achieved by schemes employing high redundancy, with MC coming first. SP and MP, that employ zero redundancy, achieve the highest delay. As this table shows, the trend in terms of delay is slightly different in the simulation results. MC and NC perform better in terms of delay than

	MP	MC	NC	G-NC	SP
Delay (Slots)	335.3	154.4	48.6	10138.6	80.2
Throughput (Pkts/Slot)	0.101	0.072	0.077	0.054	0.109
Inter-arrival times (Slots)			19.9	4449.1	
Failed pkts	22701	19857	13307	37652	3386

Table 2.3: Simulation results for the topology depicted in Fig. 2.3(a). Three paths with four hops each), where $d_h = 40$ m, $d_v = 120$ m.

	MP	MC	NC-L	NC-U	G-NC-L	G-NC-U	SP
Delay (Slots)	647.6	64.2	76.5	81.0	620.0	729.0	35.1
Throughput (Pkts/Slot)	0.077	0.033	0.074	0.071	0.057	0.046	0.156
Inter-arrival times (Slots)			31.3	43.5	183.0	405.0	
Failed pkts	61218	103649	41785	41154	69925	92947	478

Table 2.4: Simulation results for the topology depicted in Fig. 2.3(b). Seven paths with two hops each, where $d_h = 40$ m, $d_v = 10$ m.

MP, however SP proves better than MC. Moreover, NC appears to achieve lower delay than MC. The reason for this re-arrangement, in terms of delay, is related to interference and how accurately it is captured by the analytical framework. As already described, MC replicates the initial flow on all paths, while NC based forwarding splits into *k* subflows. As a result, path utilization is more intense in the case of MC. As also shown in Tables 2.2 and 2.3, MC experiences 199.9% and 49.2% more failed packets, for the two instances of the topology depicted in Fig. 2.3(a) (where $d_v = 80$ m and $d_v = 120$ m respectively). The gap in terms of failed packets, becomes even more notable when MC is compared with SP. However, the analytical framework assumes the same link error probability, for links utilized by MP, SP, and NC, without taking into account different interference conditions that may arise due to different utilization of the paths employed.

As far as, numerical results for throughput are concerned, Table 2.5 shows that, the lowest the redundancy employed, the higher the throughput achieved, for schemes employing multiple paths, with MP coming first. SP that utilizes a single path to the destination achieves the lowest throughput among all schemes. The simulation results reveal the same trend, apart from the case of SP, which seems to achieve the best throughput among all. As already discussed, fixed link error probabilities for all links, which remain the same, independently of the forwarding scheme employed, fail to accurately capture inter-path interference.

Another interesting observation, concerning simulation results for network coding based-forwarding, is that, greedy network coding variant (G-NC - that injects packet generations continually into the network, without waiting for the previous ones to be decoded) has a poor performance both in terms of throughput and delay. It is also interesting to compare the average inter-arrival times for packets that belong to the same generation for this variant and the

	Simulation				Numerical	
	$d_h = 40m, d_v = 80m$		$d_h = 40m, d_v = 120m$		Error=$\{0.2, 0.4\}$	
Rank	Delay	Throughput	Delay	Throughput	Delay	Throughput
1	NC	SP	NC	SP	MC	MP
2	SP	MP	SP	MP	NC	NC
3	MC	NC	MC	NC	SP,MP	MC
4	MP	G-NC	MP	MC		SP
5	G-NC	MC	G-NC	G-NC		

Table 2.5: Numerical vs simulation results. Node disjoint paths, end-to-end coding, symmetric links. Three paths assumed, with four-hops each.

one that waits for a packet generation to be decoded first before issuing the next one. As Tables 2.2 and 2.3 show, G-NC experiences significantly higher inter-arrival times, when compared to NC. The reason for this gap, is the larger inter-path interference imposed on the network by the parallel presence of multiple generations on the paths employed. This is also obvious from the percentages of failed packets presented in the aforementioned tables. For the two scenarios explored ($d_v = 80$ m and $d_v = 120$ m), based on the topology with three paths and four hops, G-NC experiences 145.7% and 182.9% more failed packets. Consequently, introducing *idle times* between successive packet generations, proves gainful both in terms of throughput and delay.

	Simulation		Numerical	
	$d_h = 40$ m, $d_v = 10$ m		Error=$\{0.2, 0.4\}$	
Rank	Delay	Throughput	Delay	Throughput
1	SP	SP	MC	MP
2	MC	MP	NC-L	NC-L
3	NC-L	NC-L	NC-U	NC-U
4	NC-U	NC-U	SP,MP	MC
5	G-NC-L	G-NC-L		SP
6	MP	G-NC-U		
7	G-NC-U	MC		

Table 2.6: Numerical vs simulation results. Node disjoint paths, end-to-end coding, symmetric links. Seven paths assumed, with with two hops each.

Table 2.6, compares the throughput and delay trends derived from the numerical results presented in Table I of [21] and the simulation results of Table 2.4, for the case of a network consisting of seven node-disjoint paths with two hops each. As far as network coding based schemes are concerned, end-to-end coding is assumed.

As numerical results in this table show, the higher the redundancy employed by a scheme, the lower the delay it achieves. NC-L, that can decode the generation when at least three linear independent combinations are successfully received, achieves lower delay than NC-U that requires at least four. As simulation results show, the analytical framework captures the trend in terms of delay for all schemes, apart from SP, which, as in the previous topology explored, achieves the lowest delay among all schemes. As already discussed, SP experiences the lowest inter-path interference than all schemes. This is also obvious from the number

	MP	MC	NC	G-NC	SP
Delay (Slots)	8.1	3.7	11.4	22.1	5.0
Throughput (Pkts/Slot)	0.361	0.194	0.261	0.290	0.188
Inter-arrival times (Slots)			6.8	15.8	
Failed pkts	1299	2224	1389	1492	30

Table 2.7: Simulation results. Three paths with one hop each, where the distance between the source and the destination (d_h) is 40 m.

	MP	MC	NC-L	NC-U	G-NC-L	G-NC-U	SP
Delay (Slots)	18.7	5.5	23.0	26.4	44.0	76.8	5.0
Throughput (Pkts/Slot)	0.364	0.118	0.215	0.197	0.219	0.193	0.188
Inter-arrival times (Slots)			14.1	18.9	30.9	61.5	
Failed pkts	6952	17263	8600	8595	9225	10461	30

Table 2.8: Simulation results. Seven paths with one hop each, where the distance between the source and the destination (d_h) is 40 m.

of failed packets. The analytical framework discussed however, assumes a fixed link error probability, which is independent of the scheme employed and thus, the amount of inter-path interference present in the network.

As far as throughput is concerned, the simulation results included in Table 2.6 show that the analytical framework captures the trend in terms of throughput, missing only the case of SP. More precisely, higher throughput is achieved by schemes employing multiple paths in parallel and a low degree of redundancy, with MP coming first. It also interesting to note again that, the greedy variant of the network coding-based forwarding scheme, achieves poor performance, both in terms of delay and throughput

2.3.2 Non-disjoint paths, hop-by-hop coding, symmetric links

	Simulation		Analytical	
	$d_h = 40$ m,		Error={0.2, 0.4}	
Rank	Delay	Throughput	Delay	Throughput
1	MC	MP	MC	MP
2	SP	G-NC	NC	NC
3	MP	NC	SP,MP	MC
4	NC	MC		SP
5	G-MC	SP		

Table 2.9: Numerical vs simulation results. Non-disjoint paths, hop-by-hop coding, symmetric links. Three single-hop paths assumed, where the distance between the source and the destination is 40 m.

Table 2.9, compares the throughput and delay trends, for the numerical results presented in Table II of [21] and the simulation results of Table 2.7, for the case of a network consisting of three single hop paths.

The main difference between the numerical and the simulation results is the rank on NC, in terms of delay, which appears to achieve the highest delay in the simulation results. Recall that, sources of traffic transmit on each slot with a probability equal to 0.2. As a result, the probability of two or more packets overlapping during a slot is 10.4%, for the topology explored. This suggests that, packet transmissions do not overlap very frequently. Indeed, by comparing the number of failed packets for each scheme between Tables 2.3 and 2.7, it is obvious that in the scenario explored in Table 2.9, the interference is less significant. As also shown in Table 2.7, NC experiences slightly more failed packets than MP. Note also that, before transmitting each coded packet for NC, the transmitter spends some slots waiting, due to the probability with which it accesses the channel. For the rest of the section, this idle time at sources, will be referred to as, *random access waiting*. The poor performance of NC is due to the fact that the overhead required to receive two coded packets, mainly due to random access waiting waiting, is not compensated by the gain in terms of delay. As far as throughput is concerned, the analytical framework explored accurately captures the trend in the simulation results: schemes employing multiple paths and a lower degree of redundancy, achieved higher throughput. It is also interesting to note that, in the absence of significant interference, the greedy NC variant (G-NC), achieves higher throughput than NC.

	Simulation		Analytical	
	$d_h = 40$ m,		Error={0.2, 0.4}	
Rank	Delay	Throughput	Delay	Throughput
1	SP	MP	MC	MP
2	MC	G-NC-L	NC-L	NC-L
3	MP	NC-L	NC-U	NC-U
4	NC-L	NC-U	SP,MP	MC
5	NC-U	G-NC-U		SP
6	G-NC-L	SP		
7	G-NC-U	MC		

Table 2.10: Numerical vs simulation results. Non-disjoint paths, hop-by-hop coding, symmetric links. Seven single-hop paths assumed, where the distance between the source and the destination is 40 m.

Table 2.10, compares the throughput and delay trends, for the numerical results presented in Table II of [21] and the simulation results of Table 2.8, for the case of a network consisting of seven single hop paths. As far as network coding based schemes are concerned, hop-by-hop coding process is assumed in the analysis.

In the scenario, where seven single hop paths are considered instead of three, the probability of two or more packet transmissions overlapping increases and consequently, transmitters experience increased interference. As Table 2.10 show, network coding based forwarding schemes, experience higher delay than all other schemes. The main reason for which the analytical framework discussed misses the trend in terms of delay is that, it does not capture interference conditions accurately, when different forwarding schemes are employed. As Table 2.8 shows, MP experiences fewer failed packets than NC. The reason for that is that, it splits the incoming flow into more subflows, of lower rate, when compared to NC (also discussed at the beginning of Section 2.3). The analytical framework however, considers a fixed error probability, independently of intensity with which each path is utilized by the corresponding forwarding scheme. When the flow injected, on the paths employed in parallel, increases, the inter-path interference also increases so the success probability declines.

Concerning throughput, both the analytical framework and the simulation results, indicate that higher throughput is achieved by schemes employing multiple paths and a low degree of redundancy. The only exception is MC, which achieves the lowest throughput, as shown by the simulation results included in Table 2.10. As also shown in Table 2.8, MC is the scheme that experiences the larger number of failed transmissions.

2.3.3 Non-symmetric links

2.3.3.1 Non-symmetric links - SNR based link error probabilities

In this section, wireless scenarios where different links may have different success probabilities, are explored. The numerical and simulation results used in this table are derived from Table III of [21] and Table 2.7 respectively.

	Simulation		Numerical	
	$d_h = 40$ m,		{e1,e2,e3}={0.3,0.4,0.5}	
Rank	Delay	Throughput	Delay	Throughput
1	MC	MP	MC	MP
2	SP	G-NC	NC	NC
3	MP	NC	SP	MC
4	NC	MC	MP	SP
5	G-NC	SP		

Table 2.11: Numerical vs simulation results. Asymmetric links in terms of error probability. Three single-hop paths assumed, where the distance between the source and the destination is 40 m.

Numerical results show that, the highest the redundancy employed, the lowest the delay achieved. For throughput, best performance is achieved by schemes employing multiple paths and low redundancy. As also discussed in Section 2.3.2, the main difference between the numerical and the simulation results is the rank on NC in terms of delay, which appears to achieve the highest delay in the simulation results. Considering the transmission probability for each interface/node, which is set to 0.2 in the simulation setup, the probability of two or more transmissions overlapping is low and thus, the inter-path interference experienced is not expected to be significant. The poor performance of NC is due to the fact that the overhead required to receive two coded packets, mainly due to random access waiting, is not compensated by the gain in terms of delay.

As far as throughput is concerned, both the simulation and the numerical results, show that, schemes that employ multiple paths in parallel along with low redundancy, achieve the highest throughput. It is also interesting to note that, the greedy network coding variant (G-

NC), achieves higher throughput than the variant that waits for the previous packet generation to be decoded before injecting the new one into the network. This is due to the low inter-path interference. More on that, as Table 2.7 shows, G-NC experiences only 7.4% more failed packets when compared to NC.

2.3.3.2 Non-symmetric links with SINR-based link error probabilities

	Simulation		Numerical	
Scheme	Delay (Slots) Slots	Throughput Packets/Slot	Delay Slots	Throughput Packets/Slot
SP	0.92	0.996	1.0	0.998
MP	3.91	0.734	4.0	0.748
MC	2.1	0.368	1.7	0.577
G-NC	10.7	0.568	2.7	0.738
NC	5.0	0.608	2.7	0.738

Table 2.12: Numerical and simulation results for the topology consisting of three single hop paths where the distance between the source and the destination is 40 m. Link error probabilities are SINR-based.

	Simulation		Numerical	
	$d_h = 40$ m,		Error={SINR model}	
Rank	Delay	Throughput	Delay	Throughput
1	SP	SP	SP	SP
2	MC	MP	MC	MP
3	NC	NC	NC	NC
4	MP	MC	MP	MC
5	G-NC	G-NC		

Table 2.13: Numerical vs simulation results. Asymmetric links in terms of error probability. Three paths assumed, with one hop each. SINR-based link error probabilities.

Concerning the extension of the analytical framework presented in Section 2.2.2, where link error probabilities are captured through the SINR model, delay and throughput results, for all forwarding schemes explored, are presented in Table 2.12, while throughput and delay trends are summarized in Table 2.13. The simulation setup is the same as the one discussed in Section 2.3, with the only difference that SINR threshold is assumed to be 1.0 and the transmission probability for different interfaces is also assumed 1.0. A transmission probability equal to one is employed, since in the extended version of the analytical framework, we assume that each node/interface transmits with a probability equal to 1.0, on each time slot.

Results presented in Table 2.13, concerning the rank, both in terms of delay and throughput, for the various forwarding schemes, show that the analytical framework, where link error probability is captured through the SINR model, captures in an exact manner the underlying trends. This is also due, to the match between the transmission probability assumed in the corresponding models and the simulation setup. Table 2.12 also shows that, for the case of SP and MP, the analytical framework also captures accurately, the delay and throughput observed in the simulation scenarios.

Part of our future work is to extended the analytical framework, by including transmission probability for each interface/node in the corresponding throughput and delay expressions. Some preliminary results concerning this part of the thesis have been published in [22, 23].

Chapter 3

Flow allocation on multiple paths for maximizing average aggregate flow throughput

3.1 Introduction

In this chapter, we consider random access, wireless mesh networks, with multi-packet reception capabilities. Further on, multiple flows are routed to their destinations through node-disjoint paths. The issue addressed in this part of the thesis is the following: allocation of flow on multiple paths that exhibit both intra- and inter-path interference, in order to maximize average aggregate flow throughput, while also providing bounded delay. A distributed flow rate allocation scheme is suggested, for maximizing the average aggregate flow throughput (AAT), while also providing bounded delay. For the purposes of the suggested scheme, flow rate allocation is formulated as an optimization problem. It also employs a simple model for the AAT that captures both intra- and inter-path interference through the SINR model.

The chapter is divided into two main parts based on how interference is handled. In the first part, interference is treated as noise while in the second part, *successive interference cancelation (SIC)* is employed. Both parts of this chapter are organized in the same way. First, the system model is presented, which is common for both parts. Then, for each part of this chapter, the corresponding analysis applied, is overviewd. What follows is a description of the simulation setup employed. Finally, an extensive presentation of the evaluation process is provided including both numerical and simulation results. Being more precise, for the first part of this chapter, where interference is treated as noise and comprises the largest part of this chapter, the evaluation process addresses the following issues: first, the accuracy of the suggested model for capturing the AAT observed in the simulation scenarios is explored. For this purpose, both illustrative and some random wireless scenarios are employed. Additionally, the proposed scheme is compared, in terms of throughput and delay, with the following flow allocation schemes: *Best Path* that optimally utilizes the best path available, *Full Multipath* that assigns the maximum possible flow (one packet per slot) on each path, and a scheme where different flows forward traffic through the paths employed on a round robin fashion. At the third part of the evaluation process, a variant of the suggested flow allocation scheme is considered, where interference is approximated by taking into account only the *dominant* interfering nodes for a link. For this variant, the accuracy of the model for capturing the AAT observed in the simulation scenarios is also explored. In the last part of the evaluation process, the proposed scheme is also compared in terms of flow delay (defined in a subsequent section) with the aforementioned flow allocation schemes.

3.2 System model

Static, wireless mesh networks are assumed, with the following properties:

- Random access to the shared medium, where each node transmits independently of all other nodes based on its transmission probability only, requiring no coordination among them. For flow originators, transmission probability denotes the rate at which they inject packets into the network (flow rate). For the relay nodes, transmission probability is fixed to a specific value and no control is assumed.
- Time is slotted and each packet transmission requires one timeslot.
- Flows among different pairs of source and destination nodes carry unicast traffic of same-sized packets.
- All nodes use the same channel and rate, and are equipped with multi-user detectors being thus, able to successfully decode packets from more than one transmitter at the same slot [51].
- We assume that all nodes are half-duplex and thus, cannot transmit and receive simultaneously.
- Additionally, all nodes always have packets available for transmission.
- As far as routing is concerned, multiple node disjoint paths are assumed to be available by the routing protocol, one for each flow. Moreover, source routing is assumed, ensuring that packets of the same flow are routed to the destination along the same path. Apart from that, for each node, its position, transmission probability, or flow rate, along with an indication of whether it is a flow originator, are assumed known to all other nodes. This information can be periodically propagated throughout the network through a link-state routing protocol. Implementation details concerning these assumptions are presented in Appendix A.

3.3 Interference treated as noise

This section presents the channel model, analysis, and the corresponding evaluation, of the proposed flow allocation scheme, for the case where interference is treated as noise.

3.3.1 Channel model

The channel model used in this part of the thesis, is the same one, as the one presented in Section 2.2.1.2 of the previous chapter and is also quoted here, for the convenience of the reader [47]. In the wireless environment, a packet can be decoded correctly by the receiver if the received SINR exceeds a certain threshold. Assume a set of nodes, denoted by $\mathcal{T}$, that are also active, during the same slot with node i. Let $\mathcal{P}_{rx}(i,j)$ be the signal power received from node i at node j. Treating interference from neighbouring links as noise, $\mathrm{SINR}(i,j)$ is then expressed through:

$$\mathrm{SINR}(i,j) = \frac{\mathcal{P}_{rx}(i,j)}{\eta_j + \sum_{k \in T \setminus \{i\}} \mathcal{P}_{rx}(k,j)}. \tag{3.1}$$

In the above equation, η_j denotes the receiver noise power at j. We assume that a packet transmitted by i, is successfully received by j, if and only if, $\mathrm{SINR}(i,j) \geq \gamma_j$, where γ_j is a threshold characteristic of node j. The wireless channel is subject to fading; let $\mathcal{P}_{tx}(i)$ be the transmitting power of node i and $r(i,j)$ be the distance between i and j. The power received by j, when i transmits, is $\mathcal{P}_{rx}(i,j) = \mathcal{A}(i,j)g(i,j)$, where $\mathcal{A}(i,j)$ is a random variable representing channel fading. Under Rayleigh fading, $\mathcal{A}(i,j)$ is exponentially distributed [48]. The received power factor $g(i,j)$ is given by $g(i,j) = P_{tx}(i)(r(i,j))^{-\alpha}$, where α is the path loss exponent with typical values between 2 and 4. The success probability of link (i,j), when the transmitting nodes are in $\mathcal{T}$, is given by

$$p^j_{i/T} = \exp\left(-\frac{\gamma_j \eta_j}{v(i,j)g(i,j)}\right) \prod_{k \in T \setminus \{i,j\}} \left(1 + \gamma_j \frac{v(k,j)g(k,j)}{v(i,j)g(i,j)}\right)^{-1}, \tag{3.2}$$

where $v(i,j)$ is the parameter of the Rayleigh random variable for fading. The analytical derivation for this success probability ,which captures the effect of interference on link (i,j) from transmissions of nodes in set $\mathcal{T}$, can be found in [49].

3.3.2 Analysis

In this section, we present how aggregate throughput optimal flow rate allocation is formulated as an optimization problem for random topologies.

The suggested method for formulating aggregate throughput optimal flow rate allocation as an optimization problem, for random topologies, is a procedure consisting of three steps. We demonstrate this procedure assuming multiple flows that are forwarded to the same destination. The same analysis however, can be applied for the case where multiple flows have different destination nodes. First, the notations used in the analysis are presented and are also summarized in Table 3.1. $\mathcal{V}$ denotes the set of the nodes and $|\mathcal{V}| = \mathrm{N}$. We assume m flows $f_1, f_2, ..., f_m$, that need to forward traffic to the destination node D. $\mathcal{R} = \{r_1, r_2, ..., r_m\}$ represents the set of m disjoint paths employed by these flows. $|r_i|$ is used to denote the number of links in path r_i. $\mathcal{I}_{i,j}$ is the set of nodes that cause interference to packets sent from *i* to *j*. For example, if all network nodes are assumed to contribute with interference to link (i,j) and $j \neq D$, then $\mathcal{I}_{i,j} = \mathcal{V} \setminus \{i,j,D\}$ and thus, the set of nodes that cause interference to that link, has size $\mathcal{L}_{i,j} = |\mathcal{I}_{i,j}| = |\mathcal{V}| - 3$. Further on, $Src(r_k)$ is used to denote the source node of the

Table 3.1: Notations.

Notation	Definition
$\mathcal{V}$	Set of nodes. $\lvert V\rvert = N$
q_i	Transmission probability for node i
$f_1, f_2, ..., f_m$	m flows
r_i	Path i employed by flow f_i
$\mathcal{R} = \{r_1, r_2, ..., r_m\}$	Set of node disjoint paths
$\lvert r_i\rvert$	Num of links in path r_i
$\mathcal{I}_{i,j}$	Interfering nodes for link (i,j)
$\mathcal{I}_{i,j}[n]$	Id of nth interfering node for link (i,j)
$\mathcal{L}_{i,j} = \lvert\mathcal{I}_{i,j}\rvert$	Number of nodes that interfere with transmissions on (i,j)
$Src(r_k)$	Source node of the k^{th} flow
$\mathcal{P}_{r_k} = \prod_{(i,j)\in r_k} p^j_{i/i}$	End-to-end success probability for path r_k
$\bar{\mathcal{T}}_{i,j}$	Average throughput for (i,j) (Pkts/slot)
$\bar{\mathcal{T}}_{r_k}$	Average throughput for k^{th} flow (Pkts/slot)

k^{th} flow, employing path r_k. $\bar{T}_{i,j}$ and $\bar{T}_{r_k}$ denote the average throughput, measured in packets per slot, achieved by link (i, j) and flow f_k forwarded over path r_k, respectively. Let also $\mathcal{I}_{i,j}[n]$ denote the id of the nth interfering node for link (i, j). For each node i, q_i, denotes its transmission probability, given that there is a packet available for transmission in its queue. As already discussed, for flow originators, it indicates the rate at which flow is injected on a path, while for relay nodes it is assumed fixed to a specific value. Finally, the *end-to-end success probability* for path r_k is expressed through $\mathcal{P}_{r_k} = \prod_{(i,j)\in r_k} p^j_{i/i}$.

The first step of the suggested method consists of deriving the expression for the average throughput of a specific link (i, j). Average throughput for that link, $\bar{\mathcal{T}}_{i,j}$, is expressed through the probability of a successful packet reception over that link and is denoted by (3.3). The step of expressing a link's average throughput is also clarified through a simple topology in Section 3.3.2.1.

$$\bar{\mathcal{T}}_{i,j} = \sum_{l=0}^{2^{\mathcal{L}_{i,j}}-1} \mathcal{P}_{i,j,l} q_{i,j} \prod_{n=1}^{\mathcal{L}_{i,j}} q^{b(l,n)}_{\mathcal{I}_{i,j}[n]} (1 - q_{\mathcal{I}_{i,j}[n]})^{1-b(l,n)}, \tag{3.3}$$

where

$$q_{i,j} = \begin{cases} q_i & j = D \\ q_i(1 - q_j) & j \neq D \end{cases},$$

$$\mathcal{P}_{i,j,l} = p^j_{i/i\cup\{I_{i,j}[n],\ \forall\ n:\ b(l,n)\neq 0)\}},$$

$$b(l, n) = l \ \&\ 2^{n-1},\ \ \&\ \text{is the logical bitwise AND operator.}$$

As also discussed above, node *i* is active during a slot, with probability q_i, given there is a packet available for transmission at its queue. Note that, transmission probability and position for every node can be propagated periodically to all other nodes through routing protocol's topology control messages. Position information is used to infer each link's success probability based on (3.2). As a flow's data rate is increased, the interference imposed on other links is also increased. Estimating thus a link's (i,j) average throughput, requires enumerating all possible subsets of active transmitters. The process of expressing a link's average throughput is also explained through an illustrative topology later in this section. Assuming that all nodes contribute with interference to transmissions over link (i,j) and a network with N nodes, all such subsets of interfering nodes for (i,j) are $2^{\mathcal{L}_{i,j}}$. For large networks, enumerating all subsets of active transmitters may be computationally intractable. In Section 3.3.3.1.3, we explore a variant of the suggested flow allocation scheme where only the *k* dominant interferers are taken into account for expressing the throughput of link (i,j). As also discussed in that section, dominant interferers for that link are considered those that contribute with the most significant amount of interference, on average, to packets received by *j*. In (3.3), l enumerates all possible subsets of active transmitters, while $b(l,n)$ becomes one if, the n^{th} node in $\mathcal{I}_{i,j}$ is assumed active in the l^{th} subset examined. For each such subset, indexed by l in the product term of (3.3), the corresponding success probability of link (i,j), given that this subset of nodes is active, is expressed through $\mathcal{P}_{i,j,l}$.

The average aggregate throughput achieved by all flows is expressed through: $\bar{\mathcal{T}}_{aggr} = \sum_{k=1}^{m} \bar{\mathcal{T}}_{r_k}$, where $\bar{\mathcal{T}}_{r_k} = \underset{(i,j)\in r_k}{min} \bar{\mathcal{T}}_{i,j}$. The second step of the suggested method consists of maximizing the average aggregate throughput, while also guaranteeing bounded packet delay, which results in non-smooth optimization problem P1:

$$\underset{\mathcal{S}}{\text{Maximize}} \sum_{k=1}^{m} \min_{(i,j)\in r_k} \bar{\mathcal{T}}_{i,j} \qquad (P1)$$

s.t:

$$(S1):\ 0 \le q_{Src(r_k)} \le 1,\ k = 1, ..., m$$

$$(S2):\ \bar{\mathcal{T}}_{Src(r_k),i} \le \bar{\mathcal{T}}_{j,l},$$
$$\{\forall i,j,k,l : (Src(r_k),i),\ (j,l) \in r_k, |r_k| > 1\},$$

where $\mathcal{S} = \{q_{Src(r_k)},\ k = 1, ..., m\}$. Constraint set *S1*, ensures that the maximum data rate for any flow does not exceed one packet per slot, while also allowing paths to remain un-utilized. Constraint *S2*, ensures that the flow injected on each path, that is the throughput of that path's first link, is limited by the flow that can be serviced by any subsequent link of that path. In this way, data packets are prevented from accumulating at the relay nodes, guaranteeing thus, bounded packet delay. For the rest of the chapter, this constraint will be referred to as *bounded delay constraint*. It should be noted that, the above optimization problem is a non-smooth one due to the *min* term present in the target function.

P1 can be transformed to the following smooth optimization problem:

$$\underset{\mathcal{S}'}{\text{Maximize}} \sum_{k=1}^{m} \begin{cases} \bar{\mathcal{T}}_{Src(r_k),D}, & |r_k| = 1 \\ q'_{Src(r_k)}, & |r_k| > 1 \end{cases} \qquad (P2)$$

$$\begin{aligned} & s.t.: \\ & \quad (S1): \ 0 \le q_{Src(r_k)} \le 1, \ k = 1, ..., m \\ & \quad (S2): \ \bar{\mathcal{T}}_{Src(r_k),i} \le \bar{T}_{j,l}, \\ & \qquad\qquad \{\forall i, j, k, l : (Src(r_k), i), \ (j, l) \in r_k, |r_k| > 1\} \\ & \quad (S3): \ 0 \le q'_{Src(r_k)} \le 1, \ \{\forall k : |r_k| > 1\} \\ & \quad (S4): \ q'_{Src(r_k)} \le \bar{\mathcal{T}}_{i,j}, \ \{\forall i, j, k : |r_k| > 1, \ (i, j) \in r_k\}, \end{aligned}$$

where $\mathcal{S}' = \{q_{Src(r_k)}, \ k = 1, ..., m\} \cup \{q'_{src(r_k)} : \ |r_k| > 1\}$. For the rest of the chapter, we will refer to optimization problem P2 above, as the *flow allocation optimization problem*.

Based on the above optimization problem, a scheme that calculates on a distributed manner the flow that should be assigned on each path, in order to maximize AAT, can be implemented as follows: assume that each node periodically announces the following information to all other nodes through routing protocol's control messages: a)position, b)transmission probability, and c)an indication of whether it is a flow originator. In case where a node is a flow originator, (c) can carry information about the destination node of the corresponding flow. Using (c), each flow originator can infer, both relay nodes and other flow originators, along with the destination node to which they need to forward traffic. Position information can be used to infer each node's position, along with distance for each pair of nodes. In this way, success probability for each link can be calculated based on (3.2). Apart from that, based on received position information, for all other nodes, each node is able to infer its own view of the topology. If node position, along with flow source and destination node pairs information, is available to all flow sources, then the inferred topology can be searched for a set of multiple node disjoint paths. An example of such an approach, based on the Dijkstra algorithm, is presented in Appendix A. Having the multiple paths (denoted by $r_1, r_2, ..., r_m$ above) available, along with transmission probability for each relay node, each flow source formulates its own instance of the flow allocation optimization problem and thus, estimates the flow rate that it should assign on the path employed, without any further coordination with other flow sources. In this way, flow rates are estimated on a distributed manner, given the information propagated by routing protocol's control messages. Finally, in order to ensure that packets of the same flow are indeed forwarded to the destination through the inferred path, source routing needs to be adopted. Such a scheme, that is based on above flow the allocation optimization problem, will be referred to as *Throughput Optimal Flow Rate Allocation (TOFRA)* scheme, for the rest of the chapter. Note also that, for a given traffic scenario (set of flows), the term *TOFRA AAT* will be used to denote the average aggregate throughput achieved by all flows, when the flow rate injected on each path employed, is determined by solving a scenario-specific instance of the corresponding flow allocation optimization problem.

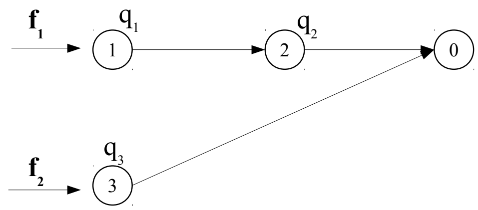

Figure 3.1: Illustrative topology.

3.3.2.1 Demonstration through a simple topology

In this section, the formulation of the flow allocation optimization problem, is demonstrated through the simple topology presented in Fig. 3.1. Two flows namely, f_1 and f_2, originating from nodes, 1 and 3, are forwarded to destination node 0 through paths r_1: $1 \rightarrow 2 \rightarrow 0$ and r_2: $3 \rightarrow 0$, respectively. We further assume that, transmissions on a specific link cause interference to all other links. Before presenting each link's average throughput, consider link $(2, 0)$ as an example. Transmitters that cause interference to packets sent from 2 to 0, constitute set $\mathcal{I}_{2,0} = \{1, 3\}$ and thus, $\mathcal{L}_{2,0} = 2$. There are three possible subsets of nodes that may cause interference on link $(2, 0) : \{1\}, \{3\}, \{1, 3\}$. When $l = 3$ in (3.3), it enumerates the third subset of interfering nodes, with $b(l, n)$ becoming one, for both $n = 1$ and $n = 2$.

The average throughput per link is presented in (3.4a)-(3.4c).

$$\bar{\mathcal{T}}_{1,2} = q_1(1-q_2)(1-q_3)p^2_{1/1} + q_1(1-q_2)q_3p^2_{1/1,3}, \tag{3.4a}$$

$$\begin{aligned}\bar{\mathcal{T}}_{2,0} &= q_2(1-q_1)(1-q_3)p^0_{2/2} + q_2q_1(1-q_3)p^0_{2/2,1} \\ &\quad + q_2(1-q_1)q_3p^0_{2/2,3} + q_2q_1q_3p^0_{2/1,2,3},\end{aligned} \tag{3.4b}$$

$$\begin{aligned}\bar{\mathcal{T}}_{3,0} &= q_3(1-q_1)(1-q_2)p^0_{3/3} + q_3q_1(1-q_2)p^0_{3/1,3} \\ &\quad + q_3(1-q_1)q_2p^0_{3/2,3} + q_3q_1q_2p^0_{3/1,2,3}.\end{aligned} \tag{3.4c}$$

Recall that, q_1 and q_3, denote the data rates for flows f_1 and f_2, respectively. Aggregate average throughput (AAT) achieved by all flows, can be expressed through (3.5).

$$\begin{aligned}&\bar{\mathcal{T}}_{aggr} = \bar{\mathcal{T}}_{r_1} + \bar{\mathcal{T}}_{r_2}, \quad where, \\ &\bar{\mathcal{T}}_{r_1} = \min\{\bar{\mathcal{T}}_{1,2}, \bar{\mathcal{T}}_{2,0}\}, \quad \bar{\mathcal{T}}_{r_2} = \bar{\mathcal{T}}_{3,0}\end{aligned} \tag{3.5}$$

Average aggregate throughput optimal flow rate allocation, consists of identifying rates, q_1 and q_3, that maximize AAT, while also guaranteeing bounded packet delay. These rates can be found by solving the following optimization problem:

$$
\begin{aligned}
\underset{q_1, q_3}{\text{Maximize}} \quad & \bar{\mathcal{T}}_{30} + min\{\bar{\mathcal{T}}_{12}, \bar{\mathcal{T}}_{20}\} \\
\text{subject to} \quad & 0 \leq q_i \leq 1,\ i \in \{1,3\} \quad (g1)-(g4) \\
& \bar{\mathcal{T}}_{12} \leq \bar{\mathcal{T}}_{20} \qquad\qquad\quad (g5)
\end{aligned}
$$

Constraint (g5), in the above optimization problem, constitutes the bounded delay constraint for path r_1. According to third step of the process presented in the previous subsection, the above non-smooth optimization problem can be transformed to the following smooth optimization problem:

$$
\begin{aligned}
\underset{q_1^{'}, q_1, q_3}{\text{Maximize}} \quad & \bar{\mathcal{T}}_{30} + q_1^{'} \\
\text{subject to} \quad & 0 \leq q_i \leq 1,\ i \in \{1,3\} & (g1)-(g4) \\
& \bar{\mathcal{T}}_{12} \leq \bar{\mathcal{T}}_{20}, & (g5) \\
& q_1^{'} \leq \bar{\mathcal{T}}_{12}, & (g6) \qquad (P3) \\
& q_1^{'} \leq \bar{\mathcal{T}}_{20}, & (g7) \\
& 0 \leq q_1^{'} \leq 1 & (g8)-(g9)
\end{aligned}
$$

As far as the type of the above optimization problem is concerned, it is first transformed to the standard form. In order to be convex, both the objective function and all functions related to the inequality constraints must be convex functions. By exploring the second order conditions for convexity, the Hessian of each such function must be positive semi-definite. Consider constraint (g5) in the above optimization problem as an example. $g_5(\vec{q}) = \bar{\mathcal{T}}_{12} - \bar{\mathcal{T}}_{20}$, where $\vec{q} = (q_1, q_3, q_1^{'})$, and $H(g_5(\vec{q})) = \begin{bmatrix} d^2 g_5/d^2_{q_1} & d^2 g_5/(d_{q_1} d_{q_3}) & d^2 g_5/(d_{q_1} d_{q_1^{'}}) \\ ... & ... & ... \\ ... & .. & d^2 g_5/d^2_{q_1^{'}} \end{bmatrix}$

Assuming a vector $\vec{x} = (a, b, c)$ of real non-zero elements, $\vec{x} H(g(\vec{q})) \vec{x}^T = 2abk$, where $k = -p^2_{1/1}(1 - q_2) + p^2_{1/1,3}(1 - q_2) - p^0_{2/2} q_2 + p^0_{2/1,2} q_2 + p_2$. Since, a and b, have real non-zero values, $2abk$ can be < 0 and thus, function $g_5(\vec{q})$ is not convex. Consequently, the above optimization problem is not convex.

3.3.3 Evaluation

The evaluation process consists of two main parts. The first one, presented in Section 3.3.3.1, focuses on the evaluation of the proposed flow allocation scheme and employs some indicative scenarios, along with several random ones, for that purpose. In the second part of the evaluation process, presented in Section 3.3.3.2, the technique of simulated annealing for solving the corresponding flow allocation optimization problem is evaluated. The evaluation consists of exploring the accuracy with which simulated annealing approaches the global maximum and also the time required to identify it.

Parameter	Value
d	400 m
Relay transmission probability	0.5
Path Loss Exponent	3.0
Transmit Power	0.1 W
Noise power	7×10^{-11} W

Table 3.2: Network parameters for the scenario based on topology of Fig. 3.1.

3.3.3.1 Flow allocation scheme evaluation

3.3.3.1.1 Motivating scenarios for the proposed flow allocation scheme. Before presenting simulation results, for a grid topology and some random wireless scenarios, we further motivate flow rate allocation on multiple paths, using numerical results derived from two simple wireless scenarios with different values for certain network parameters.

The first scenario explored, is based on the topology depicted in Fig 3.1. Let $d(i, j)$ denote the distance between nodes i and j. Network parameters for this scenario are summarized in Table 3.2.

For the illustrative purpose of this section, we assume that $d(1, 2) = d(2, 0) = d(3, 1) = d$, $d(3, 0) = \sqrt{5}d$, $d(3, 2) = \sqrt{2}d$. Further on, the path loss exponent assumed is 3, while transmission probability for relay node 2, is 0.5. It should also be noted that, for the numerical results derived in this section, interference is treated as noise. Flow rates, q_1 and q_3, that achieve maximum average aggregate throughput (AAT), for SINR threshold values $\gamma = \{0.25, 0.5, ..., 2\}$, are estimated by solving the optimization problem (P3), using the simulated annealing technique. Note also that, multi-hop path $r_1 : 1 \rightarrow 2 \rightarrow 0$ exhibits higher end-to-end success probability than path $r_2 : 3 \rightarrow 0$, for all γ values considered (end-to-end success probability is defined in Section 3.3.2 of this chapter).

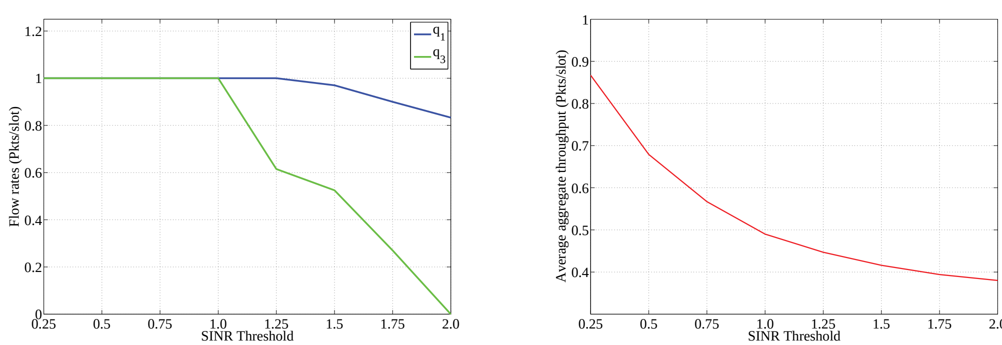

(a) Flow rates

(b) AAT

Figure 3.2: Flow rates assigned on each path and average aggregate throughput (AAT) for the simple topology in Fig. 3.1.

Parameter	Value
d	200 m
Path loss expon	3.0
Relay tx prob	0.5
Noise power	1x10^{-12} w
Tx power	0.01 w
SINR thres	γ

	γ=1.0	γ=5.0
q0	0.636	0.560

	γ=1.0	γ=5.0
q5	0.909	0.0

	γ=1.0	γ=5.0
q9	1.0	0.692

	γ=1.0	γ=5.0
q12	0.725	0.0

	γ=1.0	γ=5.0
q17	1.0	0.689

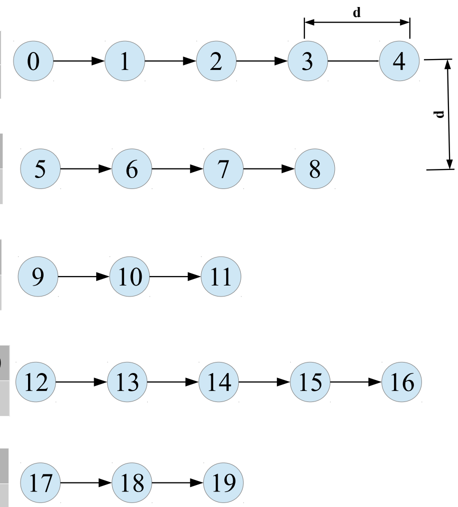

Figure 3.3: Flow assignment for different γ values for a grid-based scenario.

Fig. 3.2(a), presents the flow rates assigned on paths, r_1 and r_2, that maximize AAT, for the topology depicted in Fig. 3.1 and $\gamma = \{0.25, 0.5, ..., 2\}$. Fig. 3.2(b), presents the corresponding AAT achieved, by each pair of flow rates depicted in Fig. 3.2(a). As these figures show, the maximum AAT is achieved by full rate utilization of both paths, for SINR threshold values up to 1.0, suggesting that, inter-flow interference is balanced by the gain in throughput. For SINR threshold values larger than 1.0, utilization of path r_2, which exhibits lower end-to-end success probability, declines. This is due to the fact that, for large SINR threshold values, the effect of interference imposed on path r_1, becomes more significant. Moreover, for γ values larger than 1.0, the multi-packet reception capability at destination node 0 declines. At the same time, flow forwarded through path r_2, manages to deliver only a small portion of its traffic to destination node 0.

The second motivating scenario, along with the corresponding values for specific network parameters, are summarized in Fig. 3.3. The scenario presented in this figure, is based on a grid-like topology, where five flows originate from nodes 0, 5, 9, 12, and 17, respectively, and are forwarded to destination nodes 4, 8, 11, 16, and 19. Flow rates, q_0, q_5, q_9, q_{12}, and q_{17}, are derived by solving a topology specific instance of the flow allocation optimization problem (P2) presented in Section 3.3.2, for two different γ values, using the simulated annealing technique. The flow rate assigned on each path, for each γ value considered, are also presented in Fig. 3.3.

As this figure shows, for $\gamma = 1.0$, all paths are utilized at a high rate, despite the significant amount of both-intra and inter-path interference. This is even more prominent for paths lying in the middle of the topology, such as, the ones sourced at nodes 5, 9, and 12, which are expected to experience the largest amount of inter-path interference. The reason for such a high path utilization is that, when a γ value, as low as 1.0 is used, receiving nodes are more

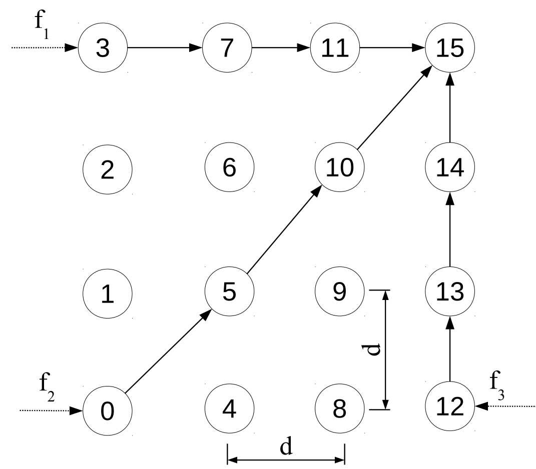

Figure 3.4: Grid-based network topology.

tolerant to interference. In such a case, higher average throughput is achieved over a link when more flow is assigned on it. More on that, as Fig. 3.3 also shows, when all receivers employ a higher SINR threshold value (e.g. equal to 5.0), the suggested flow allocation scheme employs the paths that exhibit the highest topological separation in terms of distance. Paths sourced at nodes 5 and 12 for example, are assigned zero flow (zero packets per slot). Considering again the case of $\gamma = 1.0$, Fig. 3.3 shows that paths with a larger number of hops are assigned lower flow when compared to shorter ones. This is due to the fact that the average throughput achieved over a path is limited by the average throughput of the bottleneck link along it.

3.3.3.1.2 Grid Scenario. After demonstrating the proposed flow allocation scheme through two motivating scenarios, the evaluation process, which employs both numerical and simulation results, is presented. The evaluation process explores four issues. The first one, is the accuracy of the model employed by the proposed scheme, for capturing the average aggregate flow throughput (AAT) observed in the simulated scenarios. For that reason, a grid-based scenario, along with several random ones, are employed. Secondly, the proposed scheme is compared, both in terms of AAT and flow delay (defined on a subsequent paragraph), with other simple flow allocation schemes. On the third part of the evaluation process, a variant of the proposed flow allocation scheme is explored where interference is approximated by considering only the *dominant* interfering nodes for a specific link. Finally the variance of the AAT observed in the simulated scenarios is addressed for the case of the suggested scheme (TOFRA).

As a first step, towards evaluating the accuracy of the model employed for capturing the AAT observed in the simulated results, the grid topology depicted in Fig. 3.4 is considered. Both vertical and horizontal distance (d), for all pairs of nodes d, is set to 100 m. Two traffic scenarios are explored, also depicted in Fig. 3.4. In the first scenario, two flows f_1 and f_2,

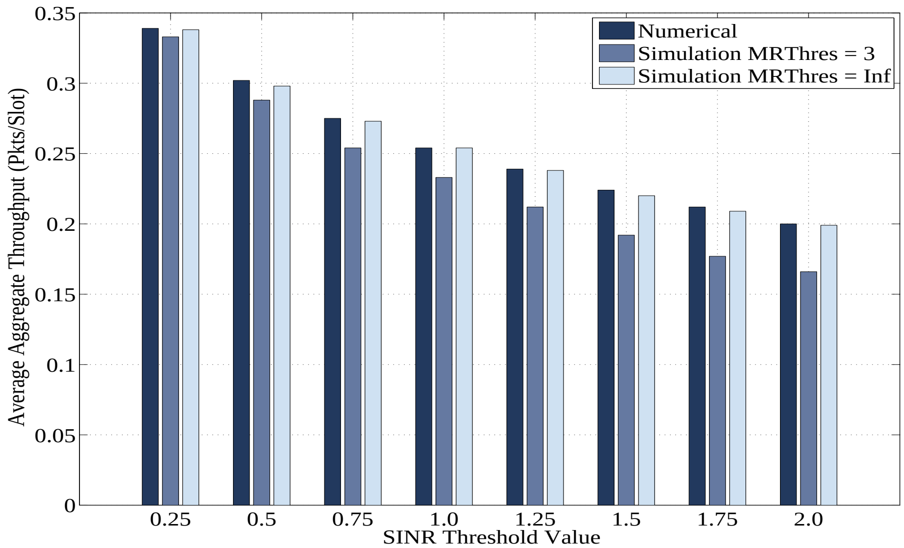

Figure 3.5: TOFRA AAT: Numerical vs. simulation results for the two flows grid-based scenario. Two TOFRA variants simulated based on maximum retransmit threshold (MRThres) value.

originated at nodes 3 and 0, respectively, are routed to destination node 15 through paths r_1: $3 \rightarrow 7 \rightarrow 11 \rightarrow 15$ and r_2: $0 \rightarrow 5 \rightarrow 10 \rightarrow 15$. In the second scenario, a third flow f_3 is also considered and it is routed through path r_3: $12 \rightarrow 13 \rightarrow 14 \rightarrow 15$. The effect of interference on success probability and thus, on throughput is captured by considering different values of the SINR threshold (γ). A low γ value indicates high tolerance to interference, while a large value would suggest low interference tolerance and thus, higher packet error probability. Flow rates, $\{q_0, q_3\}$, and $\{q_0, q_3, q_{12}\}$, for the two and three flows scenarios, respectively, are derived by solving a topology specific instance of the flow allocation optimization problem presented in Section 3.3.2 using the simulated annealing technique.

Figs. 3.5 and 3.6, compare numerical with simulation results concerning AAT, for γ values $\{0.25, 0.5, ..., 2.0\}$, and the two aforementioned traffic scenarios. Simulation results for the AAT, are derived by assigning on each path, the flow determined by the flow allocation optimization problem and calculating average aggregate throughput for all flows. For each traffic scenario and different γ value, two different variants of the proposed scheme are simulated. In the first one, the maximum retransmit threshold is 3.0, while in the second one it is infinite (as also shown in Table 3.3), suggesting that a packet is not dropped from a queue, after a specific number of failed retransmissions. Simulation results are derived using the Ns2 simulator with the modules and modifications presented in Appendix A. Values for certain Ns2 cross layer parameters are presented in Table 3.3. Moreover, all nodes share the same channel, transmission rate and γ value. Flow sources generate constant bit rate UDP flows. Queues for all nodes are kept backlogged for the whole simulation period using the modification presented

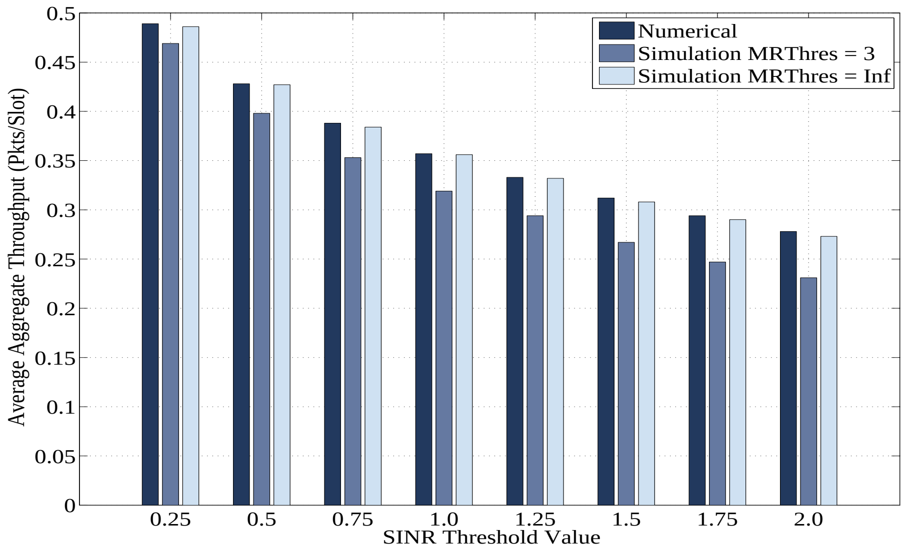

Figure 3.6: TOFRA AAT: Numerical vs. simulation results for the three flows grid-based scenario. Two TOFRA variants simulated based on maximum retransmit threshold (MRThres) value.

in Section A.3 of Appendix A.

As these figures show, for all γ values considered and a maximum retransmit threshold equal to 3.0, the model employed by the proposed flow allocation scheme, overestimates the AAT observed in the simulated scenarios. Moreover, this overestimation is more prominent when a larger γ value is employed. The average deviation over all γ values employed, between the AAT derived by our analysis and the simulated one, is 11.6% and 12.8%, for the two and three flows scenarios, respectively. The main reason for this overestimation is that, when a packet is dropped after three consecutive failed transmissions, and no other packet is available at the transmitting node's queue, a *dummy* packet (also discussed in Appendix A) is inserted in its queue. This is due to the assumption in the analysis, that there is always a packet available for transmission at each node's queue. However, dummy packets are not taken into account in AAT estimation. In the analysis presented in Section 3.3.2 however, the probability of a packet being dropped due to having reached the maximum retransmit threshold is disregarded. More on that, the probability of a packet being dropped due to reaching the maximum retransmit threshold, becomes more probable when a larger γ value is employed. Larger γ values imply lower link success probabilities. Another reason for the overestimation of the AAT, observed in the simulated scenarios, by the model considered, is the following: in the analysis, we have assumed that whenever a packet is transmitted, it is a packet carrying data. In the simulated scenarios however, all nodes, either perform periodic emission of routing protocol's control messages, or forwarded specific received control packets (topology control messages for the simulation setup presented in Appendix A). This means that some slots are spent carrying

Parameter	Value
Max Retransmit Threshold	3 or Inf
Contention Window	5
Path Loss Exponent	4.0
Transmit Power	0.1 W
Simulation Time	20.000 slots

Table 3.3: Network parameters for the scenario based on the grid-based topology of Fig. 3.4.

routing protocol's control messages, instead of data packets, resulting in our analysis overestimating the AAT observed in the simulated results. The second reason for AAT overestimation though, is less important due to the large intervals over which control packets are generated and the small number of nodes participating in the multipath set. Fig. 3.5 and 3.6 also show that, when an infinite value is assumed for the maximum retransmit threshold in the simulated scenarios, numerical and simulation results are very close. More precisely, the average deviation, over all γ values, between the AAT derived by our analysis and the simulated one, is, 0.82% and 0.87%, for the two traffic scenarios (two and three flows respectively).

It is also interesting to observe the data rates assigned to each path. In the three flows scenario, flow f_2 is the one that experiences the most significant inter-path (or inter-flow) interference due to transmissions from flows f_1 and f_3. Inter-path interference between flows f_1 and f_3 is mitigated by the topological separation of the paths utilized. Using a γ value equal to 0.5 for example, flows f_1 and f_3 are both assigned a data rate of 0.284 packets per slot while f_2 a rate of 0.187 packets per slot. This shows that, the proposed scheme *prefers* paths that are topologically separated and thus, experience low inter-path interference.

3.3.3.1.3 Random Wireless Scenarios. In this section, the proposed flow allocation scheme is evaluated, using Ns2 simulations for random wireless scenarios. The evaluation process presented in this section, consists of four parts. In the first one, the accuracy of the model employed by the flow allocation scheme discussed in Section 3.3.2, for capturing the average aggregate flow throughput (AAT), is explored. In the second part, the suggested flow allocation scheme (TOFRA) is compared with other flow allocation schemes, in terms of AAT. In the third part of this section, we explore the trade-off between accurately capturing the AAT observed in the simulation scenarios and the complexity in expressing a link's average throughput. More precisely, the interference experienced by the a link is approximated by considering only the dominant interfering nodes. In the last part of this section, TOFRA along with the other flow allocation schemes discussed are evaluated in terms of average flow delay (defined in the end of the section).

For the purposes of the evaluation process, 50 nodes are uniformly distributed over an area of 500 m x 500 m. Ten different traffic scenarios are generated as follows: for each scenario, a random number of flows (with a maximum number of ten flows allowed) is generated. For each flow, a source and destination node are randomly selected among the available nodes, without allowing two flows to share the same source, or destination. The number of flows

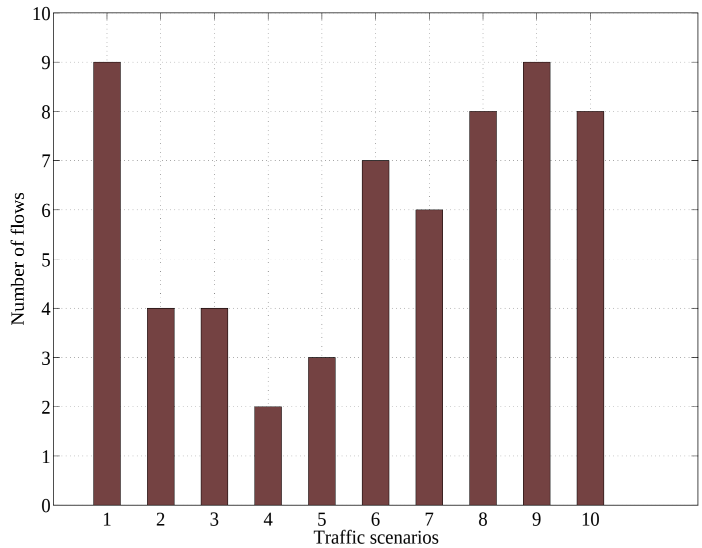

Figure 3.7: Number of flows per traffic scenario.

per scenario is summarized in Fig. 3.7. Multiple, node disjoint paths are identified for these flows, based on the process described in Appendix A. The returned multipath set is post-processed, allowing from one up to five link-hops per path and is listed for each traffic scenario in Appendix A. The topology based on which, random traffic scenarios are generated, along with two indicative such scenarios, are presented in Fig. 3.8. As part of the evaluation process, the proposed scheme is compared both in terms of AAT and flow delay (defined later), with the following simple flow allocation schemes: a) *Full MultiPath (FMP)*, b) Best path BP$_{e2e}$, and c) *Round-robin (RR)* based flow allocation. FMP, assigns one packet per slot on each path, while RR utilizes paths on an iterative manner. On each time slot, a new packet is injected on a different path. Finally, BP$_{e2e}$ employs only a single path, from all the available ones, to forward traffic, and the path selected is the one exhibiting the highest end-to-end success probability. As also discussed in Section 3.3.2, end-to-end success probability for a path r_k is expressed through: $\mathcal{P}_{r_k} = \prod_{(i,j)\in r_k} p^j_{i/i}$. The flow assigned on this path is determined by solving a scenario-specific, single path version, of the flow allocation optimization problem formulated in the aforementioned section.

The effect of interference on success probability is captured by considering different SINR threshold (γ) values. It should be noted that, the higher the SINR threshold, the higher the received SINR should be, in order to have a successful packet reception and thus, the lower the interference that should be experienced by a link. Consequently, high γ values indicate low tolerance to interference. The γ values employed, for the rest of the evaluation process, are 0.5, 1.0, 1.5, and 2.0.

Different simulation scenarios are generated as follows: for each traffic scenario and each γ value considered, all aforementioned flow allocation schemes are employed. Consider sce-

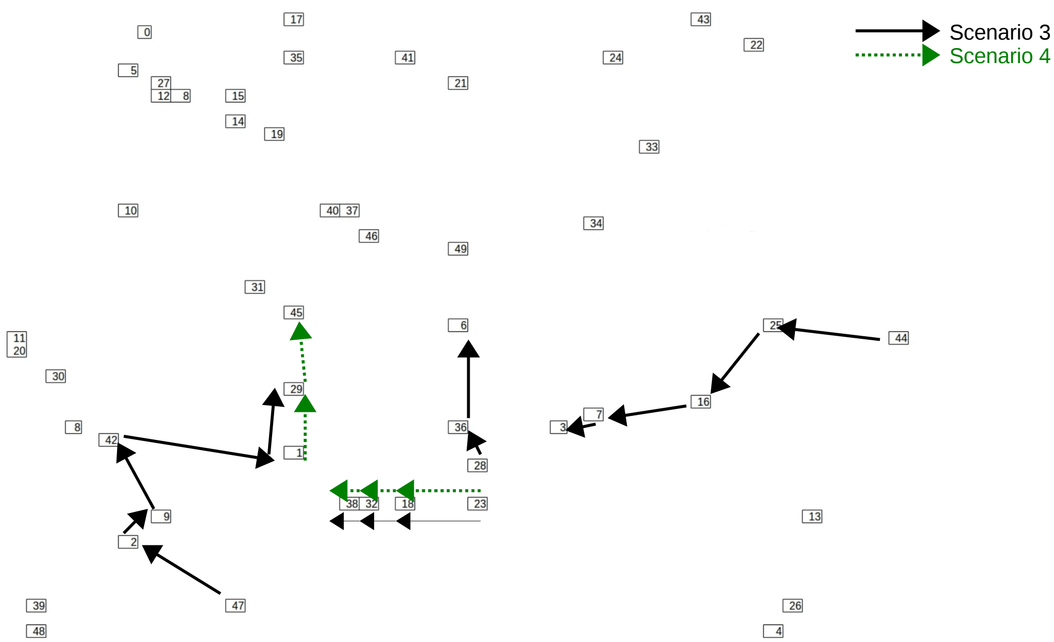

Figure 3.8: Network topology and two indicative traffic scenarios.

Parameter	Value
Max Retransmit Threshold	3 (simulated results)
Contention Window	5
Path Loss Exponent	4.0
Transmit Power	0.1 W
Noise Power	1×7^{-11} W
Packet size	1500 bytes
Traffic type	UDP
Simulation Time	20.000 slots

Table 3.4: Network and simulation parameters for the random traffic scenarios based on Fig. 3.8.

nario 4, depicted in Fig. 3.8, for example, and assume $\gamma = 1.0$. Four different simulation scenarios are generated based on it. In the first one, the proposed flow allocation scheme (TOFRA) is applied for determining the flow to be assigned on each path. In the second one, FMP is employed, which assigns one packet per slot on both paths, presented in the corresponding traffic scenario. In the third simulation scenario, the two paths, sourced at nodes 1 and 23, are utilized on an iterative manner. Finally, in the fourth simulation scenario, BP$_{e2e}$ utilizes only one path, the one exhibiting the highest end-to-end success probability, which is $23 \rightarrow 18 \rightarrow 32 \rightarrow 38$, for this scenario. It should also be noted that, for the case of TOFRA and BP$_{e2e}$, the flow assigned on the paths employed, is derived by solving a scenario-specific instance of the flow allocation optimization problem, using simulated annealing. Each simulation scenario thus, is a tuple composed from three things: a)traffic scenario: $\{1, 2, ..., 10\}$, b)γ value: $\{0.5, ..., 2.0\}$, and c)flow allocation scheme: $\{$ TOFRA, FMP, RR, BP$_{e2e}$ $\}$. The Ns2 simulation setup used in the evaluation process, is described in detail in Appendix A. Values for certain network parameters, used in the simulations and also in the analysis, in order to derive numerical results, are presented in Table 3.4. Note that, the maximum retransmit threshold is set to 3 for the simulated results only. In the analysis however, the effect of this threshold was disregarded, implying that a packet is not dropped after exceeding a predefined number of failed retransmissions. As also discussed in Section 3.3.3.1.2, this difference in the maximum retransmit threshold used in the simulated scenarios and the one assumed in the analysis, is one source of deviation between simulated and numerical results concerning average aggregate flow throughput (AAT).

In the first part of the evaluation process, the accuracy of the model employed by the suggested flow allocation scheme, for capturing the AAT observed in the simulated scenarios is explored. Two variants of the proposed flow allocation scheme are simulated. In the first one, queues of all the relay nodes, are kept backlogged, for the whole simulation period. As also discussed in the simulation setup in Appendix A, if a queue is found empty during a slot, a dummy packet is inserted in that queue. Dummy packet transmissions are taken into account while inferring active transmitters, for estimating the received SINR on a link. However, they are not taken into account for AAT calculation. In Figs. 3.9-3.12, this variant is labelled as

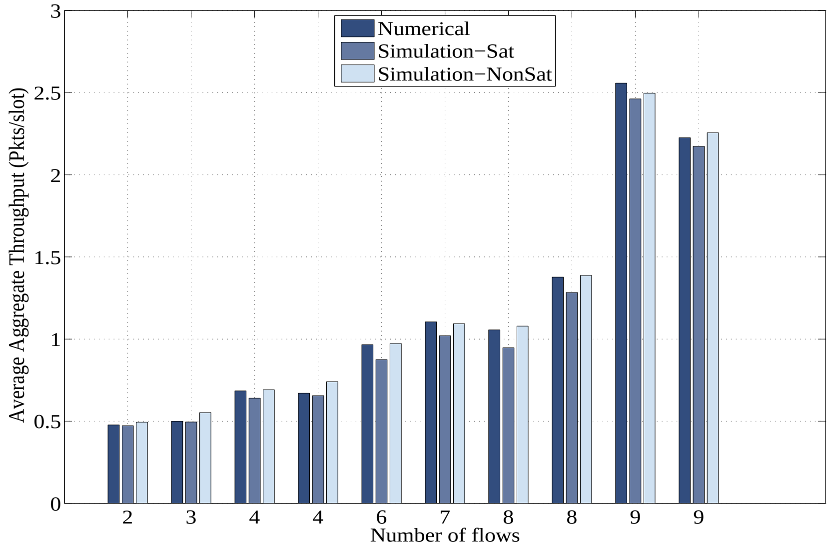

Figure 3.9: TOFRA AAT: Numerical vs. simulation results for $\gamma = 0.5$. Simulation results for two TOFRA variants one with saturated queues (Simulation-Sat) and one with non saturated queues (Simulation-NonSat).

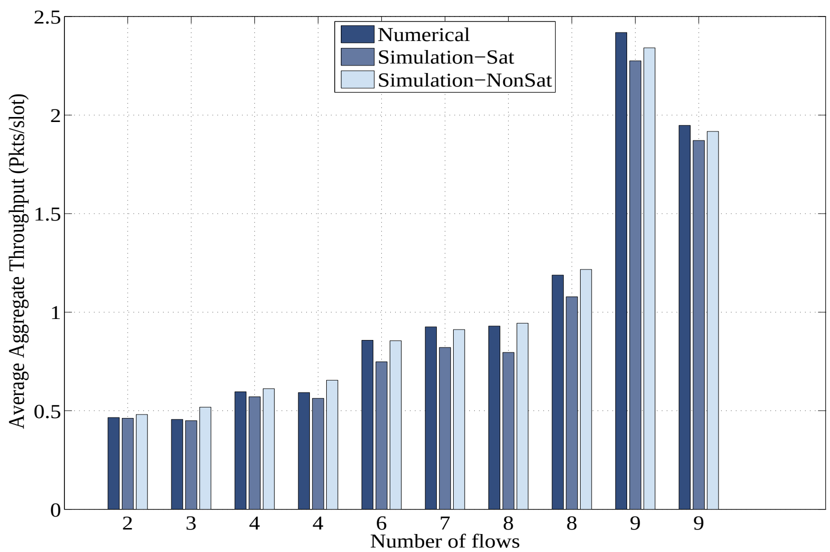

Figure 3.10: TOFRA AAT: Numerical vs. simulation results for $\gamma = 1.0$. Simulation results for two TOFRA variants one with saturated queues (Simulation-Sat) and one with non saturated queues (Simulation-NonSat).

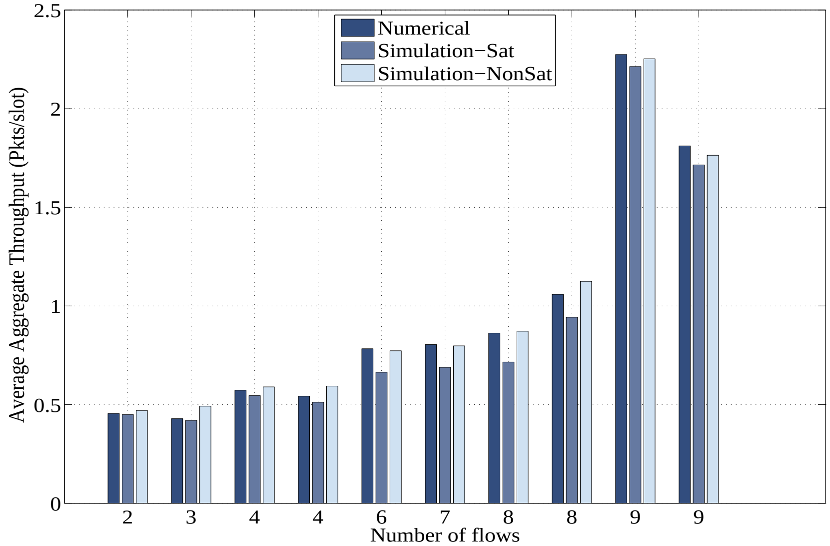

Figure 3.11: TOFRA AAT: Numerical vs. simulation results for $\gamma = 1.5$. Simulation results for two TOFRA variants one with saturated queues (Simulation-Sat) and one with non saturated queues (Simulation-NonSat).

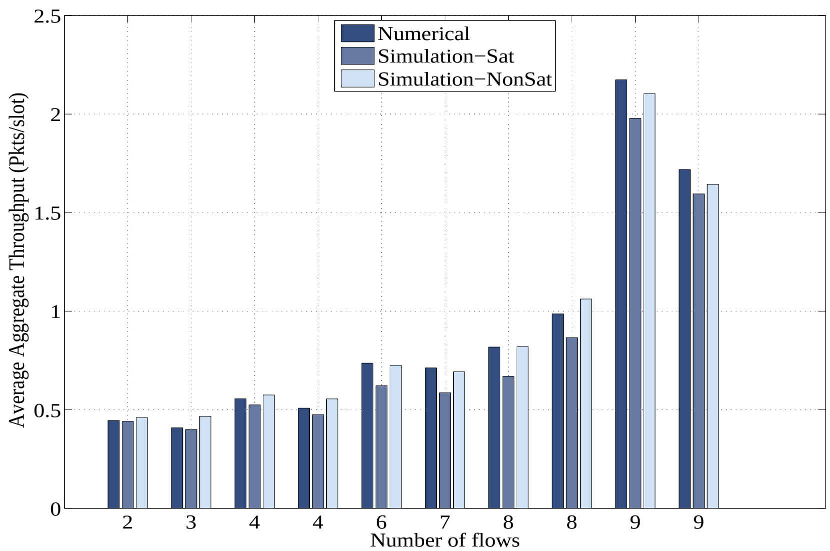

Figure 3.12: TOFRA AAT: Numerical vs. simulation results for $\gamma = 2.0$. Simulation results for two TOFRA variants one with saturated queues (Simulation-Sat) and one with non saturated queues (Simulation-NonSat).

Simulation-Sat. The main purpose of this variant is, to explore whether the suggested mode for AAT, accurately captures MAC-layer interplay and the effect of interference on AAT. For the second TOFRA variant simulated, the assumption for saturated relay queues is removed. All simulation scenarios are replayed, allowing the queue of relay nodes, to have no packets available for transmission during a specific slot. In the aforementioned figures, this variant is labelled as *Simulation-NonSat*. It should also be noted that, for both variants, sources of traffic are backlogged for the whole simulation period.

Figures 3.9 to 3.12, compare analytical with simulation results, concerning average aggregate throughput (AAT), for SINR threshold values 0.5, 1.0, 1.5, and 2.0, and the ten different wireless scenarios explored. Simulated results for both TOFRA variants are presented. For the case of the TOFRA variant, where queues for relay nodes are kept backlogged for the whole simulation period, the average deviation over all simulated scenarios, between the analytical and simulation results, is 5.5%, 7.6%, 9.0%, and 10.9%, respectively, for the four SINR threshold values considered. In all the scenarios and for all the γ values considered, the model employed by the TOFRA scheme overestimates the AAT observed in the simulation results. The reasons for this overestimation were also discussed in Section 3.3.3.1.2. The first one, is related to the maximum retransmit threshold. In the analysis employed, its effect is disregarded and thus, no packet is dropped after exceeding a certain number of failed retransmissions. In the simulated results however, it is set to 3.0, which means that a packet that is unsuccessfully transmitted for three times, it will be dropped. If there is no other packet available in the transmitter's queue, a dummy packet will be inserted (in case where TOFRA is simulated with the saturated queues assumption) instead. Dummy packets however, are not taken into account for AAT calculation. More on the effect of maximum retransmit threshold on TOFRA's AAT, consider scenario, 8 with $\gamma = 1.0$, as an example. Simulated AAT for the proposed scheme, when queues are saturated and the maximum retransmit threshold is 3, is 16.6% lower than the corresponding numerical value. When the corresponding simulation scenario is replayed with an infinite value for the maximum retransmit threshold, the corresponding deviation between numerical and simulated AAT drops to 1.9%. The second reason, for the overestimation of the AAT observed in the simulated scenarios is the following: in the analysis, it is assumed that whenever a packet is transmitted it is a packet carrying data. In the simulated scenarios however, all nodes either perform periodic emission of routing protocol's control messages, or forward received control packets (topology control messages for the simulation setup presented in Appendix A). This means that, specific slots are spent carrying routing protocol's control messages, instead of data packets, resulting in our analysis overestimating the AAT observed in the simulated results. The second reason for AAT overestimation though, is less important due to the large intervals over which control packets are generated and the small number of nodes participating in the multipath set.

Figs. 3.9-3.12, also compare the AAT estimated by the model employed and the simulated one when the assumption of saturated queues at the relays is removed. There are three reasons that shape the gap between the analytical and the simulated AAT for TOFRA, when queues are not saturated, with all three reasons stemming from analysis' assumptions. The first two reasons were described in the previous section and result in our analysis overestimating the AAT observed in the simulated results. The third reason has an opposite effect on AAT and is

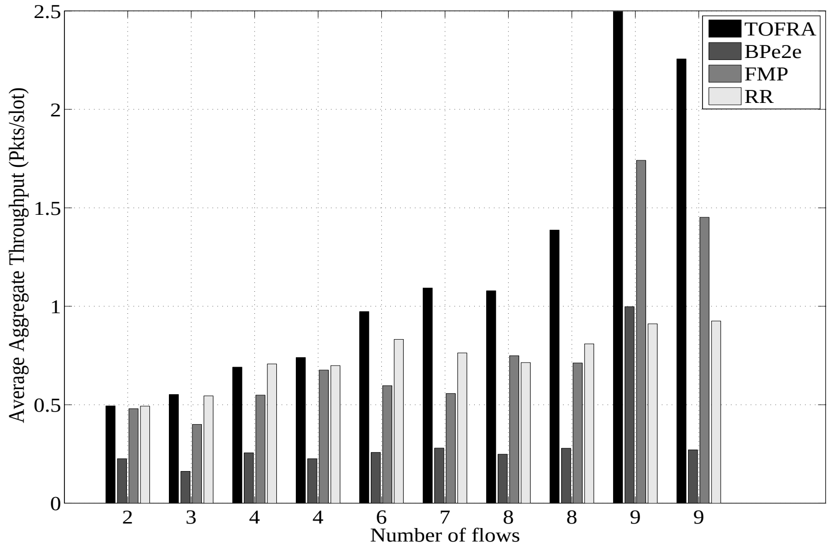

Figure 3.13: Simulation results [$\gamma = 0.5$]: AAT for TOFRA, FMP, BP$_{e2e}$, and RR.

related to the saturated queues assumption present in the analysis. According to this assumption, whenever a relay node attempts to transmit a packet there is always one available for transmission in its queue. In the simulated scenarios however, this is not always the case. As a result, the actual interference experienced by transmissions along a link, is lower than the one assumed in the analysis and thus, the actual average throughput for a link may be higher than the one calculated by the analysis applied. The effect of this is that, the model employed may underestimate the average throughput of a specific links and thus, may underestimate the AAT. For each γ value employed, the average deviation between numerical and simulated results, concerning AAT, is estimated over all ten traffic scenarios explored. The corresponding average deviation values are 3.1%, 3.7%, 4.0%, and 4.7%, respectively, for $\gamma = 0.5, 1.0, 1.5, 2.0$. Note that, for each traffic scenario, the absolute value of the deviation of simulated from numerical AAT is considered. It is interesting to note that, the deviation between numerical and simulated results, concerning AAT, is lower for the case where the assumption of saturated queues is removed. This is however, due to the contradictory effects on AAT, between the assumption of saturated queues and the assumptions concerning the maximum retransmit threshold, and the occupation of certain slots by routing protocol's control traffic.

For the rest of the evaluation process, only queues of flow originators will be kept backlogged for the whole simulation period. Queues for relay nodes may be empty during a specific slot.

Fig 3.13-3.16, depict the average aggregate flow throughput (AAT), achieved by all aforementioned schemes, for the ten random scenarios employed. Each figure corresponds to one of the different SINR threshold values considered (0.5, 1.0, 1.5, and 2.0). As these figures show, the proposed flow allocation scheme (TOFRA) achieves significantly higher ATT than full

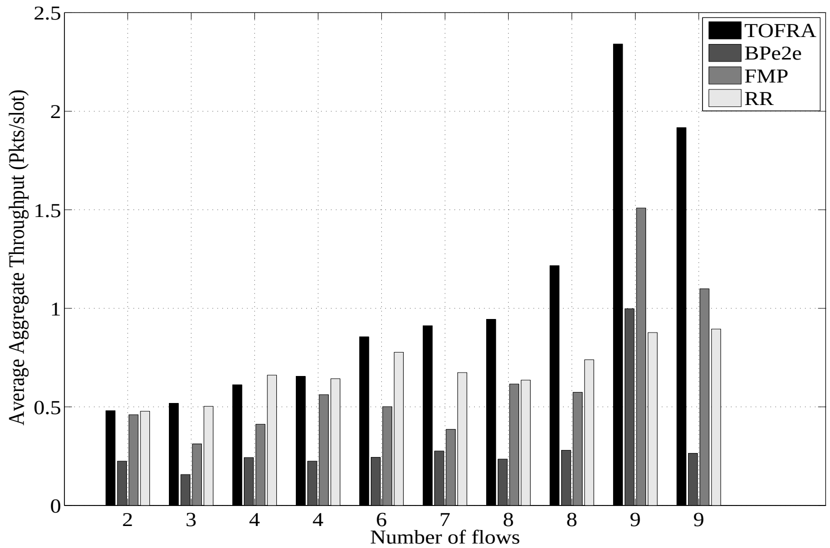

Figure 3.14: Simulation results [$\gamma = 1.0$]: AAT for TOFRA, FMP, BP$_{e2e}$, and RR.

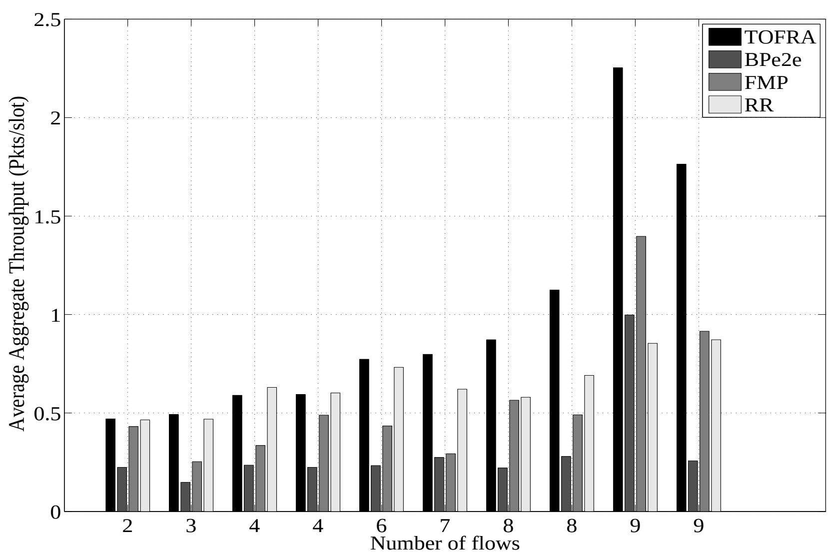

Figure 3.15: Simulation results [$\gamma = 1.5$]: AAT for TOFRA, FMP, BP$_{e2e}$, and RR.

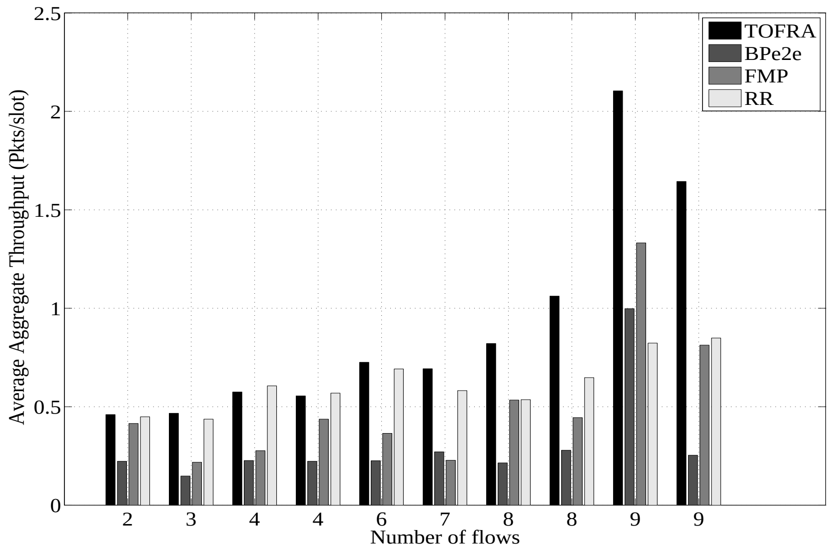

Figure 3.16: Simulation results [$\gamma = 2.0$]: AAT for TOFRA, FMP, BP$_{e2e}$, and RR.

multipath (FMP). The main reason for this is that, it takes into account the effect of both intra- and inter-path interference on throughput. FMP on the other hand, assigns the maximum flow data rate on each path (one packet per slot), disregarding the effect of interference. TOFRA achieves 47.3%, 63.7%, 78.9%, and 91.5% higher AAT, on average, over all ten scenarios, than FMP, for $\gamma = 0.5, 1.0, 1.5, 2.0$, respectively. The proposed scheme also outer-performs BP$_{e2e}$, for all traffic scenarios and γ values. This is however expected, since TOFRA exploits the diversity among the available paths and is able to aggregate resources from different paths on an interference-aware manner. The average gain of TOFRA over BP$_{e2e}$ is 293.7%, 256.4%, 2391.1%, and 222.1%, for the four γ values considered.

As far as round robin (RR) scheme is concerned, the average gain of TOFRA over RR, in terms of AAT, is 50.5%, 43.7%, 41.7%, and 39.1%, for $\gamma = 0.5, 1.0, 1.5, 2.0$, respectively. Comparing TOFRA with RR reveals the following trend: in scenarios where a low number of flows is present (≤ 4), the gain of TOFRA over RR is insignificant. Moreover, in specific scenarios, and especially when a larger γ value is employed, RR achieves slightly higher AAT than TOFRA. This is the case for scenario 2 and all γ values, and scenario 3 and γ values 1.5, and 2.0, respectively. In scenarios with a larger number of flows, TOFRA outer-performs RR. The advantage of RR over TOFRA is that, alternating among the available paths, on an iterative manner, it reduces both inter-path interference and packet failures along each path, due to half-duplex node operation. However, round-robin based flow allocation is expected to exhibit poor performance in two cases: firstly, in scenarios where a larger number of flows is present and thus, a larger number of paths is utilized. In a scenario with K flows, employing K paths for example, each path will remain idle before being assigned another packet to forward, for $K - 1$ slots. Secondly, RR is expected to achieve significantly lower AAT than TOFRA

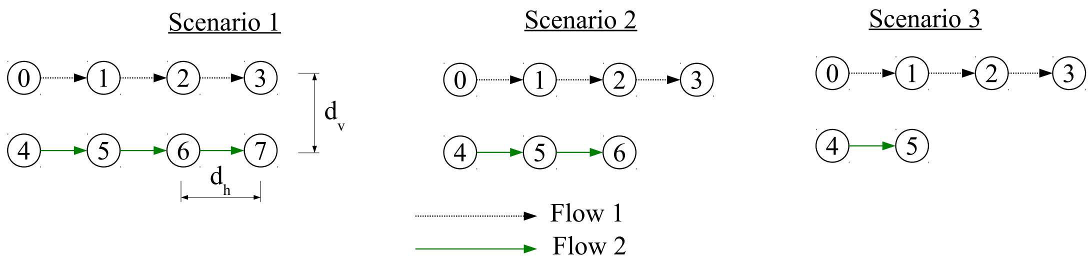

Figure 3.17: Scenarios with different diversity between paths, in terms of hop-count.

Parameter	Value
Max Retransmit Threshold	3
Relay transmission probability	0.5
Path Loss Exponent	3.0
Transmit Power	0.01 W
Noise Power	1×10^{-12} W
d_h, d_v	100 m
Simulation Time	20.000 slots

Table 3.5: Network and simulation parameters for the scenarios described in Fig. 3.17.

in scenarios where there is a large degree of diversity among the available paths. The reason for this is that, RR assigns packets on paths on a periodic manner, without adjusting flow rate based on their quality. For highlighting the importance of path diversity on RR' and TOFRA's performance, the illustrative scenarios depicted on Fig. 3.17 are employed. Three different scenarios are explored. In each of them, two flows are assumed, source at nodes 0, and 4, respectively. The different scenarios correspond to different degrees of diversity between the available paths with diversity referring to number of hops per path. In scenario 3 for example, included in Fig. 3.17, paths $0 \to 1 \to 2 \to 3$ and $4 \to 5$ exhibit the highest diversity among all other scenarios, since they consists of four and two link-hops, respectively. Values for certain network parameters, that are used for deriving numerical and simulated results, concerning average aggregate flow throughput (AAT), are listed in Table 3.5. The performance gain in terms of AAT of TOFRA over RR, for the aforementioned scenarios and network parameters, is summarized in Table 3.6. As this table shows, for scenario 1, where there is zero diversity in terms of number of hops per path, RR achieves higher AAT than TOFRA when a larger γ value is employed. When however, the diversity between the paths is significantly higher (scenario 3), the proposed scheme achieves significantly higher performance than RR, even for a larger γ values, where the effect of inter-path interference becomes more important.

In the third part of the evaluation process, a variant of the proposed flow allocation scheme is explored, where the way in which interference is captured by the suggested average ag-

Scenario	γ	Gain
1	1.0	$+2.1\%$
1	3.0	-17.2%
2	1.0	$+7.2\%$
2	3.0	-11.9%
3	1.0	$+31.4\%$
3	3.0	$+91.9\%$

Table 3.6: Gain of TOFRA over RR for the three illustrative scenarios of Fig. 3.17.

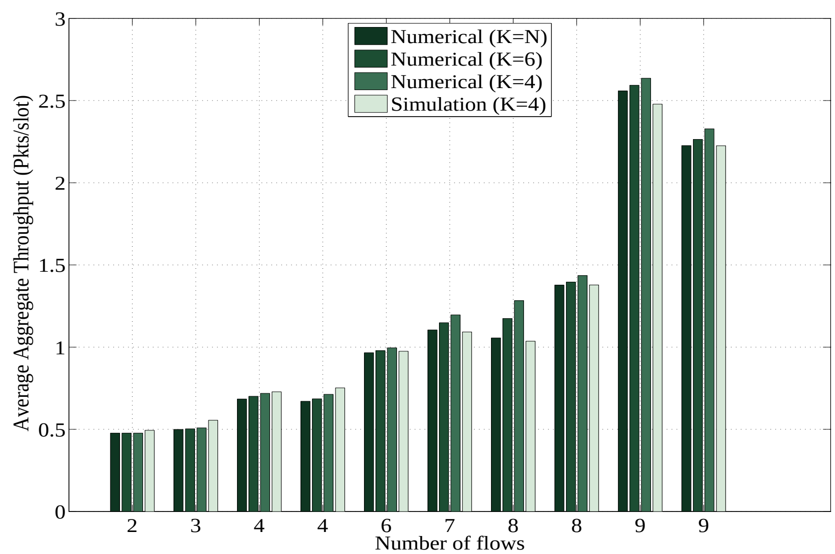

Figure 3.18: Numerical and simulation results for TOFRA's AAT and different number of dominant interfering nodes for $\gamma = 0.5$.

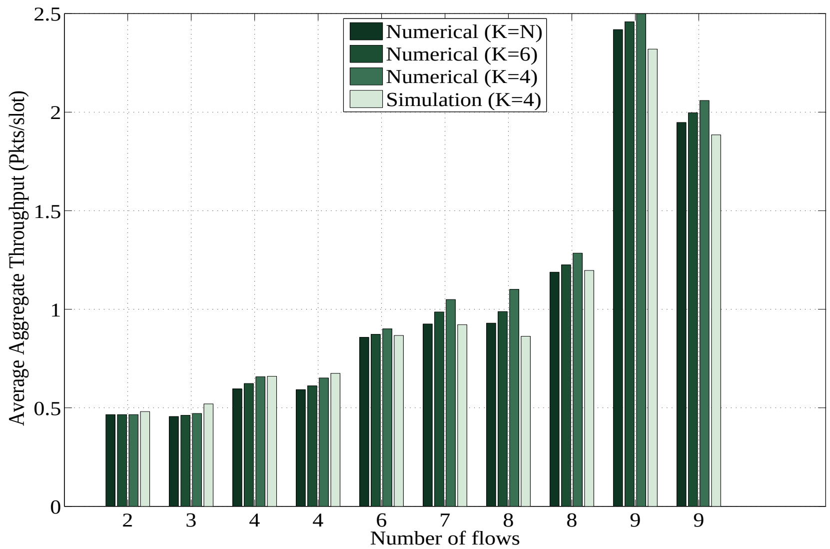

Figure 3.19: Numerical and simulation results for TOFRA's AAT and different number of dominant interfering nodes for $\gamma = 1.0$.

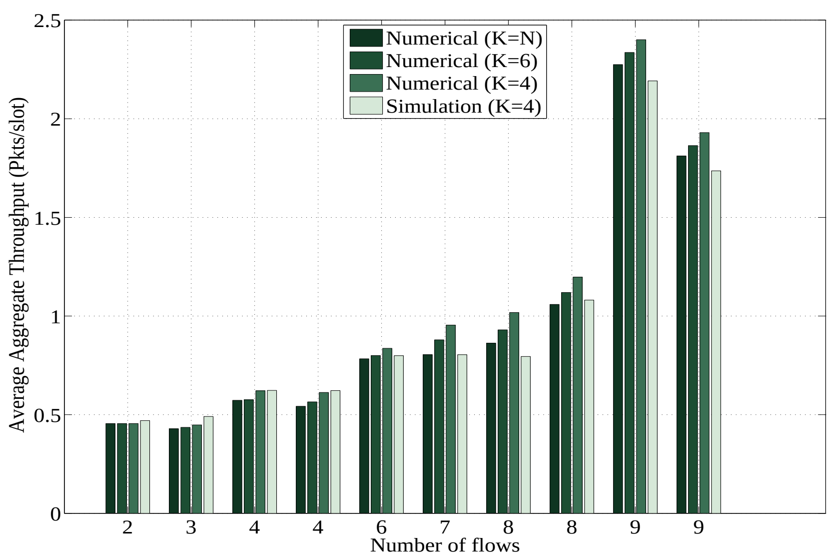

Figure 3.20: Numerical and simulation results for TOFRA's AAT and different number of dominant interfering nodes for $\gamma = 1.5$.

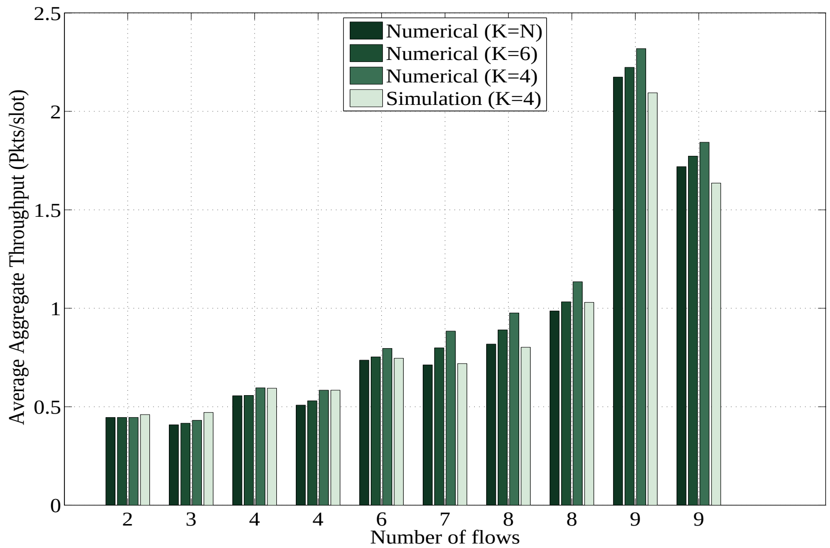

Figure 3.21: Numerical and simulation results for TOFRA's AAT and different number of dominant interfering nodes for $\gamma = 2.0$.

gregate flow throughput (AAT) model, is relaxed. The goal is to reduce the complexity of expressing a link's average throughput and thus, the complexity of expressing AAT. As already described in Section 3.3.2, the first step of the process for formulating flow allocation as an optimization problem, is deriving the expression for a specific link's average throughput. Relaxing the way in which interference relations are captured takes place in this part of the process.

Instead of considering all possible interfering nodes for expressing the average throughput achieved over a link, we approximate the interference imposed on it, by taking into account only the *K dominant interferers*. The term dominant interferers, refers to transmitters that contribute on average, with the highest amount of interference, to packet receptions over a specific link and thus, have the most significant effect on its success probability. The purpose of this part of the evaluation process is to explore the trade-off between, reduced complexity in formulating flow allocation as an optimization problem and accuracy in capturing the average aggregate throughput observed in the simulated scenarios. For each wireless scenario and γ value (0.5, 1.0, 1.5, and 2.0), the flow allocation problem employed by the TOFRA scheme, is formulated and solved through the simulated annealing technique, considering each time a different number (K) of dominant interfering nodes ($K = 2, ..., 6$). In this way, the proposed scheme estimates the rates that achieve maximum AAT, along with the corresponding AAT value, for each traffic scenario, γ value, and different number of interfering nodes. Numerical results concerning AAT that are estimated on this way are presented in Figs. 3.18-3.21, with labels *Numerical (K=N)*, *Numerical (K=6)*, and *Numerical (K=4)*, based on the number of dominant interfering nodes considered. Note that, label *Numerical (K=N)*, indicates numerical results derived by the flow allocation optimization problem, by considering all interfering nodes for each link. These results, are the same with the numerical results concerning TOFRA's AAT, used in the first part of the evaluation process and presented in Figs. 3.9-3.12, therein.

When the number of interfering nodes considered for expressing each link's average throughput is reduced, TOFRA overestimates the maximum AAT that can be achieved, by all flows present in the traffic scenario considered. Comparing numerical results concerning TOFRA's AAT, for $K = N$, and $K = 6$, the average overestimation over all traffic scenarios is 2.6%, 3.0%, 3.6%, and 3.9%, for $\gamma = 0.5, 1.0, 1.5$, and 2.0, respectively. The corresponding values, for the case where numerical results for $K = N$, and $K = 4$ are compared, are 5.7%, 7.7%, 9.4%, and 10.8%. As Figs. 3.18-3.21 also show, this overestimation becomes more significant for large γ values, where the effect of interference on success probability becomes more acute. These results show that, considering only a small number of dominant interfering nodes for each link, results in TOFRA estimating an AAT value, that differs insignificantly from the one estimated when all interfering nodes are taken into account.

What is most interesting though, is to explore whether the AAT estimated through TOFRA's model, when considering only the K dominant interfering nodes for each link, differs significantly from the actual AAT observed in the simulated scenarios. It should be noted that, simulated results concerning TOFRA's AAT, for each traffic scenario and SINR threshold (γ) value, are derived by injecting on each path employed, the flow rate determined by the TOFRA scheme and calculating the AAT achieved by all flows. It is also important to note that, while estimating the received SINR for a specific packet, all active transmitters are taken into account for interference inference, implying that, the actual interference experienced by a link in the simulated scenarios, is higher than the one considered by the TOFRA variant, where interference for each link is approximated by considering the dominant interfering nodes only.

Observing Figs. 3.18-3.21 shows that, for all γ values and for most scenarios, TOFRA's AAT, in the simulated scenarios, is lower than the one estimated by the analysis employed (flow allocation optimization problem). This is expected however, since in the analysis, only a subset of all the interfering nodes (the dominant ones) are considering for expressing a specific link's average throughput. To be more precise, TOFRA's AAT observed in the simulated scenarios, is lower than the corresponding numerical values for 6, 6, 6, and 7 out of ten traffic scenarios, for $\gamma = 0.5, 1.0, 1.5$, and 2.0, respectively. It is also interesting to note that, in some scenarios, the simulated AAT is higher than the one estimated by the flow allocation optimization problem. The reason for this, was also discussed in the first part of the evaluation process, in the beginning of this section, and is related to the saturated queues assumption present in our analysis. Even if only the dominant interfering nodes are considered for a specific link, it is assumed that these nodes will always have a packet available for transmission in their queues. However, this is not always the case in the simulated scenarios and so, the actual interference experienced by a link, from these dominant interferers, may be lower than the one estimated by our analysis. In this way, the effect of interference underestimation, by considering only the dominant interfering nodes for each link, is counter-balanced. For each traffic scenario and γ value, the absolute value of the deviation between numerical and simulated AAT is estimated, for the case, where both of them are derived by considering only

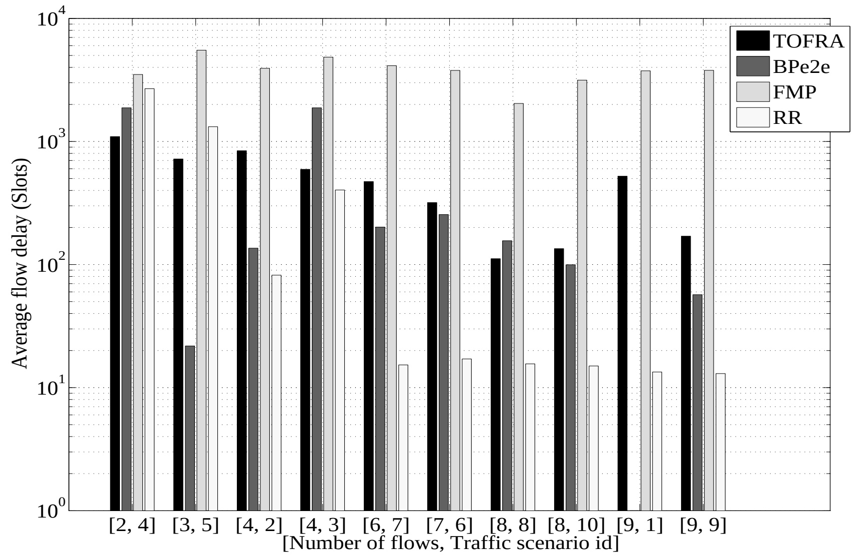

Figure 3.22: Average flow delay per flow allocation scheme for $\gamma = 0.5$.

the four dominant interfering nodes for each link. The average value of this deviation, over all traffic scenarios, is 6.8%, 8.5%, 9.6%, and 9.6%, respectively, for $\gamma = 0.5, 1.0, 1.5$, and 2.0. These results show that, the gain of reduced complexity for expressing a link's average throughput, comes at an insignificant cost in the accuracy with which simulated AAT for the proposed scheme is captured by the analysis employed.

In the last part of this section, the aforementioned flow allocation schemes are compared in terms of delay. More precisely, the average flow delay, measured in slots, for each scheme is estimated. Before discussing simulation results, the following definitions are necessary: for each flow, *end-to-end flow delay* will be used to denote the average per packet end-to-end delay, for all packets forwarded by that flow. End-to-end delay for a packet, is the interval between, that packet's first transmission attempt at the source of the flow and the time when the packet is successfully received at the destination of the corresponding flow. For the rest of the section average flow delay will be referred to as, flow delay.

Figs. 3.22-3.25, illustrate the average flow delay for each scheme, for all the random scenarios explored and SINR threshold values 0.5, 1.0, 1.5, and 2.0. The y-axis of these plots is in the log scale, in order to make it possible to compare delay for FMP with other schemes. In all the simulation scenarios, full multipath (FMP) achieves by far larger average flow delay than all other schemes. For scenario 9 for example, and $\gamma = 0.5$, average flow delay for FMP is 3786.5 slots, while the corresponding values for TOFRA, BP$_{e2e}$, RR are 170.0, 56.9, and 13.0 slots, respectively. The main reason for this gap, in terms of flow delay, is that FMP assigns one packet per slot on each path, without taking into account, intra- or inter-path interference. As a result, certain packets may experience a larger number of retransmissions until they are delivered to their final destinations. Moreover, FMP does not adjust the rate with which it in-

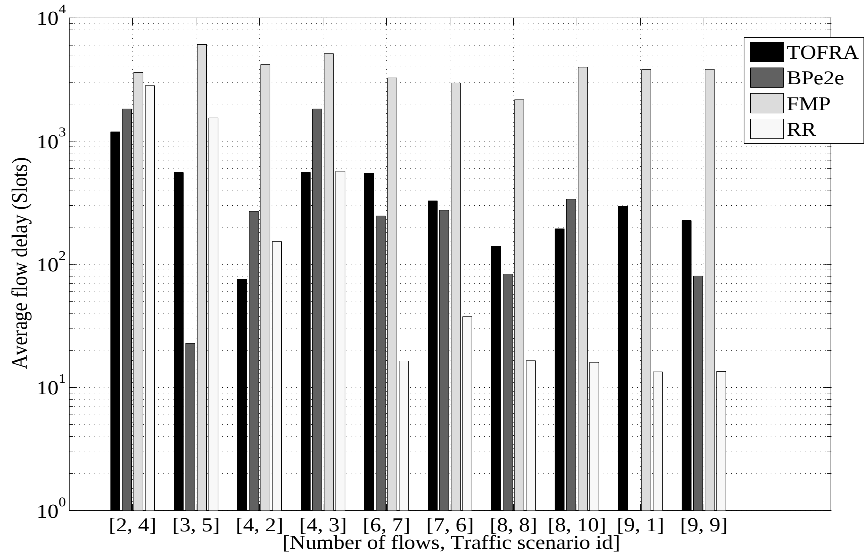

Figure 3.23: Average flow delay per flow allocation scheme for $\gamma = 1.0$.

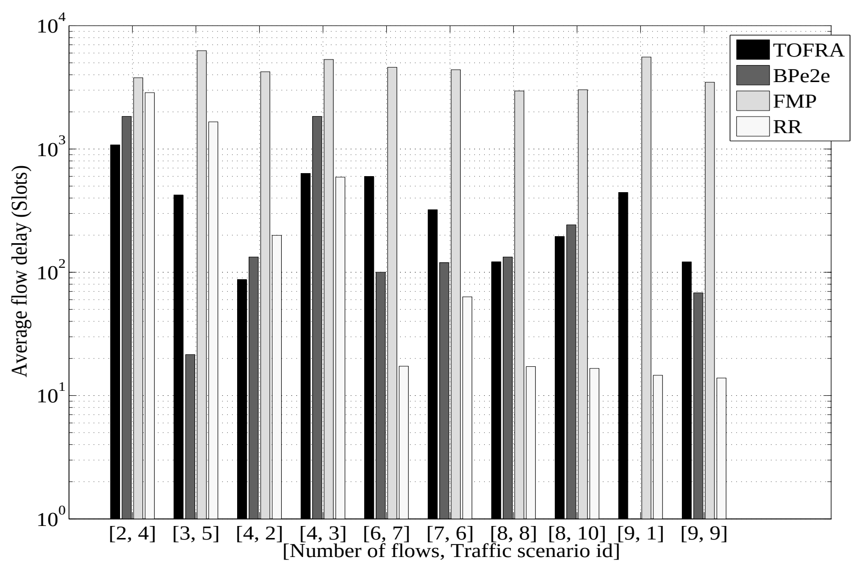

Figure 3.24: Average flow delay per flow allocation scheme for $\gamma = 1.5$.

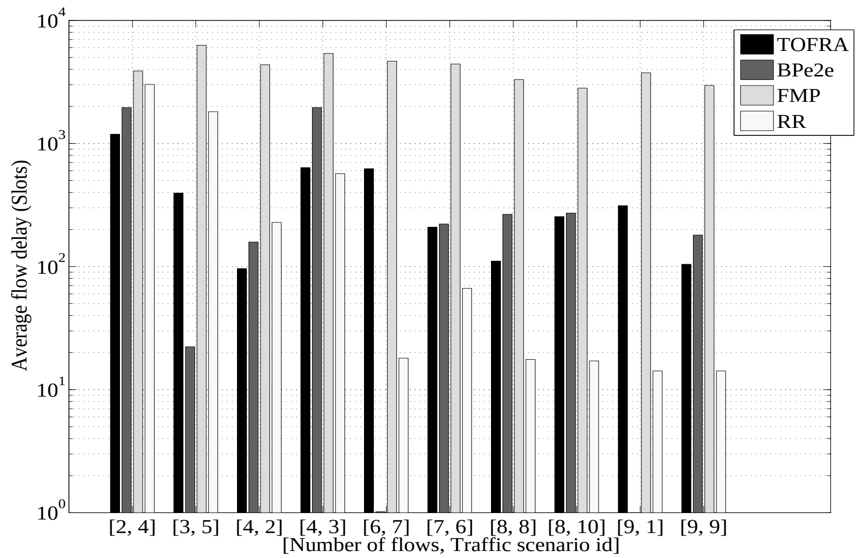

Figure 3.25: Average flow delay per flow allocation scheme for $\gamma = 2.0$.

jects traffic into each path, based on the rate with which the bottleneck link along the path can service incoming traffic. As a result, packets will accumulate at the queue of the transmitter of the corresponding bottleneck link, experiencing large queueing delay.

Figs. 3.22-3.25 also show that, for the majority of the scenarios and γ values explored, RR achieves significantly lower flow delay than TOFRA. This is mainly due to the low rate at which RR utilizes each path, especially in scenarios with many flows, where each path is revisited less often for being assigned a packet. This infrequent utilization of paths, in cases where numerous flows are forwarded in parallel, prevents RR from assigning more flow rate on a path than the one that can be serviced by its bottleneck link.

Another interesting trend, revealed in the aforementioned figures, concerns the comparison in terms of flow delay, of TOFRA and BP$_{e2e}$. BP$_{e2e}$, although it utilizes a single path and thus, avoids packet retransmissions due to increased inter-path interference, it does not achieve lower flow delay than TOFRA in all the scenarios explored. The reason for this (also discussed through some explanatory cases on subsequent paragraphs of this section) is that, in certain scenarios, BP$_{e2e}$ may experience higher queueing delay. Moreover, TOFRA can take advantage of the path diversity and disperse traffic among the available paths. This may result in a more moderate utilization of certain paths.

Apart from these trends, there are also some interesting cases which need further discussion. In scenarios, 3 and 4, for example, best-path (BP$_{e2e}$) experiences significantly higher flow delay than all other scenarios, for all γ values. In these scenarios, best-path utilizes path $23 \rightarrow 18 \rightarrow 32 \rightarrow 38$. The large flow delay is due to queueing delay experienced at relay node 18. Recall also that, best-path selects the path with the highest end-to-end success probability and determines the flow assigned to it, by solving a single path version of the flow allocation optimization problem presented in Section 3.3.2. The bounded delay constraint employed by that optimization problem, limits the average throughput that can be achieved over link $(23, 18)$, to be lower, or equal, to the corresponding average throughput achieved over links $(18, 32)$ and $(32, 18)$. In this way, it prevents relay nodes, 18 and 32, from receiving more flow than the one they can service. However, while expressing the average throughput of link $(23, 18)$, due to the saturated queues assumption in the analysis applied, it is assumed that relay node 32, will always have a packet available for transmission and thus, it will always contribute with interference to transmissions over link $(23, 18)$. In the simulated results however, this relay node does not always have a packet available for transmission in its queue. More precisely, simulated results show that, relay 32 is active for 23.0% of the total slots constituting the simulation duration. If a packet was always available for transmission and based on the assumption of a fixed contention window for each relay, equal to 5, that relay node should have been noticed active (transmitting), for approximately 28.57% of the total slots. The consequence of this is that, due to lower actual interference experienced by link $(23, 18)$, from relay 32, in the simulated scenario, this link will actually achieve higher average throughput than the one estimated by the analysis employed and thus, considered in the bounded delay constraint. This gap between the simulated and numerical average throughput, for a specific link, may result in bounded delay constraint violation.

The aforementioned gap between the simulated and numerical throughput for a link, is also the reason for the vastly larger flow delay experienced by the TOFRA flow allocation scheme in scenario 2 with $\gamma = 0.5$, when compared to other γ values for the same scenario. As Figs. 3.22-3.25 show, flow delay for the TOFRA scheme is 840.9 slots for $\gamma = 0.5$ and scenario 2. The corresponding values for γ values 1.0, 1.5, and 2.0 are 75.9, 87.1, and 96.2 slots, respectively. The average throughput observed in the simulated scenario 2 with $\gamma = 0.5$, for link $(42, 1)$, is 0.298 packets/slot, while for link $(1, 29)$ is 0.203 slots. This suggests that relay, 1 receives traffic at a rate higher than the one it can service it, resulting in packets accumulating at its queue. More on that, Table 3.7 shows the average queue length, for the relay nodes of each path employed, for scenario 2 and γ values $\{0.5, 1.5\}$. As this table shows, the average queue length, for the first relay of the first flow (that is, node 1), is more than 700 packets, for scenario 2 and $\gamma = 0.5$. Average queue length for other relay nodes is by far lower. The second interesting case, concerns BP$_{e2e}$ and scenario 2. The path employed in this scenario is $46 \rightarrow 40 \rightarrow 31$. For $\gamma = 0.5$, flow delay for BP$_{e2e}$ is 156.2 slots, while for $\gamma = 1.5$, it is 133.0 slots. What is expected though, when a larger γ value is employed, is higher flow delay due to the increased number of retransmissions that will be required for a successful packet reception. On the other hand, a lower SINR threshold (γ) value would result in a higher success probability on link $(46, 40)$ and thus, in a larger number of packets *waiting* at relay's 40 queue for transmission. Indeed, in the simulated results, the average queue length of relay 40 was 37.7 packets for $\gamma = 0.5$ and 28.2 for $\gamma = 1.5$.

Figs. 3.22-3.25 also show that, in scenarios, 4 and 5, for all γ values employed, round robin (RR) experiences significantly higher flow delay than all other scenarios. This is expected though and reveals a significant disadvantage of round robin-based flow allocation. RR utilizes the available paths on an iterative manner without adjusting the flow injected on each path based on the flow it can handle. As a result, queue build-up is probable to be observed at

(Flow id, Relay id)	$\gamma = 0.5$	$\gamma = 1.5$
(1,1)	729.1	0.0002
(1,2)	4.1	0.0007
(1,3)	0.3	0
(2,1)	0.07	5.5
(2,2)	0.31	1.9
(2,3)	0.02	0.5
(3,1)	1.8	1.2
(3,2)	0.6	0.6
(3,3)	0.1	0.1
(4,1)	82.5	38.3

Table 3.7: Average queue length per relay, for traffic scenario 2.

γ	Min variance	Max variance
0.5, 1.0, 1.5, and 2.0	1×10^{-4}	1×10^{-3}

Table 3.8: Min and max AAT variance over all traffic scenarios and SINR threshold values.

certain relay nodes. This phenomenon is also expected to be more prominent in scenarios where a few paths are employed and thus, each path is re-visited more often by RR. Indeed, in the simulated results and for certain relay nodes, average queue length values are, as high as, 397.0 and 378.3 packets, implying that large flow delay values are due to queueing delay.

As Figs. 3.22-3.25 also show, for the case of scenario 2 and $\gamma = 1.5$, flow delay for BP$_{e2e}$ is 133.0 slots, while for TOFRA it is 87.1 slots. The intuition however, is that BP$_{e2e}$ should experience lower delay than TOFRA, since it will not suffer packet retransmissions due to inter-path interference. In this scenario, BP$_{e2e}$ employs path $27 \rightarrow 12 \rightarrow 14$. For the case of TOFRA, the end-to-end delay, for the flow traversing this path, is 170.9 slots. The end-to-end delays however, for the other three flows are 88.4, 59.9, and 29.1 slots, respectively, resulting in a lower average flow delay when compared to BP$_{e2e}$. This is due to the fact that, TOFRA can exploit diversity among multiple paths, in order to maximize average aggregate flow throughput, which may result in a more moderate flow assignment on paths, compared to BP$_{e2e}$.

Finally, Table 3.8 shows the minimum and maximum AAT variance value, over all traffic scenarios explored and the four γ values considered.

3.3.3.2 Simulated annealing evaluation

In the second part of the evaluation process, the technique of simulated annealing, for solving the corresponding flow allocation optimization problem, is evaluated. The evaluation consists of exploring the accuracy with which simulated annealing approaches the global maximum and also the time required to identify it.

First, the accuracy with which simulated annealing approaches the global maximum, to the flow allocation optimization problem, is explored. Towards this direction, a brute force search algorithm is implemented. The brute force algorithm explores all different combinations, of different values, for the optimization problem's variables. Different values of a specific variable are generated using a specific step size with values for that variable ranging in $[0, 1]$.

Consider as an example, the flow allocation optimization problem generated for wireless scenario 4, where two flows are present (as also shown in Fig. 3.7). The source nodes of these two flows are nodes, 1 and 23, respectively, and the flow rates injected into the network by these two nodes are represented by variables q_1 and q_{23}. The aforementioned brute force algorithm for solving the flow allocation problem, with a step size of 0.5 for example, would consider all possible combinations of the following values for q_1 and q_{32}, respectively: $\{0.0, 0.5, 1.0\}$, $\{0.0, 0.5, 1.0\}$. The combination of flow rates, that achieves the highest average aggregate throughput, would be returned as the solution to the flow allocation optimization problem.

It should be noted that, the larger the step size employed by the brute force (BF) algorithm, the finer the distance between the solution returned by the BF algorithm and the actual one that achieves the global optimum (maximum average aggregate throughput). However, using a small step size, would result in a large number of values considered for each variable and thus, in a large number of possible combinations of different variable values, especially for problems with a large number of variables. For that reason, for evaluating the accuracy with which simulated annealing approaches the globally optimum set of flows rates (the ones that achieve maximum AAT), among all ten wireless scenarios depicted in Fig. 3.7, we employ the scenarios with the fewest number of paths. The scenarios selected for this part of the evaluation process are 2, 3, 4, and 5 where 4, 4, 2, and 3 flows are present, respectively. For each such scenario, and each SINR threshold value $(0.5, 1.0, 1.5$, and $2.0)$, the solution to the flow allocation problem, identified by the simulated annealing technique and the brute force algorithm, are compared in terms of achieved AAT.

As a first step for evaluating the solution to the flow allocation optimization problem, returned by simulated annealing, Figs. 3.26(a)-3.26(b) compare the average aggregate throughput (AAT) achieved by SA (denoted by TOFRA$_{SA}$), with the one returned by a brute force algorithm with step 0.01 (denoted by TOFRA$_{BF}$). The traffic scenario considered is scenario 4 (out of the ten random wireless employed in Section 3.3.3.1.3), where two flows are present. The flow rates that need to be fixed, so as to maximize AAT, are q_1 and q_{23}, respectively. Moreover, two different SINR threshold (γ) values are considered, 0.5, and 2.0. Note that in Figs. 3.26(a)-3.26(b), both the x- and y-axis depict values from 0.0 to 0.6 and correspond to values for q_1 and q_{23}, respectively. Values for the AAT, measured in packets per slot, are presented on the vertical, z-axis. Values for the AAT, that are equal to 0.0, correspond to a combination of flow rates that does not constitute a feasible solution to the flow allocation optimization problem. This suggests that, the bounded delay constraint (also discussed in Section 3.3.2) is violated. As the aforementioned figures show, the solution identified by simulated annealing, lies very close to the pair of, q_1 and q_{23} values, that achieve the highest AAT according to the BF algorithm.

Tables 3.9-3.10, compare the AAT achieved, by the solution identified by simulated annealing (denoted by TOFRA$_{SA}$) and the one achieved by a brute force algorithm with step

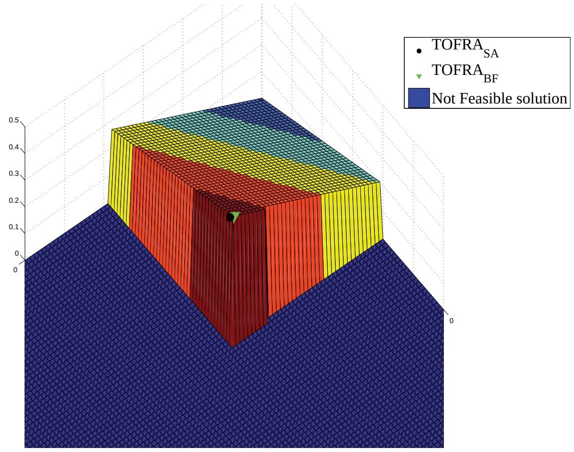

(a) $\gamma = 0.5$

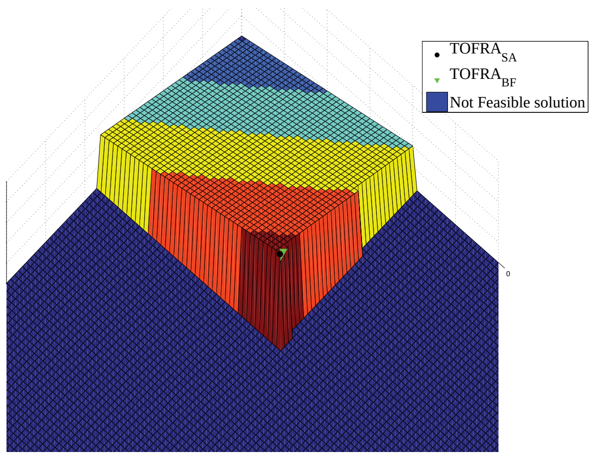

(b) $\gamma = 2.0$

Figure 3.26: Simulated annealing vs. brute force solution to the flow allocation optimization problem for scenario 4 and two SINR thresholds.

size 0.001 (denoted by TOFRA$_{BF}$), for scenarios $2, 3, 4, 5$ and γ values $0.5, 1.0, 1.5$ and 2.0. As these tables show, for all scenarios and γ values employed, the AAT achieved by simulated annealing is very close to the one achieved by the brute force algorithm. More precisely, for all scenarios and γ values, the AAT achieved by the brute force algorithm is slightly lower than the one achieved by the simulated annealing technique. This is due to the coarse step size employed by BF algorithm. Employing a finer step size would result in a more detailed search through the solution space, at the cost however of higher execution time.

The second step for evaluating simulated annealing, explores the time required to solve the flow allocation optimization problem, formulated by the TOFRA scheme. For that reason, all ten random wireless scenarios, discussed in Section 3.3.3.1.3, are employed, along with γ values $0.5, 1.0, 1.5$ and 2.0. Figs. 3.27(a)-3.27(d), present the time required to solve the

	$\gamma = 0.5$		$\gamma = 1.0$	
Scenario	TOFRA$_{SA}$	TOFRA$_{BF}$	TOFRA$_{SA}$	TOFRA$_{BF}$
1	0.684413	0.683707	0.596185	0.596140
2	0.670753	0.670312	0.592394	0.591420
3	0.477030	0.476944	0.465426	0.465570
4	0.499512	0.498854	0.456220	0.455306

Table 3.9: Maximum AAT: Simulated annealing vs. brute force for four random wireless scenarios, $\gamma = \{0.5, 1.0\}$ and BF step = 0.001.

	$\gamma = 1.5$		$\gamma = 2.0$	
Scenario	TOFRA$_{SA}$	TOFRA$_{BF}$	TOFRA$_{SA}$	TOFRA$_{BF}$
1	0.573005	0.572894	0.555879	0.554739
2	0.542730	0.542494	0.508299	0.507774
3	0.455060	0.454899	0.445710	0.445170
4	0.428703	0.428294	0.408472	0.408010

Table 3.10: Maximum AAT: Simulated annealing vs. brute force for four random wireless scenarios, $\gamma = \{1.5, 2.0\}$ and BF step = 0.001.

flow allocation optimization problem by simulated annealing, for two different variants of the TOFRA scheme. The first one, denoted as *TOFRA$_{SA}$ (k=N)*, is the variant where all interfering nodes are taken into account for expressing a link's average throughput. The second variant, denoted as *TOFRA$_{SA}$ (k=4)*, is the variant where only the four dominant interfering nodes are considered for expressing each link's average throughput. More details on this variant were also presented in Section 3.3.3.1.3.

As Figs. 3.27(a)-3.27(d) show, for the case of TOFRA$_{SA}$ (k=4), where only the four dominant interfering nodes are taken into account, for expressing a link's average throughput, the time required to solve the corresponding flow allocation optimization problem, is as high as 10 seconds, for scenarios with a large number of flows. For scenarios with a lower number of flows, such as, 2, 3, 4, and 5, the corresponding time is significantly lower. It is also interesting to note that, for the case of TOFRA$_{SA}$ (k=N), the time required to solve the corresponding flow allocation optimization problem is significantly higher for larger SINR threshold values. This is due to the fact that, while enumerating the nodes that contribute with interference to transmissions over a link (i, j), only nodes whose success probability to node j is larger or equal to 1% are taken into account. For larger γ values, the number of nodes whose success probability to each receiver j of a link (i,j) is larger than 1%, decreases.

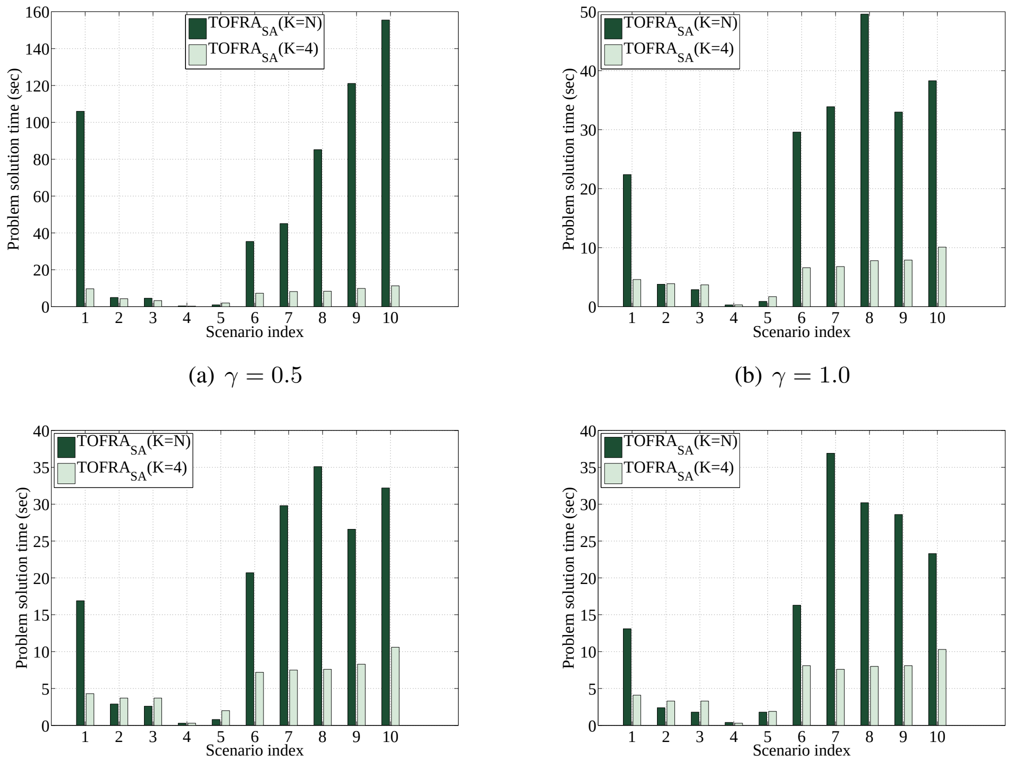

(a) $\gamma = 0.5$ (b) $\gamma = 1.0$

(c) $\gamma = 1.5$ (d) $\gamma = 2.0$

Figure 3.27: Time required to solve the flow allocation optimization problem through simulated annealing for two TOFRA variants. TOFRA$_{SA}$ (k=N) considers all interfering nodes, while TOFRA$_{SA}$ (k=4) only the four dominant ones.

3.4 Successive Interference cancelation

The severe effect of interference on network performance is even more prominent when multiple paths are utilized in parallel. Successive interference cancelation (SIC) is a promising physical layer technique for handling interference and improving network performance [51–55]. The performance of TDMA-based, conflict-free, scheduled multi-hop networks is explored in [56] when SIC is enabled at either all nodes or, at some of them. A framework studying the performance of SIC in wireless networks, using tools from Stochastic Geometry, is provided in [57]. A comprehensive survey on the performance of SIC, for single- and multiple-antenna OFDM and spread OFDM (OFCDM) systems is provided in [58]. Authors in [59], study the extent of throughput gains with SIC, from a MAC layer perspective and propose a SIC-aware scheduling algorithm. The maximum stable throughput region for the two-user interference channel is derived in [60]. The case of receivers performing SIC is also considered in the same study.

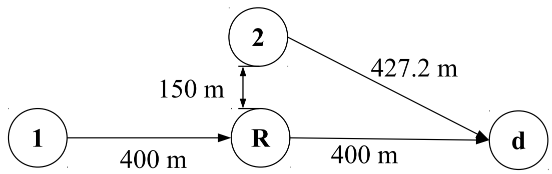

Figure 3.28: Illustrative scenario.

3.4.1 Channel model

In this section, the flow allocation scheme discussed in Section 3.3, is reconsidered. The main difference is that, instead of treating interference as noise (IAN), a variant of the proposed scheme is explored, where successive interference cancelation (SIC) is applied at receiving nodes. More precisely, we explore the gain that can be achieved, at the network layer, when successive interference cancellation is employed, instead of treating interference as noise. The variant of the proposed flow allocation scheme, where SIC is employed, instead of treating interference as noise, is evaluated both in terms of throughput and delay. It should be noted that, the system model assumed for this section is the same as the one presented in Section 3.2.

For the case where, receiving nodes are assumed to perform successive interference cancellation, a block fading channel model with Rayleigh fading is considered, i.e. the fading coefficients, $\mathcal{A}(j,i)$, remain constant during one timeslot, but change independently from one timeslot to another, based on a circularly symmetric complex Gaussian distribution, with zero mean and unit variance. The noise is assumed to be additive white Gaussian with zero mean and unit variance. With $\mathcal{P}_{tx}(j)$, we denote the transmission power of node j, and $\mathrm{r(j,i)}$ is the distance between transmitter j and receiver i, with a being the path loss exponent.

Let $\mathcal{D}_{j,i}^{\mathcal{T}}$ denote the event that, node i is able to decode the packet transmitted from node j, given a set of active transmitters, denoted by $\mathcal{T}$. To illustrate how successive interference cancellation is applied at receivers, the topology shown in Fig. 3.28 is employed.

For this topology, $\mathcal{D}_{1,R}^{\{1,2\}}$ denotes the event that the relay (R) can decode the information from the first node, when nodes 1 and 2, are active ($\mathcal{T} = \{1,2\}$). When only j is active, the event $\mathcal{D}_{j,i}^{\{j\}}$ is defined as

$$\mathcal{D}_{j,i}^{\{j\}} \triangleq \left\{R_j \leq \log_2\left(1 + \mathcal{A}(j,i)(r(j,i))^{-a}\mathcal{P}_{tx}(j)\right)\right\}, \tag{3.6}$$

which is equivalent to $\mathcal{D}_{j,i}^{\{j\}} = \left\{2^{R_j} - 1 \leq \mathcal{A}(j,i)(r(j,i))^{-a}\mathcal{P}_{tx}(j)\right\}$.

For convenience, we define $\mathrm{SNR}_{ji} \triangleq \mathcal{A}(j,i)(r(j,i))^{-a}\mathcal{P}_{tx}(j)$ and $\gamma_j \triangleq 2^{R_j} - 1$. The probability that the link ji is not in outage, when only j is active, is given by the following equation: [48]

$$\Pr\left(\mathcal{D}_{j,i}^{\{j\}}\right) = \Pr\left\{\mathrm{SNR}_{ji} \geq \gamma_j\right\} = \exp\left(-\frac{\gamma_j (r(j,i))^{-a}}{\mathcal{P}_{tx}(j)}\right). \tag{3.7}$$

Let us consider the case that, the relay node R treats interference from node 2 as noise, when both nodes 1 and 2 are active. The event $\mathcal{D}_{1R}^{\{1,2\}}$ is given by

$$\mathcal{D}_{1,R}^{\{1,2\}} \triangleq \left\{R_1 \leq \log_2\left(1 + \frac{\mathcal{A}(1,R)(r(1,R))^{-a}\mathcal{P}_{tx}(1)}{1 + \mathcal{A}(2,R)(r(2,R))^{-a}\mathcal{P}_{tx}(2)}\right)\right\}, \tag{3.8}$$

which is equivalent to

$$\mathcal{D}_{1,R}^{\{1,2\}} = \left\{\gamma_1 \leq \frac{\mathcal{A}(1,R)(r(1,R))^{-a}\mathcal{P}_{tx}(1)}{1 + \mathcal{A}(2,R)(r(2,R))^{-a}\mathcal{P}_{tx}(2)} \triangleq \mathrm{SINR}_{1R}\right\}. \tag{3.9}$$

The probability that the channel $(1, R)$ is not in outage, when both nodes 1 and 2 are active, is given by [48]:

$$\begin{aligned} \Pr^{IAN}\left(\mathcal{D}_{1,R}^{\{1,2\}}\right) &= \Pr\left\{\mathrm{SINR}_{1R} \geq \gamma_1\right\} = \\ = \exp\left(-\frac{\gamma_1 (r(1,R))^{a}}{\mathcal{P}_{tx}(1)}\right)&\left[1 + \gamma_1 \frac{\mathcal{P}_{tx}(2)}{\mathcal{P}_{tx}(1)}\left(\frac{r(1,R)}{r(2,R)}\right)^{a}\right]^{-1}. \end{aligned} \tag{3.10}$$

Let us consider the case that, the relay node R, deploys successive interference cancellation (SIC), when both nodes, 1 and 2, are active. If the relay R knows the codebook of the node 2, it can perform SIC by first decoding the message sent by 2, removing its contribution (interference) to the received signal, and then decoding the message coming from node 1. The relay R is able to decode the interference, when both nodes 1 and 2 are active, if the following conditions are satisfied

$$R_2 \leq \log_2\left(1 + \frac{\mathcal{A}(2,R)(r(2,R))^{-a}\mathcal{P}_{tx}(2)}{1 + \mathcal{A}(1,R)(r(1,R))^{-a}\mathcal{P}_{tx}(1)}\right), \tag{3.11}$$

$$R_1 \leq \log_2\left(1 + \mathcal{A}(1,R)(r(1,R))^{-a}\mathcal{P}_{tx}(1)\right), \tag{3.12}$$

which are equivalent to

$$\gamma_2 = 2^{R_2} - 1 \leq \frac{\mathcal{A}(2,R)(r(2,R))^{-a}\mathcal{P}_{tx}(2)}{1 + \mathcal{A}(1,R)(r(1,R))^{-a}\mathcal{P}_{tx}(1)} \triangleq \mathrm{SINR}_{2R} \text{ and } \gamma_1 \leq \mathrm{SNR}_{1R}. \tag{3.13}$$

The event $\mathcal{D}_{1,R}^{\{1,2\}}$ is given by $\mathcal{D}_{1,R}^{\{1,2\}} = \{\mathrm{SINR}_{2R} \geq \gamma_2\} \cap \{\mathrm{SNR}_{1R} \geq \gamma_1\}$, and the probability that R can decode the transmitted information from 1 (given that both 1 and 2 are active) is given by (3.14) [60].

$$\Pr^{SIC}\left(\mathcal{D}_{1,R}^{\{1,2\}}\right) = \Pr\left\{\{\mathrm{SINR}_{2R} \geq \gamma_2\} \cap \{\mathrm{SNR}_1 \geq \gamma_1\ \}\right\}$$
$$= \exp\left(-\frac{\gamma_1(r(1,R))^a}{\mathcal{P}_{tx}(1)}\right)\exp\left[-\frac{\gamma_2(1+\gamma_1)(r(2,R))^a}{\mathcal{P}_{tx}(2)}\right]\left[1+\gamma_2\frac{\mathcal{P}_{tx}(1)}{\mathcal{P}_{tx}(2)}\left(\frac{r(2,R)}{r(1,R)}\right)^a\right]^{-1}. \tag{3.14}$$

For the rest of this chapter, for reasons of brevity, the probability that node i is able to decode the packet transmitted from node j, given a set of active transmitters denoted by $\mathcal{T}$, ($\Pr(\mathcal{D}_{j,i}^{\{\mathcal{T}\}})$) will be denoted by $p^i_{j/\mathcal{T}}$.

3.4.2 Analysis

The method for formulating flow allocation on multiple disjoint paths, as an optimization problem, is the same as the one presented in Section 3.3.2 of this chapter. Average link throughput is also expressed through (3.3) in this section. The only modification incorporated, concerns transmission probabilities at the relay nodes. In the aforementioned equation for average link throughput, probability $q_{i,j}$ is rewritten accordingly:

$$q_{i,j} = \begin{cases} q''_i & j = D \\ q''_i(1-q''_j) & j \neq D \end{cases}, \tag{3.15}$$

$$q''_i = \begin{cases} q_i & , i \neq relay \\ q_i \mathbb{1}[q_{Src(r(i))} > 0] & , j = relay \end{cases} \tag{3.16}$$

In the above equation, $\mathbb{1}[q_{Src(r(i))} > 0]$, denotes an indicator function whose value becomes one if $q_{Src(r(i))} > 0$ and zero otherwise. The reason for employing it is the following: assume that the flow assigned on a path is zero packets per slot. This means that, relay nodes along this path, will have no packets to transmit to their next hops. However, while enumerating all interfering nodes for expressing a specific link's average throughput through (3.3), relay nodes that belong to a path to which zero flow is assigned, will be assumed to contribute with interference. This is due to the assumption mentioned in the system model that all nodes always have packets available for transmission. Employing however, the indicative function present in (3.16), a relay node i that belongs to a path where zero flow is assigned ($q_{Src(r(i))} = 0$), will not be considered to contribute with interference.

3.4.3 Evaluation

The evaluation process presented in this section, consists of three parts. In the first one, the accuracy of the model employed by the TOFRA scheme, for capturing the average aggregate flow throughput (AAT) observed in the simulated scenarios is explored. In the second part, the gain in terms of throughput that can be achieved at the network level, by combining TOFRA flow allocation scheme with SIC is explored. Finally, the effect of SIC on end-to-end flow delay is discussed.

For the rest of the section, the notion of asymmetry for two interfering links, will be

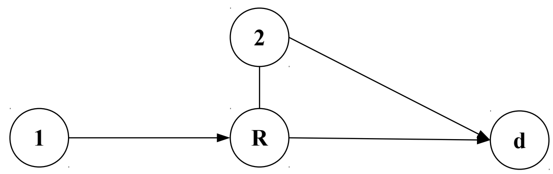

	Topology 1	Topology 2	Topology 3
r(1,R)(m)	400	400	400
r(R,d) (m)	400	300	300
r(2,R) (m)	150	150	150
r(2,d) (m)	427.2	430	200

Figure 3.29: Wireless topologies explored.

used to denote the difference between the average received SNR over them. As far as SIC is concerned, it has been shown that performance gain increases with the asymmetry among interfering links [59]. For that reason, three different topologies are explored, based on the one presented in Fig. 3.29. Different topology instances are derived by fixing the distances between pairs of nodes. The corresponding distance values employed are summarized in the table incorporated in the same figure. For all three topologies, two unicast flows are assumed, sourced at nodes, 1 and 2, respectively. Flow f_1, is forwarded to d, through path $1 \rightarrow R \rightarrow d$, while flow f_2, through $2 \rightarrow d$. Assuming such a traffic scenario, in topology 1 depicted in Fig. 3.29, transmissions along link $(1, R)$ experience interference from node 2. If similar SINR threshold (γ) values, for all transmitters are further assumed, then the received signal on R from 2, constituting the interference, is received with higher power compared to the signal received from 1. On a similar manner, in topologies 1 and 2, transmissions along link $(2, d)$ experience interference from R. The signal constituting interference from R is received with higher power at d, than the signal carrying data packets sent from 2.

Based on these remarks, different approaches are explored, for each topology presented in Fig. 3.29, depending on how interference is handled at each receiving node. For topologies 1 and 2, three different approaches are explored. In the first one, interference at nodes R, d is treated as noise. In the second approach, SIC is applied on R, as described in Section 3.4.1. In the third one, destination d, first tries to decode the message from R, remove its contribution (interference) to the received signal, and then decode the message from 2. Finally, as far as topology 3, depicted in Fig. 3.29, is concerned, three approaches are also explored. The first two approaches are the same with topologies 1 and 2. In the third one however, where the destination resides closer to transmitting node 2 instead of R, d first tries to decode the message received from 2 (interference), remove its contribution to the received signal, and then decode the message from node R. For the rest of the section, we will also use the term successive interference cancellation to describe how interference is handled at destination d. To distinguish among the different approaches discussed above for handling interference, they

Parameter	Value
Max Retransmit Threshold	3
Contention Window	5
Path Loss Exponent	3.0
Packet size	1500 bytes
Simulation duration	20.000 slots
Transmission power	0.1 W
Noise power	$7 \times 10^{-11} W$

Table 3.11: Values for network parameters, used to derive numerical and simulation results.

are labelled after: *IAN*, *SIC(R)*, *SIC(R,d)*, with SIC(R,d) denoting that SIC is applied at both R and d.

As far as allocation of flow (data rates) on different paths is concerned, three different schemes are explored. The first scheme is TOFRA (presented in Section 3.3.2). As also discussed in Section 3.3.3.1.3, *Full MultiPath (FMP)* assigns one packet per slot on each path. Finally, the third scheme explored, employs only a single path to forward traffic to the destination. Based on how *best* path is identified, we explore two variants: in the first one, denoted as BP$_{e2e}$, best path is considered as the one, exhibiting the highest end-to-end success probability, expressed through: $\mathcal{P}_{r_k} = \prod_{(i,j)\in r_k} p^j_{i/i}$. In the second variant, denoted as BP$_{wb}$, best path is defined as the one that has the *widest* bottleneck link, which can be formulated as identifying path r_k : $\arg\max_{k} \min_{(i,j)\in r_k)} p^j_{i/i}$. In the first two topologies explored, BP$_{wb}$ utilizes path $1 \to R \to d$ to the destination, while in the third one, $2 \to d$. BP$_{e2e}$ on the other hand, deploys path $2 \to d$, for all three topologies explored. Applying SIC for the topologies presented in Fig. 3.29 is meaningless, since when path $2 \to d$ is used, destination d receives no interference, while in the case of $1 \to R \to d$, the interference received at d, from 1, is insignificant due to the large distance between them. For both aforementioned best-path variants, the flow assigned on the utilized single path, is calculated by solving a single-path version of the optimization problem (P2), presented in Section 3.3.2, through the simulated annealing technique.

For the purposes of the evaluation process, Ns2 simulations are employed, where the required modifications and modules are presented in Appendix A. Table 3.11 presents the values used for several Ns2 parameters.

Different simulation scenarios are generated as follows: for each topology presented in Fig. 3.29, one of the aforementioned flow allocation schemes is employed. For each flow allocation scheme, three variants are simulated based on how interference is handled at each receiving node. The variant denoted by *FMP-IAN* for example, assigns one packet per slot on each path, while interference is treated as noise at each receiver. For *FMP-SIC(R)*, SIC is assumed at receiving node R. To capture the effect of interference on success probability, four different SINR threshold values are employed: 0.5, 1.0, 1.5, and 2.0. In each simulation scenario, flows carrying constant bit rate, UDP traffic, are generated while simulation period is 20.000 slots. Queues for flow originators are kept backlogged for the whole simulation period.

Topology	γ	Flow allocation scheme	q_1	q_2	AAT_{num} Pkts/Slot	AAT_{sim} Pkts/Slot
1	0.5	TOFRA-IAN	0.0	1.0	0.973	0.970
1	0.5	TOFRA-SIC(R)	0.287	1.0	1.045	1.045
1	0.5	TOFRA-SIC(R,d)	0.287	1.0	1.057	1.069
1	1.0	TOFRA-IAN	0.0	1.0	0.946	0.943
1	1.0	TOFRA-SIC(R)	0.227	1.0	0.920	0.920
1	1.0	TOFRA-SIC(R,d)	0.227	1.0	0.931	0.951
1	1.5	TOFRA-IAN	0.0	1.0	0.921	0.918
1	1.5	TOFRA-SIC(R)	0.189	1.0	0.840	0.848
1	1.5	TOFRA-SIC(R,d)	0.189	1.0	0.846	0.875
1	2.0	TOFRA-IAN	0.0	1.0	0.896	0.891
1	2.0	TOFRA-SIC(R)	0.164	1.0	0.783	0.802
1	2.0	TOFRA-SIC(R,d)	0.164	1.0	0.783	0.802

Table 3.12: Simulation vs numerical results for the AAT achieved by each TOFRA variant. Topology 1.

For the relay node present in Fig. 3.29, the queue may become empty during a slot. That is, not saturated queues assumption is simulated, for relay nodes.

In the first part of the evaluation process, we explore whether, the proposed model accurately captures the average aggregate flow throughput (AAT) observed in the simulation results. Tables 3.12 - 3.14, summarize the flow rates assigned on each path, along with the corresponding value for AAT achieved by TOFRA, derived from both the numerical and the simulation results. Recall that, flow rates assigned on each path, are identified by sources, by solving a topology specific instance of the flow allocation optimization problem presented in Section 3.3.2. The path loss exponent assumed for deriving numerical results is 3.0 and link distances are those presented in Fig. 3.29.

The average deviation between the AAT derived from the model described in Section 3.3.2 and the one observed in the simulated results, is 1.42%, over all topologies, γ values and TOFRA variants employed. There are several reasons for this deviation and were already discussed in the evaluation section related to the grid-based scenarios and the random wireless ones. For convenience of the reader, they are also quoted in this section. The main reason is related to the assumption of the model, for AAT, concerning saturated queues at the relay nodes. In our analysis, it is assumed that whenever a relay node attempts to transmit a packet, there is always one available at its queue. In the simulated scenarios however, a relay node's queue may be empty at a specific slot. In this way however, the considered model for the AAT overestimates the interference experienced by any link in the simulated scenarios and thus, underestimates the average throughput achieved over that link. Due to the assumption concerning saturated queues at the relay nodes, it also overestimates the collision probability at each relay node, due to concurrent packet transmission and reception events. At the end of this section, we also discuss how this underestimation of a link's average throughput may also

Topology	γ	Flow allocation scheme	q_1	q_2	AAT_{num} Pkts/Slot	AAT_{sim} Pkts/Slot
2	0.5	TOFRA-IAN	0.0	1.0	0.972	0.968
2	0.5	TOFRA-SIC(R)	0.350	1.0	1.005	1.004
2	0.5	TOFRA-SIC(R,d)	0.350	1.0	1.084	1.116
2	1.0	TOFRA-IAN	0.0	1.0	0.945	0.942
2	1.0	TOFRA-SIC(R)	0.315	0.0	0.889	0.886
2	1.0	TOFRA-SIC(R,d)	0.315	0.0	0.975	1.023
2	1.5	TOFRA-IAN	0.0	1.0	0.919	0.916
2	1.5	TOFRA-SIC(R)	0.288	1.0	0.815	0.817
2	1.5	TOFRA-SIC(R,d)	0.288	1.0	0.896	0.958
2	2.0	TOFRA-IAN	0.0	1.0	0.894	0.894
2	2.0	TOFRA-SIC(R)	0.267	1.0	0.760	0.764
2	2.0	TOFRA-SIC(R,d)	0.268	1.0	0.833	0.901

Table 3.13: Simulation vs numerical results for the AAT achieved by each TOFRA variant. Topology 2.

affect queueing delay. Apart from that, in the analysis presented in Section 3.3.2, a packet is not assumed to be dropped after a larger number of failed retransmissions. In the simulation parameters presented in Table 3.11 however, a maximum retransmit threshold equal to 3.0 is adopted. This suggests that, after three failed transmissions, a specific packet is dropped. This may result in lower throughput for the link over which that packet is retransmitted, but will also result in reduced interference imposed on neighbouring links. Finally, in the analysis, we have assumed that whenever a packet is transmitted, it is a packet carrying data. In the simulated scenarios however, all nodes, either perform periodic emission of routing protocol's control messages, or forwarded specific received control packets (topology control messages for the simulation setup presented in Appendix A). This means that, specific slots are spent carrying routing protocol's control messages, instead of data packets, resulting in our analysis overestimating the AAT observed in the simulated results.

In the second part of the evaluation process, we explore the gain in terms of throughput that can be achieved by employing SIC, instead of treating interference as noise (IAN). More precisely, we explore the AAT achieved by the aforementioned flow allocation schemes, when different approaches for handling interference are followed (discussed above). Figures 3.30 - 3.32, present the corresponding AAT values for the three topologies summarized in Fig. 3.29.

Figures 3.30-3.32 show that, applying SIC instead of IAN, at both receiving nodes R, d, proves gainful in terms of AAT, when γ=0.5. For the case of the TOFRA flow allocation scheme, the gain is 10.2%, 15.2%, and 13.2%, respectively, for the three topologies explored. The corresponding values for FMP are 10.7%, 16.9%, and 2.6%, respectively. It should also be noted that, the gain in terms of throughput, for SIC, is less significant when it is applied only to receiver R. For γ=0.5, employing SIC at R, instead of IAN, results in 7.7%, 3.7%, and 3.1% higher AAT, for the three topologies explored. Applying SIC on R, increases the

Topology	γ	Flow allocation scheme	q_1	q_2	AAT$_{num}$ Pkts/Slot	AAT$_{sim}$ Pkts/Slot
3	0.5	TOFRA-IAN	1.0	1.0	1.011	1.015
3	0.5	TOFRA-SIC(R)	0.153	1.0	1.062	1.047
3	0.5	TOFRA-SIC(R,d)	0.297	1.0	1.158	1.149
3	1.0	TOFRA-IAN	0.0	1.0	0.994	0.993
3	1.0	TOFRA-SIC(R)	0.098	1.0	0.990	0.987
3	1.0	TOFRA-SIC(R,d)	0.267	1.0	1.093	1.086
3	1.5	TOFRA-IAN	0.0	1.0	0.991	0.989
3	1.5	TOFRA-SIC(R)	0.074	1.0	0.946	0.966
3	1.5	TOFRA-SIC(R,d)	0.247	1.0	1.045	1.037
3	2.0	TOFRA-IAN	0.0	1.0	0.988	0.985
3	2.0	TOFRA-SIC(R)	0.060	1.0	0.915	0.954
3	2.0	TOFRA-SIC(R,d)	0.232	1.0	1.006	1.001

Table 3.14: Simulation vs numerical results for the AAT achieved by each TOFRA variant. Topology 3.

success probability on link $(1, R)$, from 9.3% to 95.1%, for γ=0.5 and from 2.3% to 81.5% for γ=2.0. Consequently, transmitter 1 will manage to deliver a larger portion of its traffic to R, when SIC is employed at R, instead of IAN, which will also result in an increased number of packets transmitted from R to d. This, will have a negative effect on the average throughput of link $(2, d)$, since it will experience increased interference. Indeed, for the first topology presented in Fig. 3.29, γ=0.5 and the TOFRA flow allocation scheme, when interference is treated as noise at all the receivers, the fraction of data packets, transmitted over $(2, d)$, that are retransmitted due to due to noise, signal attenuation, interference, and fading, is 2.7%. In the scenario where SIC is employed at R, the corresponding fraction of retransmitted packets increases to 14.1%. This shows that, improving the success probability at a relay node, by applying SIC, will also increase the interference imposed on its next hop. Consequently, the number of packets that are retransmitted will increase, limiting the gain in terms of AAT. As Figs. 3.30-3.32 also show, for higher γ values, applying SIC instead of IAN, for the case of TOFRA, either offers insignificant gain, or results in lower average aggregate throughput. As already discussed, applying SIC at R, significantly increases the success probability on link $(1, R)$, with TOFRA also increasing the amount of flow assigned on path $1 \rightarrow R \rightarrow d$. If however, the increased interference on link $(2, d)$, is not compensated by the gain of utilizing path $1 \rightarrow R \rightarrow d$, the average aggregate flow throughput (AAT) observed, may be lower compared to the case where IAN is applied at each receiver.

As far as the relation between interfering links asymmetry and gain in terms of throughput, of SIC over IAN, is concerned, the following remark is also interesting. As already discussed above, the success probability of link $(1, R)$ increases from 9.3% to 95.1%, for γ=0.5, when SIC is employed at R, instead of IAN. Accordingly, in topology 1 for example, the success probability of link $(2, d)$ increases from 60.4% to 66.7% for γ=0.5, when SIC is employed

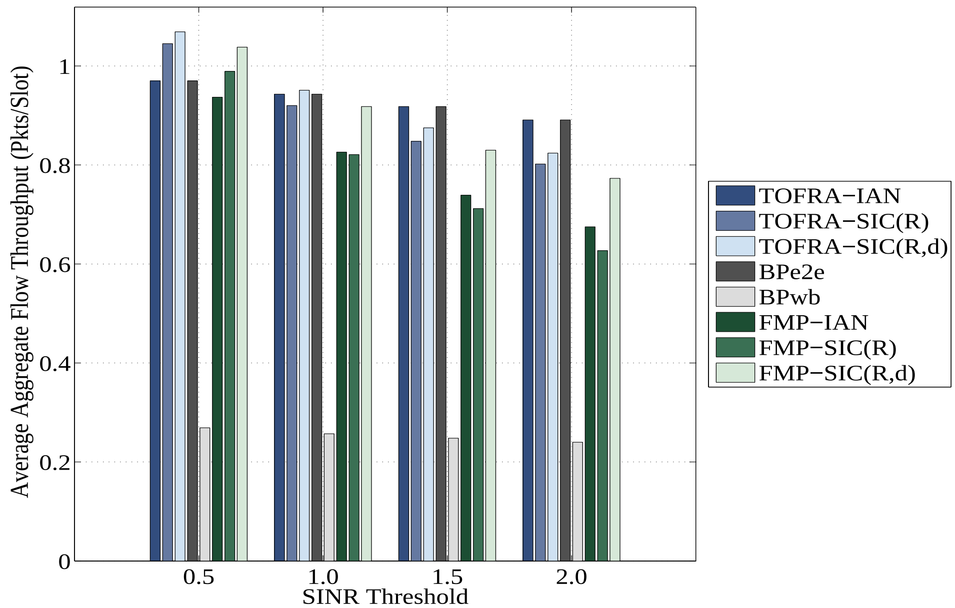

Figure 3.30: Topology 1: AAT per flow allocation variant.

at d, instead of IAN. This increase in the success probability, is significantly lower than the corresponding one for link $(1, R)$. The reason for this, is the different asymmetry between interfering links, for the two receivers. As Fig. 3.29 also shows, the distance of interfering node 2 from R is much smaller than the distance between 1 and R. The distances however, of nodes 2 and R, from d, are very similar. A notable effect of combining SIC with the TOFRA flow allocation scheme, is the utilization of paths which where assigned zero flow when IAN was applied at receiving nodes. As Tables 3.12-3.14 show, the utilization of path $1 \rightarrow R \rightarrow d$ becomes non-zero for all topologies and γ values considered, when SIC is employed.

As far as different flow allocation schemes are concerned, variants of the TOFRA scheme achieve higher AAT than the corresponding full multipath (FMP) variants, for all topologies and γ values employed. The main reason for this is that, FMP assigns one packet per slot on each path on an interference unaware manner, resulting in a higher fraction of data packets retransmitted due to interference. This performance gap becomes even more profound when large SINR threshold values are assumed: thus, the success probability of all links is decreased. Considering topology 3, with γ=0.5 for example, TOFRA-SIC(R,d) achieves 10.2% higher AAT than the corresponding FMP variant (FMP-SIC(R,d)). Compared to BP$_{e2e}$, TOFRA-IAN achieves the same AAT, for almost all scenarios explored, since they both utilize at full rate path $2 \rightarrow d$. The only exception to this is the scenario based on topology 3, where γ=0.5. In this scenario, the corresponding TOFRA variant also utilizes path $1 \rightarrow R \rightarrow d$. When TOFRA however, is combined with SIC, at both R and d and a low γ is employed, it achieves higher AAT. In topology 3 for example, when a γ value equal to 0.5 is employed, TOFRA-SIC(R,d)

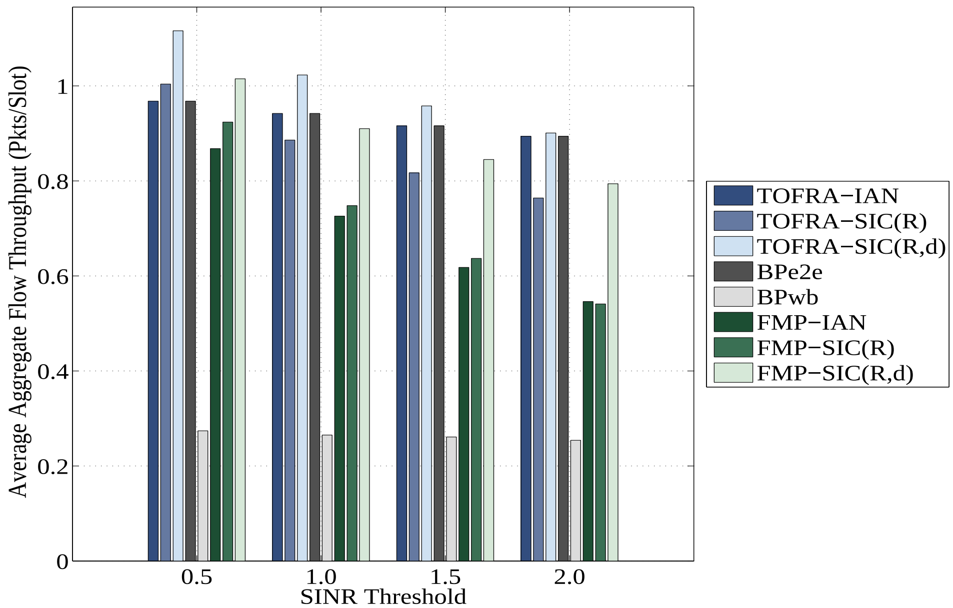

Figure 3.31: Topology 2: AAT per flow allocation variant.

achieves 15.4% higher AAT than BP$_{e2e}$. It should be noted however that, the prospect of higher throughput for TOFRA, is limited by the number of paths available. In the scenarios explored in the previous section, where several paths are employed in parallel, TOFRA outerperforms BP$_{e2e}$. Finally, best-path variant, that selects the path with the widest bottleneck link, in terms of success probability (BP$_{wb}$), utilizes path $1 \rightarrow R \rightarrow d$ for topologies 1 and 2, and $2 \rightarrow d$ for topology 3. However, as Tables 3.12-3.14 show, TOFRA assigns zero flow on path $1 \rightarrow R \rightarrow d$ for most scenarios explored, when interference is treated as noise. This shows that, utilizing this path in parallel with $2 \rightarrow d$, would result in lower AAT. As also shown in Figs. 3.30-3.32, BP$_{wb}$ achieves the lowest AAT among all schemes, for topologies 1 and 2, and performs the same with BP$_{e2e}$, for topology 3.

In the third part of the evaluation process, the aforementioned flow allocation schemes are compared in terms of delay. Moreover, the effect of applying SIC on it is explored. Similarly to Section 3.3.3.1.3, end-to-end flow delay is defined as, the average per packet end-to-end delay for all packets forwarded by that flow.

Figures 3.33-3.35 present average flow delay for the three topologies described in Fig. 3.29 and the four SINR threshold values considered. For the rest of the section, end-to-end flow delay will be referred to as *flow delay*.

As these figures show, for all three topologies explored, TOFRA-IAN achieves the same delay with BP$_{e2e}$, for all γ values considered. The only exception to this is the simulated scenario based on topology 3, with γ=0.5. In this scenario, TOFRA-IAN also assigns flow on path $1 \rightarrow R \rightarrow d$. The flow assigned on path $1 \rightarrow R \rightarrow d$, is also increased in the case where

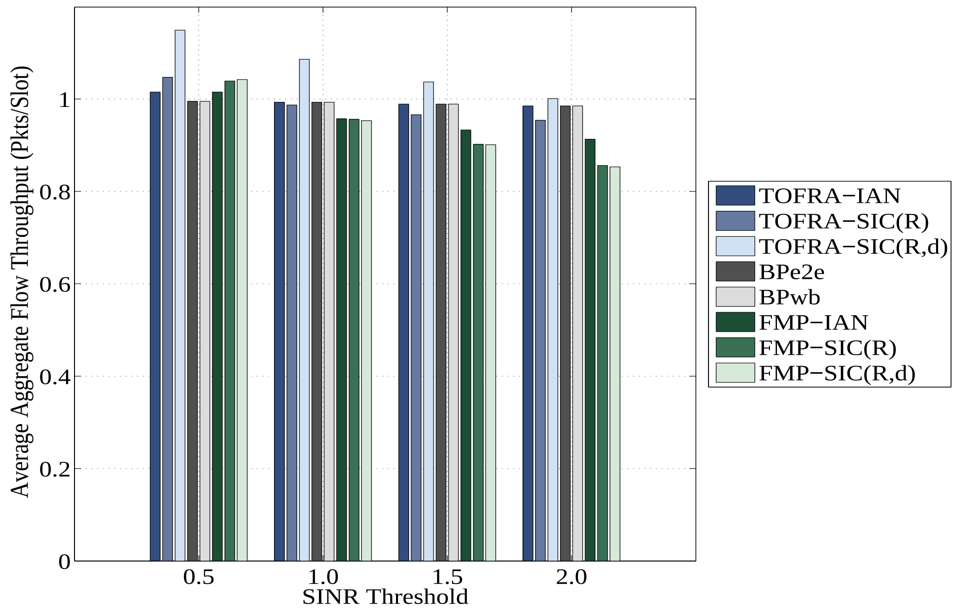

Figure 3.32: Topology 3: AAT per flow allocation variant.

TOFRA is combined with SIC. As Table 3.12 for example shows, for the second topology and γ=0.5, TOFRA assigns 0.350 packets per slot on path $1 \rightarrow R \rightarrow d$, when SIC is applied at both R and d. Consequently, a larger number of packets will experience queueing delay at R and also increased retransmissions due inter-path interference. The effect of queueing delay on flow delay, is extensively discussed in the rest of the section. This effect is also validated if BP$_{wb}$ is considered for topologies 1 and 2. In these topologies, BP$_{wb}$ forwards all packets through path $1 \rightarrow R \rightarrow d$. Figures 3.33-3.35 show that, it experiences significantly higher flow delay than all other schemes, for these two topologies, apart from full multipath variants FMP-SIC(R), FIM-SIC(R,d). The second reason behind the increased delay of TOFRA, when combined with SIC, is related to the accuracy with which, the model presented in Section 3.3.2 captures the average throughput of a link and is discussed in the next paragraph.

To validate the effect of queueing delay on flow delay, the throughput ratio (defined in Section 3.3.3.1.3) for a relay, along with average queue length are employed. For the case of relay node R, in Fig. 3.29 for example, throughput ratio is defined as: $\bar{T}(1, R)/\bar{T}(R, d)$. As also discussed in Section 3.3.3.1.3, a value for that ratio larger than one, would suggest a queue at the relay, where packets arrive at a rate faster than the rate with which they can be serviced (delivered to d). This, results in an unstable queue at the relay node and consequently in packets experiencing unbounded delay. A value for that ratio that is one, would imply a sub-stable queue at R. In this case, packets may experience increased queueing delay. Additionally, the average queue length for each node, especially for relays, is calculated from simulated results.

Figures 3.33-3.35 also show that, for all topologies and γ values explored, FMP-IAN

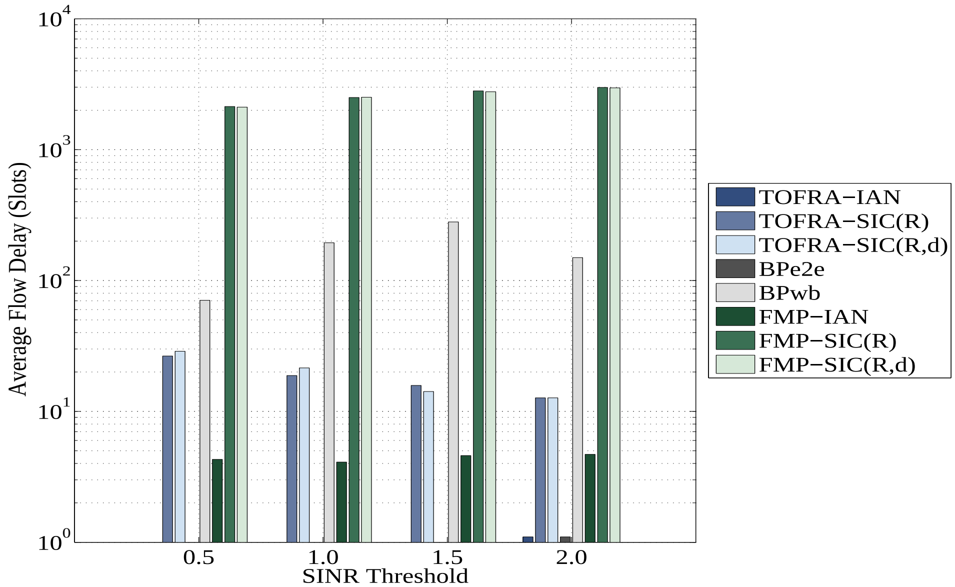

Figure 3.33: Topology 1: flow delay per flow allocation variant.

achieves significantly lower flow delay than TOFRA variants that employ SIC, although FMP is expected to experience more failed packets due to increased inter-path interference. In order to explore this delay gap between FMP and TOFRA variants, topology 2, with γ=0.5, is used as an example. Moreover, we focus on FMP-IAN and TOFRA-SIC(R,d) variants. As simulation results show, FMP-IAN indeed experiences a larger number of failed transmission due to noise, signal attenuation, interference, and fading. For link $(0, 1)$, this ratio is 81.0% for FMP-IAN and 3.6% for TOFRA-SIC(R,d). As far as path $1 \rightarrow R \rightarrow d$ is concerned, it is also interesting to note that FMP-IAN manages to deliver to R, only 8.3% of the packets sent over link $(1, R)$, while the corresponding value for TOFRA-SIC(R,d) is 68.6%. Taking into account these ratios, TOFRA-SIC(R,d) is expected to experience higher queueing delay than FMP-IAN. Indeed, the average queue length for relay node 1 is 0.09 packets, for the case of FMP-IAN, and 17.0 packets when TOFRA-SIC(R,d) is employed.

Comparing different TOFRA variants in terms of average flow delay shows than when SIC is applied, instead of IAN, average flow delay exhibits a significant increase. As Tables 3.12-3.14 show, when TOFRA is combined with SIC, maximum AAT is achieved by utilizing path $1 \rightarrow R \rightarrow d$ in parallel with $2 \rightarrow d$, for all topologies explored. The gap in terms of delay may imply that TOFRA variants that employ SIC experience increased queueing delay. To validate this, the simulation scenario based on topology 2 with γ=0.5, is used as an example. First, the throughput ratio for relay node R is estimated, for the two TOFRA variants that employ SIC, from simulation results. The value of this ratio is 1.02, and 1.01, respectively, for the two variants considered, suggesting that the queue at R becomes unstable. However, as already discussed in the first part of the evaluation process, the model employed for the

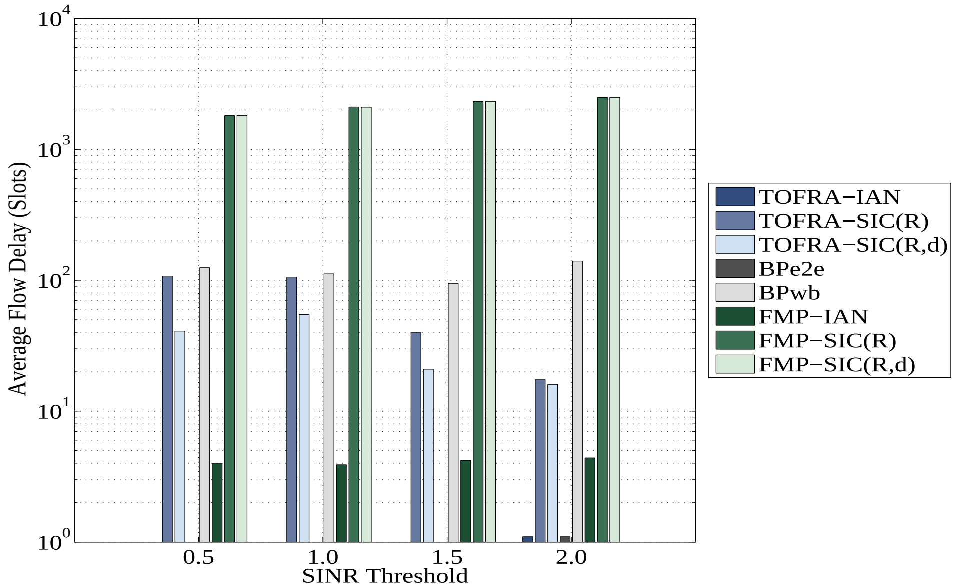

Figure 3.34: Topology 2: flow delay per flow allocation variant.

average aggregate flow throughput, may underestimate the actual average throughput of a link observed in the simulation scenarios. In this way, the average throughput of a specific link may be higher than the average throughput of a subsequent link which results in an *unstable* queue at the relay. The second reason is that, SIC improves the success probability of link $(1, R)$ and thus, increases the number of packets that are successfully delivered to R, when compared to TOFRA-IAN, resulting in a larger average queue size.

For all topologies and γ values explored, when full multipath (FMP) is combined with SIC, either at R, or both at R and d, it experiences by far higher average flow delay than all other flow allocation schemes discussed. For topology 1, in Fig. 3.29 and γ=0.5 for example, the flow delay observed in the simulation results, for FMP-SIC(R) and FMP-SIC(R,d), is 2133.9 and 2111.3 slots, respectively. However, this is expected, since FMP assigns traffic on paths an interference-unaware manner, experiencing a large number of failed packets due to increased interference. Secondly, it does not adjust the flow assigned on a path based on the one that can be serviced by its bottleneck link, resulting thus, in unstable queues at the relay nodes. For the case of topology 1 with γ=0.5 mentioned above, the throughput ratio at R for FMP-SIC(R) and FMP-SIC(R,d) is 3.680 and 3.658, respectively.

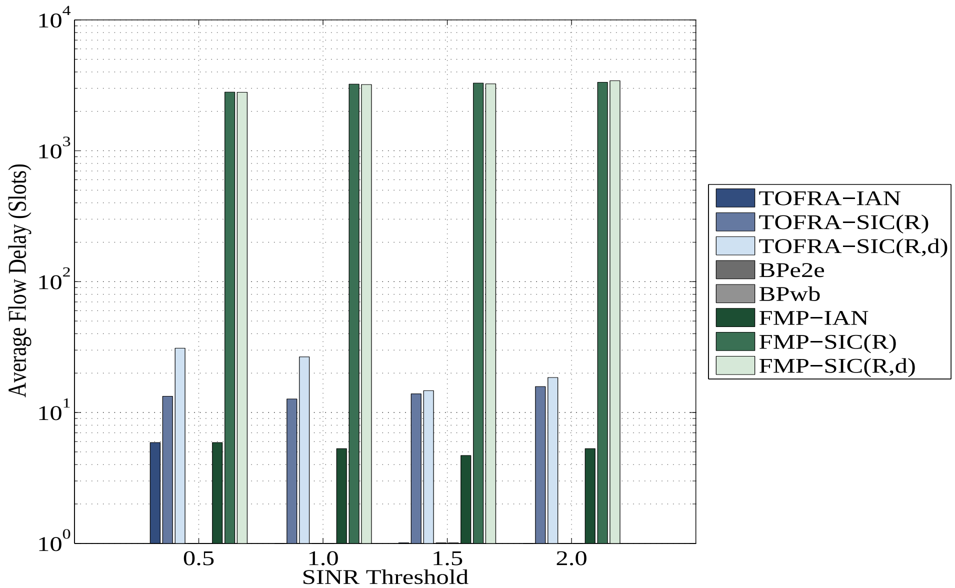

Figure 3.35: Topology 3: flow delay per flow allocation variant.

Chapter 4

Conclusions

4.1 Contributions

In the first part of the thesis, static, wireless mesh networks, are considered, with random access to the shared medium. Nodes are equipped with multiple interfaces, also having multi-packet reception capabilities, while flows carry unicast traffic. Several forwarding schemes, employing multiple paths and different degrees of redundancy are compared, both in terms of delay and throughput. For the purposes of this comparison, the analytical framework presented in [21] is employed, for expressing delay and throughput, for all schemes considered. The proposed scheme assumes fixed link error probabilities. An extension of it, is presented in the first part of the thesis, where link error probability is captured through the SINR model. Ns2 simulations are employed, in order to evaluate the accuracy of the analytical framework employed, along with the extension proposed, for capturing throughput and delay trends, for the forwarding schemes considered.

In the second part of the thesis, the issue of utilizing multiple paths in parallel, in order to maximize throughput was addressed, for random access, wireless mesh network, with multi-packet reception capabilities. A distributed flow allocation scheme was suggested, aimed at maximizing average aggregate flow throughput (AAT), while also guaranteeing bounded delay. The suggested scheme employs a simple model that captures both intra- and inter-path interference through the SINR model. Moreover, identifying flow rates that provide maximum AAT is formulated as an optimization problem. Using a simple topology we show that the corresponding optimization problem is non-convex. The suggested flow allocation scheme is evaluated through some illustrative wireless scenarios along with several random wireless ones, employing both numerical and Ns2 simulation results. As part of the evaluation process, the accuracy of the model, for capturing the AAT observed in the simulation scenarios, is explored. Moreover, the proposed scheme is compared with other simple flow allocation schemes, both in terms of flow delay and AAT. As far as interference is concerned, a variant of the proposed scheme is explored, where interference for each link is approximated by considering only the dominant interferes, for expressing a link's average throughput. The accuracy of this variant on capturing AAT observed in simulation result is evaluated. Finally, we explore the gain in terms of AAT that can be achieved, by the proposed scheme, when certain receivers employ successive interference cancellation, instead of treating interference as noise. The effect of successive interference cancellation on delay is also evaluated using Ns2 simulations.

4.2 Future Work

As far as the analytical framework, for expressing the throughput and delay, for various schemes employing different degrees of redundancy is concerned, part of our ongoing work is to extended it by incorporating transmission probabilities for all nodes.

Concerning the flow allocation scheme discussed in the second part of this thesis, for the analysis presented in Section 3.3.2 we have assumed that relay nodes employ a backoff window of fixed size and thus, transmit with a fixed probability on each slot. Part of our future work is to remove this assumption and consider a back-off window that can vary over time, based on transmission outcomes. Apart from that, the flow allocation optimization problem, presented in the second part of the thesis, is aimed at maximizing average aggregate flow throughput. As a result, in several scenarios the outcome of the optimization problem may include zero flow rate for a specific flow which means that the originator of the flow will not manage to deliver any traffic to its destination. Part of our future work, is to consider fairness issues too and explore the effect of fairness in AAT. As far as successive interference cancellation is concerned, we have explored the gain it can achieve, when combined with the proposed flow allocation scheme, for a simple topology. However, we plan to explore, how it can be employed for the case of large random topologies and whether it provides any throughput benefit. Finally, as already discussed in the part of the evaluation process that explored flow delay, although the bounded delay constraint employed by the flow allocation problem, limits the flow injected on each path based on the flow that can be serviced by any link along that path, in certain simulation scenarios, the actual average throughput for a specific link, may by slightly higher than the one considered by the corresponding constraint. As a result, the queue at the receiver of that link may become unstable with packets experiencing excess queueing delay. We are currently exploring a heuristic to tune the bounded delay constraint, in order to avoid such cases.

Bibliography

[1] T. Rappaport, *Wireless Communications: Principles and Practice*. Upper Saddle River, NJ, USA: Prentice Hall PTR, 2nd ed., 2001.

[2] Ayanoglu, C.-L. I, R. Gitlin, and J. Mazo, "Diversity coding for transparent self-healing and fault-tolerantcommunication networks," in *IEEE Transactions on Communications*, pp. 1677 – 1686, 1993.

[3] A. Tsirigos and Z. Haas, "Analysis of multipath routing, part 1: The effect of packet delivery ratio," in *IEEE Transactions on Wireless Communications vol.3 no. 1*, pp. 138–146, 2004.

[4] A. Tsirigos and Z. Haas, "Analysis of multipath routing, part 2: Mitigation of the effects of frequently changing topologies," in *IEEE Transactions on Wireless Communications*, pp. 500–511, 2004.

[5] R. Ahlswede, N. Cai, S. R. Li, and R. W. Yeung, "Network information flow," in *IEEE Transactions on Information Theory*, pp. 1204–1216, 2000.

[6] R. W. Yeung and N. Cai, "Network error correction, part i: Basic concepts and upper bounds," in *Communications in Information and Systems*, pp. 19 – 36, 2006.

[7] D. Lun, M. Medard, R. Koetter, and M. Effros, "Further results on coding for reliable communication over packet networks," in *ISIT*, 2005.

[8] G. Booker and A. Sprintson, "Design of efficient robust network codes for multicast connections," in *ISIT*, 2009.

[9] H. Bahramgiri and F. Lahouti, "Robust network coding against path failures," in *IET Communications*, pp. 272–284, 2010.

[10] P.-Y. Chen, W.-C. Ao, and K.-C. Chen, "Rate-delay enhanced multipath transmission scheme via network coding in multihop networks," *Communications Letters, IEEE*, vol. 16, no. 3, pp. 281–283, 2012.

[11] I. Woungand, S. Dhurandher, A. Anpalagan, and A. Vasilakos, *Routing in Opportunistic Networks*. Upper Saddle River, NJ, USA: Springer-Verlag New York, 1st ed., 2013.

[12] S. Katti, D. Katabi, W. Hu, H. Rahul, and M. Medard, “The importance of being opportunistic: Practical network coding for wireless environments,” in *Allerton*, 2005.

[13] S. Chachulski, M. Jennings, S. Katti, and D. Katabi, “Trading structure for randomness in wireless opportunistic routing,” in *ACM SIGCOMM*, 2007.

[14] C. Gkantsidis, W. Hu, P. Key, B. Radunovic, S. Gheorghiu, and P. Rodriguez, “Multipath code casting for wireless mesh networks,” in *CoNext*, 2007.

[15] S. Biswas and R. Morris, “Opportunistic routing in multi-hop wireless networks,” in *ACM SIGCOMM*, 2005.

[16] Y. Yuan, S. H. Y. Wong, S. Lu, and W. Arbuagh, “Romer: Resilient opportunistic mesh routing for wireless mesh networks,” in *Proceedings of IEEE WiMesh*, 2005.

[17] M. V. Pedersen, D. E. Lucani, F. H. Fitzek, C. Sorensen, and A. S. Badr, “Network coding designs suited for the real world: What works, what doesn’t, what’s promising,” in *Proceedings IEEE Information Theory Workshop*, 2013.

[18] S. Gheorghiu, A. Toledo, and P. Rodriguez, “Multipath tcp with network coding for wireless mesh networks,” in *Communications (ICC), 2010 IEEE International Conference on*, pp. 1–5, 2010.

[19] S. Y. Oh, M. Gerla, and A. Tiwari, “Robust manet routing using adaptive path redundancy and coding,” in *Proceedings of the First international conference on COMmunication Systems And NETworks*, COMSNETS’09, (Piscataway, NJ, USA), pp. 224–233, IEEE Press, 2009.

[20] M. Langberg and M. Medard, “On the multiple unicast network coding, conjecture,” in *Communication, Control, and Computing, 2009. Allerton 2009. 47th Annual Allerton Conference on*, pp. 222–227, September 2009.

[21] N. Pappas, V. Siris, and A. Traganitis, “Delay and throughput of network coding with path redundancy for wireless mesh networks,” in *Wireless and Mobile Networking Conference (WMNC), 2010 Third Joint IFIP*, pp. 1 –6, October. 2010.

[22] M. Ploumidis, N. Pappas, V. Siris, and A. Traganitis, “Evaluating forwarding schemes exploiting path diversity and degrees of redundancy in a realistic wireless environment,” in *Computer Aided Modeling and Design of Communication Links and Networks (CAMAD), 2012 IEEE 17th International Workshop on*, pp. 95–99, 2012.

[23] M. Ploumidis, N. Pappas, V. Siris, and A. Traganitis, “On the performance of network coding and forwarding schemes with different degrees of redundancy for wireless mesh networks,” *Comput. Commun.*, May 2015.

[24] L. Le, “Multipath routing design for wireless mesh networks,” in *Global Telecommunications Conference (GLOBECOM 2011), 2011 IEEE*, pp. 1 –6, December. 2011.

[25] J. Tsai and T. Moors, "Interference-aware multipath selection for reliable routing in wireless mesh networks," in *Mobile Adhoc and Sensor Systems, 2007. MASS 2007. IEEE Internatonal Conference on*, pp. 1 –6, October. 2007.

[26] A. Valera, W. Seah, and S. Rao, "Cooperative packet caching and shortest multipath routing in mobile ad hoc networks," in *INFOCOM 2003. Twenty-Second Annual Joint Conference of the IEEE Computer and Communications. IEEE Societies*, vol. 1, pp. 260 – 269 vol.1, March-3 April 2003.

[27] V. Sharma, S. Kalyanaraman, K. Kar, K. Ramakrishnan, and V. Subramanian, "Mplot: A transport protocol exploiting multipath diversity using erasure codes," in *INFOCOM 2008. The 27th Conference on Computer Communications. IEEE*, pp. 121 –125, April 2008.

[28] R. Leung, J. Liu, E. Poon, A.-L. Chan, and B. Li, "Mp-dsr: a qos-aware multi-path dynamic source routing protocol for wireless ad-hoc networks," in *Local Computer Networks, 2001. Proceedings. LCN 2001. 26th Annual IEEE Conference on*, pp. 132 –141, 2001.

[29] M. Alicherry, R. Bhatia, and L. E. Li, "Joint channel assignment and routing for throughput optimization in multiradio wireless mesh networks," *Selected Areas in Communications, IEEE Journal on*, vol. 24, pp. 1960–1971, November 2006.

[30] G. Middleton, B. Aazhang, and J. Lilleberg, "Efficient resource allocation and interference management for streaming multiflow wireless networks," in *Communications (ICC), 2010 IEEE International Conference on*, pp. 1–5, May 2010.

[31] G. Middleton, B. Aazhang, and J. Lilleberg, "A flexible framework for polynomial-time resource allocation in streaming multiflow wireless networks," *Wireless Communications, IEEE Transactions on*, vol. 11, pp. 952–963, March 2012.

[32] S. Avallone and G. Di Stasi, "A new mpls-based forwarding paradigm for multi-radio wireless mesh networks," *Wireless Communications, IEEE Transactions on*, vol. 12, pp. 3968–3979, August 2013.

[33] G. D. Stasi, J. Karlsson, S. Avallone, R. Canonico, A. Kassler, and A. Brunstrom, "Combining multi-path forwarding and packet aggregation for improved network performance in wireless mesh networks," *Computer Networks*, vol. 64, no. 0, pp. 26 – 37, 2014.

[34] X. Lin and N. Shroff, "Joint rate control and scheduling in multihop wireless networks," in *Decision and Control, 2004. CDC. 43rd IEEE Conference on*, vol. 2, pp. 1484–1489 Vol.2, December 2004.

[35] U. Akyol, M. Andrews, P. Gupta, J. Hobby, I. Saniee, and A. Stolyar, "Joint scheduling and congestion control in mobile ad-hoc networks," in *INFOCOM 2008. The 27th Conference on Computer Communications. IEEE*, pp. 619 –627, April 2008.

[36] F. Qiu, J. Bai, and Y. Xue, "Towards optimal rate allocation in multi-hop wireless networks with delay constraints: A double-price approach.," in *ICC* [36], pp. 5280–5285.

[37] Q. Gao, J. Zhang, and S. Hanly, "Cross-layer rate control in wireless networks with lossy links: leaky-pipe flow, effective network utility maximization and hop-by-hop algorithms," *Wireless Communications, IEEE Transactions on*, vol. 8, pp. 3068 –3076, June 2009.

[38] X. Wang and K. Kar, "Cross-layer rate control for end-to-end proportional fairness in wireless networks with random access," in *Proceedings of the 6th ACM International Symposium on Mobile Ad Hoc Networking and Computing*, MobiHoc '05, (New York, NY, USA), pp. 157–168, ACM, 2005.

[39] J.-W. Lee, M. Chiang, and A. Calderbank, "Jointly optimal congestion and contention control based on network utility maximization," *Communications Letters, IEEE*, vol. 10, pp. 216–218, March 2006.

[40] A. Mohsenian-Rad, J. Huang, M. Chiang, and V. Wong, "Utility-optimal random access: Reduced complexity, fast convergence, and robust performance," *Wireless Communications, IEEE Transactions on*, vol. 8, pp. 898–911, February 2009.

[41] B. Radunović, C. Gkantsidis, D. Gunawardena, and P. Key, "Horizon: balancing tcp over multiple paths in wireless mesh network," in *Proceedings of the 14th ACM international conference on Mobile computing and networking*, MobiCom '08, (New York, NY, USA), pp. 247–258, ACM, 2008.

[42] C. Gkantsidis, W. Hu, P. Key, B. Radunovic, P. Rodriguez, and S. Gheorghiu, "Multipath code casting for wireless mesh networks," in *Proceedings of the 2007 ACM CoNEXT Conference*, CoNEXT '07, (New York, NY, USA), pp. 10:1–10:12, ACM, 2007.

[43] B. Radunovic, C. Gkantsidis, P. Key, and P. Rodriguez, "An optimization framework for opportunistic multipath routing in wireless mesh networks," in *INFOCOM 2008. The 27th Conference on Computer Communications. IEEE*, pp. –, April 2008.

[44] M. Ploumidis, N. Pappas, and A. Traganitis, "Throughput optimal flow allocation on multiple paths for random access wireless multi-hop networks," in *2013 IEEE Globecom Workshops (GC Wkshps)*, pp. 263–268, December 2013.

[45] M. Ploumidis, N. Pappas, and A. Traganitis, "A flow allocation scheme for maximum throughput for random access wireless multi-hop networks," in *Fourth Nordic Workshop on System & Network Optimization for Wireless*, Yllas, Finland, 2-5 April 2013.

[46] J. Yi, A. Adnane, S. David, and B. Parrein, "Multipath optimized link state routing for mobile ad hoc networks," *Ad Hoc Netw.*, vol. 9, no. 1, pp. 28–47, 2011.

[47] N. Pappas, A. Ephremides, and A. Traganitis, "Stability and performance issues of a relay assisted multiple access scheme with mpr capabilities," *Comput. Commun.*, vol. 42, pp. 70–76, 2014.

[48] D. Tse and P. Viswanath, *Fundamentals of wireless communication*. New York, NY, USA: Cambridge University Press, 2005.

[49] G. Nguyen, S. Kompella, J. Wieselthier, and A. Ephremides, "Optimization of transmission schedules in capture-based wireless networks," in *Military Communications Conference, 2008. MILCOM 2008. IEEE*, pp. 1 –7, 2008.

[50] N. Pappas, V. A. Siris, and A. Traganitis, "Path diversity gain with network coding and multipath transmission in wireless mesh networks," in *2010 IEEE International Symposium on a World of Wireless Mobile and Multimedia Networks (WoWMoM)*, pp. 1 –6, June 2010.

[51] S. Verdu, *Multiuser Detection*. New York, NY, USA: Cambridge University Press, 1st ed., 1998.

[52] S. P. Weber, J. Andrews, X. Yang, and G. de Veciana, "Transmission capacity of wireless ad hoc networks with successive interference cancellation," *Information Theory, IEEE Transactions on*, vol. 53, pp. 2799–2814, August 2007.

[53] S. Toumpis and A. Goldsmith, "Capacity regions for wireless ad hoc networks," *Wireless Communications, IEEE Transactions on*, vol. 2, pp. 736–748, July 2003.

[54] V. Angelakis, L. Chen, and D. Yuan, "Optimal and collaborative rate selection for interference cancellation in wireless networks," *Communications Letters, IEEE*, vol. 15, pp. 819–821, August 2011.

[55] D. Yuan, V. Angelakis, L. Chen, E. Karipidis, and E. Larsson, "On optimal link activation with interference cancelation in wireless networking," *Vehicular Technology, IEEE Transactions on*, vol. 62, pp. 939–945, Feb 2013.

[56] P. Mitran, C. Rosenberg, and S. Shabdanov, "Throughput optimization in wireless multihop networks with successive interference cancellation," in *Wireless Telecommunications Symposium (WTS), 2011*, pp. 1–7, April 2011.

[57] X. Zhang and M. Haenggi, "The performance of successive interference cancellation in random wireless networks," *IEEE Transactions on Information Theory*, vol. 60, pp. 6368–6388, October 2014.

[58] N. Miridakis and D. Vergados, "A survey on the successive interference cancellation performance for single-antenna and multiple-antenna ofdm systems," *IEEE Communications Surveys Tutorials*, vol. 15, pp. 312–335, First 2013.

[59] S. Sen, N. Santhapuri, R. Choudhury, and S. Nelakuditi, "Successive interference cancellation: Carving out mac layer opportunities," *IEEE Transactions on Mobile Computing*, vol. 12, pp. 346–357, February 2013.

[60] N. Pappas, M. Kountouris, and A. Ephremides, “The stability region of the two-user interference channel,” in *2013 IEEE Information Theory Workshop (ITW)*, pp. 1–5, September 2013.

[61] “The Network Simulator NS-2.” `http://www.isi.edu/nsnam/ns/`.

[62] S. research group, “dei80211mr: a new 802.11 implementation for ns-2,” 2008. Available at http://www.dei.unipd.it/wdyn/?IDsezione=5090. [Último acesso: 18/01/2010].

Appendix A

Simulation setup

In the first part of this thesis, presented in Chapter 2, the throughput and delay were explored, for forwarding schemes employing different degrees of redundancy. In the second part of the thesis, presented in Chapter 3, different variants of a flow allocation scheme were explored, depending on how interference is treated at the receivers.

For the evaluation process, of both parts, simulator Ns2, version 2.34 [61], including support for multiple transmission rates [62], was employed. This chapter, presents some modules incorporated into Ns2, in order to meet the assumptions of the system models, described in the two parts of this thesis. The first section, presents modules and modifications, related to common assumptions between the system models adopted in the two parts of the thesis. Additionally, Section A.2 presents some modifications that were required to simulate forwarding schemes that employ different forms of redundancy. Finally, Section A.3, presents implementation details concerning the assumption of saturated queues at the relay nodes and different approaches for interference handling. These details concern the flow allocation schemes discussed in the second part of the thesis (Chapter 3).

A.1 Ns2 Simulation setup

This section, presents cross-layer implementation details, that are common for both system models adopted, in the two parts of this thesis.

Concerning medium access control, a slotted aloha-based MAC layer is implemented. Transmission of data, routing protocol control, and ARP packets is performed at the beginning of each slot, without performing carrier sensing prior to transmitting. Acknowledgements for data packets are sent immediately after successful packet reception, while failed packets are retransmitted. Slot length, T_{slot}, is expressed through: $T_{slot} = T_{data} + T_{ack} + 2D_{prop}$, where T_{data} and T_{ack} denote the transmission times for data packets and acknowledgements (ACKs), while D_{prop} denotes the propagation delay. It should be noted that, all packets have the same size, shown in Table 3.3.3.1.2. In each time slot, each node *i*, if there is a packet available for transmission in its queue, it transmits with a specific probability q_i. For flow originators, q_i denotes the rate with which flow is injected on a specific path. As far as relay nodes are concerned, transmission probabilities are determined in two ways. It can either be set to a predetermined value, or select a random number of slots before transmitting, drawn uniformly from $[0, CW]$, where CW represents the contention window for each node. The contention window (CW) is assumed fixed, with a similar value for all relay nodes and the whole simulation period.

As far as physical layer is concerned, in Chapter 2 and in the first part of Chapter 3, interference is treated as noise. Accordingly, a received packet is considered successfully received, if its received SINR exceeds a certain threshold. As also described in these chapters, the received SINR, for a specific packet transmitted over a link (i, j), is estimated through equation:

$$\mathrm{SINR}(i,j) = \frac{\mathcal{P}_{rx}(i,j)}{\eta_j + \sum_{k \in \mathcal{T} \setminus \{i\}} \mathcal{P}_{rx}(k,j)}. \tag{A.1}$$

,where $\mathcal{T}$ denotes the set of transmitters that are also active during the same time slot. In the simulated scenarios, the transmitters during each slot, that are considered to cause interference, are those transmitting data packets or routing protocol control packets. In the second part of Chapter 3, instead of treating interference as noise, certain receivers employ successive interference cancellation. For each received packet, the received SINR, or SNR, is estimated based on equations presented in Section 3.4.1 in this chapter.

Concerning routing, a protocol with the following characteristics is simulated, in for both parts of the thesis: a) source routing is employed, ensuring that packets of the same flow are forwarded to the destination through the same path b) link-state-based topology information dissemination is employed. In the first part of the thesis, presented in Chapter 2, static predefined routes to the destination are employed. In the work concerning flow allocation on multiple paths, presented in Chapter 3, an approach based on the Dijkstra algorithm is employed, to provide sources with node disjoint paths. Further details are provided in Section A.3.

A.2 Ns2 modifications concerning different degrees of redundancy

Adding support for simulating different degrees of redundancy requires the following modifications: first, each packet carries a custom sequence number. This custom sequence number is placed in the common header that all Ns2 generated packets carry. For the case of multicopy forwarding scheme, discussed in the fist part of thesis, it shares the same value for each multi-copied packet. For network coding-based forwarding, it carries the *generation id* for packets that are coded together. The second modification is related to the assumption according to which, relay nodes remove from their queues a multi-copied packet that is successfully delivered to the destination, or any packets that belong to a generation that is successfully decoded by the destination. To support this functionality, a *global ack* mechanism is emulated, which consists of a custom acknowledgement broadcasted throughout the whole network by the destination node, upon reception of a packet, or successful decoding of a packet generation. This acknowledgement, carries the sequence number of the packet received, for the case of multi-copy, and the generation id of the generation decoded, for the case of network coding-based forwarding.

A.3 Ns2 modifications concerning flow allocation on different paths

As far as the evaluation of the flow allocation schemes, discussed in Chapter 3, is concerned, the following modifications were also incorporated in Ns2. In Section 3.3.3.1.3 of this chapter, several random scenarios are employed, for evaluation the proposed flow allocation scheme. For each traffic scenario, the number of flows, along with flow source and destination are randomly selected. The scenarios considered consist of two up to nine flows. In order to populate a multipath set that contains one path for each given flow, with different paths being node-disjoint, the following approach, which is based on the Dijkstra algorithm is employed: for each flow, a shortest path is identified through the Dijkstra algorithm with cost for link (i, j) defined as $1.0 - p^j_{i/i}$, where $p^j_{i/i}$ is the success probability over a link (i, j). All relay nodes participating in that path are then removed from the available nodes and the process continues with the next flow. The returned multipath set is post-processed, allowing from one up to five link-hops per path. The paths utilized for each one of the ten random scenarios employed in Section 3.3.3.1.3 of Chapter 3, are summarized in Table A.1.

As far as queues at the relay nodes are concerned, two variants of the proposed flow allocation scheme are simulated. The first variant follows the assumption of saturated queues in the analysis, while in the second variant, queues are not assumed to be saturated. In order to implement the first variant the following patch is required in the routing module in Ns2: the first time that a relay node i successfully receives a data packet destined for a next hop j, it buffers the full header of the packet. Then, if the queue for the next hop gets empty during a subsequent slot, it creates a new dummy packet with a dummy payload and adds the header buffered. Dummy packets are not taken into account for average aggregate flow throughput calculation.

Scenario	Multipath set	Scenario	Multipath set
1	$49 \rightarrow 46 \rightarrow 37 \rightarrow 19$ $25 \rightarrow 34 \rightarrow 33$ $32 \rightarrow 18 \rightarrow 23 \rightarrow 36$ $0 \rightarrow 5 \rightarrow 27$ $31 \rightarrow 45 \rightarrow 6$ $15 \rightarrow 12 \rightarrow 10$ $28 \rightarrow 38 \rightarrow 1$ $4 \rightarrow 26 \rightarrow 13$ $11 \rightarrow 20$	6	$39 \rightarrow 2 \rightarrow 47$ $29 \rightarrow 42 \rightarrow 9$ $45 \rightarrow 31 \rightarrow 10 \rightarrow 11$ $3 \rightarrow 36 \rightarrow 6 \rightarrow 49$ $1 \rightarrow 38 \rightarrow 18$ $32 \rightarrow 23 \rightarrow 28$ $8 \rightarrow 30 \rightarrow 40$
2	$42 \rightarrow 1 \rightarrow 29 \rightarrow 45 \rightarrow 31$ $11 \rightarrow 20 \rightarrow 30 \rightarrow 8 \rightarrow 9$ $32 \rightarrow 18 \rightarrow 23 \rightarrow 28 \rightarrow 36$ $27 \rightarrow 12 \rightarrow 14$	7	$48 \rightarrow 39 \rightarrow 2$ $37 \rightarrow 19 \rightarrow 14 \rightarrow 15$ $21 \rightarrow 41 \rightarrow 35 \rightarrow 12$ $27 \rightarrow 10 \rightarrow 31 \rightarrow 40 \rightarrow 46$ $9 \rightarrow 42 \rightarrow 1 \rightarrow 38$ $26 \rightarrow 13 \rightarrow 16 \rightarrow 7$
3	$44 \rightarrow 25 \rightarrow 16 \rightarrow 7 \rightarrow 3$ $23 \rightarrow 18 \rightarrow 32 \rightarrow 38$ $47 \rightarrow 2 \rightarrow 9 \rightarrow 42 \rightarrow 1 \rightarrow 29$ $28 \rightarrow 36 \rightarrow 6$	8	$47 \rightarrow 2 \rightarrow 9$ $46 \rightarrow 40 \rightarrow 31$ $12 \rightarrow 14 \rightarrow 35 \rightarrow 41$ $0 \rightarrow 17 \rightarrow 21 \rightarrow 24$ $6 \rightarrow 49 \rightarrow 37 \rightarrow 15$ $45 \rightarrow 29 \rightarrow 1$ $19 \rightarrow 27 \rightarrow 10$ $5 \rightarrow 11$
4	$1 \rightarrow 29 \rightarrow 45$ $23 \rightarrow 18 \rightarrow 32 \rightarrow 38$	9	$40 \rightarrow 31 \rightarrow 45$ $41 \rightarrow 35 \rightarrow 15 \rightarrow 14 \rightarrow 10$ $13 \rightarrow 16$ $11 \rightarrow 20 \rightarrow 30$ $12 \rightarrow 19$ $2 \rightarrow 9 \rightarrow 42 \rightarrow 1$ $18 \rightarrow 23 \rightarrow 28$ $7 \rightarrow 3 \rightarrow 36$ $0 \rightarrow 5 \rightarrow 27$
5	$47 \rightarrow 38 \rightarrow 1 \rightarrow 29 \rightarrow 45$ $46 \rightarrow 37 \rightarrow 19 \rightarrow 14 \rightarrow 15$ $24 \rightarrow 33 \rightarrow 34 \rightarrow 49$	10	$36 \rightarrow 28 \rightarrow 32$ $48 \rightarrow 39 \rightarrow 2$ $3 \rightarrow 23$ $17 \rightarrow 15 \rightarrow 14$ $34 \rightarrow 6 \rightarrow 46 \rightarrow 37 \rightarrow 19 \rightarrow 35$ $49 \rightarrow 7$ $24 \rightarrow 21 \rightarrow 41 \rightarrow 12$ $18 \rightarrow 38 \rightarrow 1 \rightarrow 42 \rightarrow 9$

Table A.1: Multipath set employed for each one of the ten random scenarios.